ResearchGate

See discussions, stats, and author profiles for this publication at: https://www.researchgate.net/publication/235065150

Theoretical and Experimental Study of Micro Air Vehicle Powered by RF Signal at 10 GHz

Article · December 2003

CITATIONS
5

READS
2,283

1 author:



George Tsolis
Aristotle University of Thessaloniki
5 PUBLICATIONS **122** CITATIONS

SEE PROFILE

All content following this page was uploaded by George Tsolis on 15 October 2019.

The user has requested enhancement of the downloaded file.



NAVAL POSTGRADUATE SCHOOL

MONTEREY, CALIFORNIA

THESIS

THEORETICAL AND EXPERIMENTAL STUDY OF MICRO AIR VEHICLE POWERED BY RF SIGNAL AT 10 GHZ

by

George Tsolis

December 2003

Thesis Advisor:	David C Jenn
Second Readers:	Jeffrey B. Knorr
	Kevin Jones

Approved for public release; distribution is unlimited

THIS PAGE INTENTIONALLY LEFT BLANK

REPORT DOCUMENTATION PAGE			Form Approved OMB No. 0704-0188
Public reporting burden for this collection of information is estimated to average 1 hour per response, including the time for reviewing instruction, searching existing data sources, gathering and maintaining the data needed, and completing and reviewing the collection of information. Send comments regarding this burden estimate or any other aspect of this collection of information, including suggestions for reducing this burden, to Washington headquarters Services, Directorate for Information Operations and Reports, 1215 Jefferson Davis Highway, Suite 1204, Arlington, VA 22202-4302, and to the Office of Management and Budget, Paperwork Reduction Project (0704-0188) Washington DC 20503.			
1. AGENCY USE ONLY ***(Leave blank)***	**2. REPORT DATE** December 2003	**3. REPORT TYPE AND DATES COVERED** Master's Thesis	
4. TITLE AND SUBTITLE: Experimental Study of Micro Air Vehicle Powered by RF Signal at 10 GHz			**5. FUNDING NUMBERS**
6. AUTHOR(S) George Tsolis			
7. PERFORMING ORGANIZATION NAME(S) AND ADDRESS(ES) Naval Postgraduate School Monterey, CA 93943-5000			**8. PERFORMING ORGANIZATION REPORT NUMBER**
9. SPONSORING /MONITORING AGENCY NAME(S) AND ADDRESS(ES) N/A			**10. SPONSORING/MONITORING AGENCY REPORT NUMBER**
11. SUPPLEMENTARY NOTES The views expressed in this thesis are those of the author and do not reflect the official policy or position of the Department of Defense or the U.S. Government.			
12a. DISTRIBUTION / AVAILABILITY STATEMENT Approved for public release; distribution is unlimited			**12b. DISTRIBUTION CODE**

13. ABSTRACT (maximum 200 words)

The concept of using electromagnetic energy in the form of microwaves for transferring power from one point to another through free space is very old. However, the idea for powering micro air vehicles using microwaves is less than a decade old. This thesis presents a theoretical and experimental study of powering a micro air vehicle, using electromagnetic energy at the frequency of 10 GHz.

Two micro air vehicle prototypes were designed and built, and various experiments conducted in order to specify the power requirements of such a vehicle. The vehicle weighted 9-15 grams and its maximum dimension was six inches.

The rectifier antenna (rectenna) is a major component in a microwave power transmission process. A quality factor used for rectenna characterization is the conversion efficiency from microwave power to dc power. A key component in any rectenna design is the Schottky barrier diode which is used to rectify the microwave energy to dc energy.

A small rectenna array was manufactured using sixteen identical elements. Each element consisted of a circular patch antenna, a rectifying diode, and input and output low pass filters. The circuit was tested and the results showed a 10.3% conversion efficiency of the individual rectenna element, and 8.2% conversion efficiency for the total circuit.

14. SUBJECT TERMS Electromagnetic Energy, Microwaves, Micro Air Vehicle, Rectifier Antenna, Rectenna, Schottky Barrier Diode			**15. NUMBER OF PAGES** 133
			16. PRICE CODE
17. SECURITY CLASSIFICATION OF REPORT Unclassified	**18. SECURITY CLASSIFICATION OF THIS PAGE** Unclassified	**19. SECURITY CLASSIFICATION OF ABSTRACT** Unclassified	**20. LIMITATION OF ABSTRACT** UL

NSN 7540-01-280-5500 Standard Form 298 (Rev. 2-89)
Prescribed by ANSI Std. 239-18

THIS PAGE INTENTIONALLY LEFT BLANK

Approved for public release; distribution is unlimited

EXPERIMENTAL STUDY OF MICRO AIR VEHICLE POWERED BY RF SIGNAL AT 10 GHZ

George Tsolis
Major, Hellenic Air Force
B.S., Hellenic Air Force Academy, 1990

Submitted in partial fulfillment of the
requirements for the degree of

MASTER OF SCIENCE IN SYSTEMS ENGINEERING

from the

NAVAL POSTGRADUATE SCHOOL
December 2003

Author: George Tsolis

Approved by: David C. Jenn
Thesis Advisor

Jeffrey B. Knorr
Second Reader

Dan C. Boger
Chairman, Department of Information Sciences

THIS PAGE INTENTIONALLY LEFT BLANK

ABSTRACT

The concept of using electromagnetic energy in the form of microwaves for transferring power from one point to another through free space is very old. However, the idea for powering micro air vehicles using microwaves is less than a decade old. This thesis presents a theoretical and experimental study of powering a micro air vehicle, using electromagnetic energy at the frequency of 10 GHz.

Two micro air vehicle prototypes were designed and built, and various experiments conducted in order to specify the power requirements of such a vehicle. The vehicle weighted 9-15 grams and its maximum dimension was six inches.

The rectifier antenna (rectenna) is a major component in a microwave power transmission process. A quality factor used for rectenna characterization is the conversion efficiency from microwave power to dc power. A key component in any rectenna design is the Schottky barrier diode, which is used to rectify the microwave energy to dc energy.

A small rectenna array was manufactured using sixteen identical elements. Each element consisted of a circular patch antenna, a rectifying diode, and input and output low pass filters. The circuit was tested and the results showed a 10.3% conversion efficiency of the individual rectenna element, and 8.2% conversion efficiency for the total circuit.

THIS PAGE INTENTIONALLY LEFT BLANK

TABLE OF CONTENTS

I. INTRODUCTION....1

II. BACKGROUND....3
- A. WIRELESS POWER TRANSMISSION....3
- B. THE WPT PROCESS....4
  - 1. Transmission....4
  - 2. Rectification....6
- C. MICROWAVE POWERED AIR VEHICLES....17
- D. MICRO AIR VEHICLES (MAV)....23
- E. SUMMARY....25

III. RECTIFIED DIODE CHARACTERIZATION....27
- A. INTRODUCTION....27
- B. THE SCHOTTKY BARRIER DIODE....27
  - 1. Description....27
  - 2. Schottky Barrier Diode Characteristics....28
  - 3. Forward Voltage Characteristic....29
- C. HSMS 8101 SCHOTTKY BARRIER DIODE....30
- D. HSMS 8101 DIODE POWER CALCULATIONS....35
- E. IMPEDANCE MATCHING CONSIDERATIONS....37
- F. DIODE BURNOUT....41
- G. SUMMARY....41

IV. MICRO AIR VEHICLE (MAV) DESIGN....43
- A. INTRODUCTION....43
- B. BASIC ROTOR THEORY....43
  - 1. Rotor Blade Airflows....44
  - 2. Rotor Blade Forces....44
  - 3. Rotor Power Calculation....46
- C. MAV CONSTRUCTION....51
  - 1. MAV Body Construction....51
  - 2. MAV Rotor Fabrication....57
- D. MAV POWER TESTS....60
- E. SUMMARY....65

V. RECTIFIER ANTENNA (RECTENNA) DESIGN....67
- A. CIRCULAR PATCH ANTENNA....68
  - 1. Theory....68
  - 2. Design and Fabrication....73
- B. INPUT AND OUTPUT LOW PASS FILTERS....80
  - 1. Theory....80
  - 2. Design and Fabrication....84
- C. SUMMARY....90

VI. RECTENNA FABRICATION AND TESTING 91
A. RECTENNA ELEMENT FABRICATION 91
B. RECTENNA ELEMENT MEASUREMENT 92
C. RECTENNA TESTING 98
D. SUMMARY 104
VII. CONCLUSION AND RECOMMENDATIONS 107
A. CONCLUSION 107
B. RECOMMENDATIONS FOR FUTURE WORK 108
LIST OF REFERENCES 111
INITIAL DISTRIBUTION LIST 115

LIST OF FIGURES

Figure 1. Radiating module composed of a slotted waveguide antenna and a phase-locked, magnetron directional amplifier [From Ref. 2]. 6
Figure 2. The rectenna constructed by Brown for the microwave-powered helicopter. [from ref. 5]....8
Figure 3. Typical rectenna element. 8
Figure 4. Schematic showing the interconnections between the rectenna elements [From Ref. 8]. 10
Figure 5. Demonstration of beamed power over one mile distance, at the JPL Goldstone facility in the Mojave desert [From Ref. 9]. 11
Figure 6. The first thin film Rectenna element printed on mylar and Kapton F substrate [From Ref. 8]. 12
Figure 7. Schematic layout of the Texas A&M university rectenna used in METS experiment [From Ref. 8]. 14
Figure 8. Patch dual polarized rectenna manufactured by a JPL team [From Ref. 18]. 15
Figure 9. C band circular patch rectenna element. (a) Side view of the rectenna element. (b) Circular patch antenna. (c) Rectifier circuit [From Ref. 19]. 16
Figure 10. Schematic of the conformal rectenna array proposed in [Ref. 19]. 16
Figure 11. The microwave powered helicopter built by W. C. Brown in 1964 [From Ref. 5]. 17
Figure 12. The basic elements microwave powered helicopter system. [From Ref. 5]. ...18
Figure 13. Beam riding microwave power helicopter [from ref. 3]. 19
Figure 14. Artist's sketch for a microwave powered airship designed to fly at 70 kft [From Ref. 22]. 20
Figure 15. Configuration of the SHARP system [From Ref. 12]. 21
Figure 16. 4.5 m Wingspan microwave powered airplane [From Ref. 12]. 22
Figure 17. The wing of the 1/8 model of the SHARP airplane with the thin film rectenna mounted [From Ref. 23]. 22
Figure 18. Illustration of the Reynolds's number versus gross weight of various vehicles [From Ref. 24]. 24
Figure 19. Schematic of passivated type SBD together with its equivalent circuit [From Ref. 36]. 28
Figure 20. Package dimensions for HSMS 8101 SBD [From Ref. 36]. 32
Figure 21. Dc current versus dc voltage curve of the HSMS 8101 SBD for three operational temperatures [From Refs. 35, 36]. 33
Figure 22. Measured dc voltage versus dc current curve for a sample of four HSMS 8101 diodes. 35
Figure 23. HSMS 8101 Diode Computed Output Voltage Versus Input Power (Computed Using Equation 3.10). 37
Figure 24. Schottky diode AC equivalent circuit. from [Ref. 20]. 38
Figure 25. Junction resistance of HSMS 8101 SBD. 39

Figure 26. Input impedance of HSMS 8101 for various frequencies and voltage of 1 V. 41
Figure 27. Airflows in a rotor blade [From Ref. 38]. 44
Figure 28. Forces applied in a rotor blade [From Ref. 38]. 45
Figure 29. Effects of the angle of attack of the blade to the rotor thrust. (a) Low angle of attack. (b) High angle of attack [From Ref. 38]. 46
Figure 30. Fluid flow model for a helicopter rotor [From Ref. 39]. 47
Figure 31. Rotor thrust calculations (R=7.5 cm). 50
Figure 32. Rotor disc loading versus power loading (R=7.5 cm). 51
Figure 33. MAV prototype schematic layout. 53
Figure 34. Gearbox schematic layout. 54
Figure 35. Schematic layout of Maxon 10 mm motor (Manufacturer's DATA). 56
Figure 36. Schematic layout of the 7 mm coreless motor. 56
Figure 37. Rotor blade schematic layout. 58
Figure 38. Illustration of the method used for rotor blade fabrication. (a) Carbon laminates on the cylinder. (b) Blade airfoil geometry. 59
Figure 39. Calculation of the airfoil camber. 60
Figure 40. MAV hovering tethered for electrical power calculations. 61
Figure 41. Voltage versus current for hovering. 63
Figure 42. Power versus weight for hovering of the MAV prototypes. 63
Figure 43. Power versus load resistance for hovering for various weights. 64
Figure 44. Schematic of the circular microstrip patch antenna [From Ref. 44]. 68
Figure 45. Radiation conductance of the circular patch antenna [From Ref. 44]. 72
Figure 46. Computed three-dimensional radiation pattern of the circular patch antenna at 10 GHz (Microwave Studio simulation). 76
Figure 47. Computed radiation pattern of circular patch antenna (φ-component). (Microwave Studio simulation). 77
Figure 48. Computed radiation pattern of circular patch antenna (θ-component). (Microwave Studio simulation). 78
Figure 49. Computed return loss of the circular patch antenna normalized to 50 Ω. (Microwave Studio simulation). 79
Figure 50. Smith chart plot of the computed input impedance of the circular patch antenna (Microwave Studio simulation). 80
Figure 51. Maximally flat low-pass filter response for N=3 [From Ref. 32]. 81
Figure 52. Low-pass filter prototype N=2 [From Ref. 32]. 82
Figure 53. Approximate circuits for short sections of transmission lines. (a) T-equivalent circuit for a line having $\beta\ell \ll \pi/2$. (b) Equivalent circuit for small $\beta\ell$ and large Z_0. (c) Equivalent circuit for small $\beta\ell$ and small Z_0 [From Ref. 32]. 83
Figure 54. Attenuation versus normalized frequency for maximally flat filter prototypes [From Ref. 32]. 86
Figure 55. Schematic layout of the input low pass filter realized by the normalized element values. 87
Figure 56. Computed input low pass filter response. (Advance Design System simulation) 88

Figure 57. Computed output low pass filter response. (Advance Design System simulation) 90
Figure 58. Schematic layout of the rectenna element. 91
Figure 59. Rectenna element. 92
Figure 60. Block diagram of the rectenna element measurement system. 94
Figure 61. Dc output power versus microwave received (P_{rec}) for one rectenna element ($f = 9.975$ GHz) 97
Figure 62. Dc output power versus resistive load for three rectenna elements. 97
Figure 63. Rectenna efficiency measurement ($f = 9.975$ GHz) 98
Figure 64. Rectenna array in mixed connection configuration. (a) Front view, (b) Rear view. 99
Figure 65. Rectenna measurement system. 100
Figure 66. Rectenna efficiency when the elements are connected in series ($f = 9.975$ GHz) 100
Figure 67. Rectenna efficiency when the elements are connected in parallel ($f = 9.975$ GHz) 101
Figure 68. Rectenna efficiency when two series combinations of elements are connected in parallel ($f = 9.975$ GHz) 101
Figure 69. Rectenna dc output power versus incident power for series element connection ($f = 9.975$ GHz) 102
Figure 70. Rectenna dc output power versus incident power for parallel element connection ($f = 9.975$ GHz) 102
Figure 71. Rectenna dc output power versus incident power when two series combinations of elements are connected in parallel ($f = 9.975$ GHz) 103
Figure 72. Rectenna dc output voltage versus resistive load for series connection ($f = 9.975$ GHz) 103
Figure 73. Rectenna dc output current versus resistive load for parallel connection ($f = 9.975$ GHz) 104

THIS PAGE INTENTIONALLY LEFT BLANK

LIST OF TABLES

Table 1. HSMS 8101 electrical characteristics [From Ref. 36]. 31
Table 2. Input impedance for HSMS 8101 SBD for the fundamental and harmonics. 40
Table 3. Input impedance of HSMS 8101 at 10 GHz for various voltages. 40
Table 4. Characteristics of the MAV motors used for the two prototypes (Manufacturer's DATA). 55
Table 5. Measured data of the first prototype. 64
Table 6. Measured data of the second prototype. 65
Table 7. Patch data as evaluated using the PATCHD program [From Ref. 45]. 75
Table 8. Summarized computational data of patch antenna. 75
Table 9. Measured data for the first rectenna element ($f = 9.975$ GHz) 95
Table 10. Measured data for the second rectenna element ($f = 9.971$ GHz). 96
Table 11. Measured data for the third rectenna element ($f = 9.968$ GHz). 96

THIS PAGE INTENTIONALLY LEFT BLANK

ACKNOWLEDGMENTS

I would like to express my sincere gratitude to my advisor Professor David Jenn of the Naval Postgraduate School, Monterey, California. He was always optimistic in my work, giving me strength to continue working in this demanding subject. I would also like to thank Professor Jeffrey Knorr who was my second advisor for this thesis. He has never failed to stop whatever work he was doing to attend to my questions and give me solutions to various problems I faced during this project.

I would like also to express my appreciation to Assistant Professor Kevin Jones form the Aeronautics Department, whose contribution was crucial to the aerodynamic part of this project.

Last, but not least, I would like to thank my wife Chrissy and my children Helen, Sotos and Thespina for their support and devotion, without which I would not be able to fulfill the requirements of this Master's degree.

THIS PAGE INTENTIONALLY LEFT BLANK

I. INTRODUCTION

Micro air vehicles belong to a new category of uninhabited air vehicles (UAV), and are several orders of magnitude smaller than the ordinary UAVs. Recent advances in miniaturization, as a result of the evolution of micromechanics and microelectronics, allow the implementation of vehicles, which are comparable in size and functionality to small birds and insects.

However, several obstacles have to be overcome in order for a fully functional MAV to meet any operational requirements. Among them, perhaps the most important problem is providing energy for propulsion of the vehicle. Several solutions have been proposed, but none of them is capable of providing high energy density, together with high power density as required for a MAV.

In this thesis a theoretical and experimental study of a microwave powered micro air vehicle is presented. Potentially a microwave powered MAV would be an ideal solution to many problems related with the limited payload capability of the vehicle, and therefore, its endurance. The use of ground based high frequency rf energy for propulsion, minimizes or eliminates the size of the vehicle's power source, allowing at the same time the endurance of the vehicle to reach the limits of its operational life.

This thesis is organized into six chapters. Chapter II presents a thorough background of the wireless power transmission (WPT) process. Wireless power transmission is simply the transmission of power from one point to another through free space, using electromagnetic energy in the form of microwaves. A critical component in the WPT process is the rectifying antenna, rectenna, the device that receives the microwave energy and transforms it to dc energy. A detailed description of the rectenna as it has evolved over time is presented in Chapter II, and the various types of rectennas are illustrated.

Chapter III gives the fundamental analysis of the rectifying diode. The diode is the major component of the rectifying circuit. The rectenna efficiency is closely related to

the proper selection of the rectifying diode, as well as matching of the diode to the rectifying circuit. When the latter has been achieved the power losses of the rectenna are equal to the resistive losses of the diode.

In Chapter IV a detailed presentation is given of the micro air vehicle construction. The design and fabrication of two prototypes are presented, together with a basic theoretical analysis of the various aerodynamic parameters. Experimental results of propulsion power measurements are analyzed.

Chapter V covers the theoretical analysis and design of the rectenna element. As a key component in any rectenna the antenna element needs to be as efficient as possible. Thus, a thorough theoretical analysis of the circular patch antenna was performed, and verified using various computer simulations. Additionally, in Chapter V, the maximally flat response low pass filter is discussed. Since any reradiation of the harmonic signals generated by the rectification process is a major drawback in the rectenna element design, an effective input low pass filter has to be implemented. This is also the case for the output low pass filter, which is responsible for isolating the dc lines from microwave signals.

The various tests and measurements conducted for both the individual rectenna elements as well as the rectenna array are described in Chapter VI. Several electrical connections were tested to verify the more sufficient for driving the MAV motor. The low efficiency values encountered, are applied to impedance mismatches between the components of the circuit. A maximum efficiency value of 10.3% reached for the rectenna elements and 8.2% for the array. With 18.6 W of transmitted microwave power the RPM value reached from the MAV rotor was 450, which was not adequate for hovering flight.

The results of the research are summarized in Chapter VII where some recommendations for future work are also presented.

II. BACKGROUND

A. WIRELESS POWER TRANSMISSION

Power transmission by radio waves dates back to the work of Heinrich Hertz. He first demonstrated electromagnetic propagation in free space by using a complete system with a spark gap to generate high-frequency power, and detecting it at the receiving end. As part of his experimental program, he generated microwave power at a frequency of 500 MHz, corresponding to a wavelength of 60 cm. At this frequency he was able to construct parabolic reflectors of appropriate dimensions and use these to create a broad beam of microwaves, which was intercepted by another parabolic reflector, and the energy focused upon a receiving element.

Nicola Tesla was another pioneer in WPT. He carried out his experiments on WPT at the turn of the century. By means of the alternating surges of currents running up and down a mast, Tesla hoped to set up oscillations of electrical energy over large areas of the surface of the earth, and to set up standing waves into which he would immerse his receiving antennas at the optimum points.

The next attempt for transferring power using electromagnetic energy was not until 1930 where in an experiment conducted in the Westinghouse Laboratory by H. V. Noble, several hundred Watts of power were transmitted between two identical 100 MHz dipoles, located 25 ft from each other.

However, the real boost in the WPT research was the contribution of William C. Brown, from 1958 up to the late 1990's. He proposed the use of microwaves for WPT, and wrote the first published article that explored the possibilities in 1961. Then, in 1964, under an Air Force contract, he demonstrated a microwave-powered helicopter that received all the power needed for flight from a microwave beam, on a national TV news broadcast.

After the initial research on wireless power transmission, much of the subsequent work was focused on space applications. The first large project funded mainly by NASA was the Solar Power Satellite (SPS) project, during which the feasibility of transferring power collected in space from the sun to the earth using microwaves, was investigated

thoroughly. As has been proposed by Brown, gigawatts of power could be possibly collected from the sun in geostationary orbit and then be transferred to the earth in the form of microwave energy. Brown also proposed a method of combining the new (at that time) electric thruster technology with the microwave power transportation. Specifically he suggested that microwave beam power would be the ideal solution, both in cost and weight, for the high prime power requirement of an electric thruster.

SPS and related technologies had also been investigated by Japan's Institute of Space and Aeronautical Science (ISAS) for a long period of time. In 1992, a microwave powered model aeroplane was flown in verification experiment of a phased array transmitter [Ref. 18]. Further experiments consisted of investigation of the interaction of the microwave power with the ionosphere using a sounding rocket in 1993, as well as studying the feasibility and efficiency of transmitting and collecting microwave power in space.

Recently microwave power has been used for powering smart membrane systems, in applications where ultra-light weight structures are necessary, such as the shape control of inflatable membrane space antennas, smart wing concept of future aircrafts, unmanned autonomous aircraft vehicles (UAV), and satellite robot arms [Ref. 1]. Introduction of a microwave-driven membrane system based in microwave power transmission eliminates the need for complex wiring and gate switching. Thus, the total weight and fabrication cost of the system is greatly reduced.

B. THE WPT PROCESS

A complete microwave power transmission system is defined as a three step process in which: (1) dc power at the input of the system is converted into microwave power, (2) the microwave power is spread out over a transmitting aperture (antenna), the beam formed and directed at the receiver, and (3) microwave power is captured from the beam and converted back into dc power at the receiving location. The efficiency of the system is then defined as the ratio of the dc power output to the microwave power input [Ref. 2].

1. Transmission

The major reason for the lack of serious interest in WPT during the first years of the 20th century was that knowledgeable people realized that efficient point-to-point

transmission of power depended upon concentrating the electromagnetic energy into a narrow beam. The only practical manner in which this could be done would be to use electromagnetic energy of very short wavelengths and to use optical reflectors or lenses of practical dimensions.

Devices capable of generating microwave power which could allow successful energy transfer from one point to another, were not available until the late 1930's. The first of these was the velocity-modulated beam tube, first described by O. Heil and with certain modifications now is widely known as the klystron [Ref. 2]. The second device, perhaps even more important than the klystron, was the cavity magnetron developed first in Great Britain and then in the USA during WW II. Another device that potentially could be a good transmitter for WPT, was the beam crossed field amplifier, known as amplitron, which under further development could produce hundreds of kilowatts of continuous wave power. The amplitron exhibited many more advantages than any previous high power tubes. Its efficiency was greater than 70% and was capable of generating a broad range of microwave frequencies, combining good phase linearity with low phase pushing. Therefore, it was greatly attractive for high power applications of a sophisticated nature [Ref. 3].

In a beamed microwave power transmission system dc power must be converted to microwave power at the transmitting end of the system. Although many devices can perform this function, it was discovered during the comprehensive DOE/NASA study of the Solar Power Satellite (SPS) program that the microwave oven magnetron with the addition of a ferrite circulator, could perform as a phase-locked, high gain (30 dB) amplifier. The directional amplifier combined with a 64-slot slotted waveguide array to form a 600 W radiating module as shown in Figure 1 [Ref. 2].

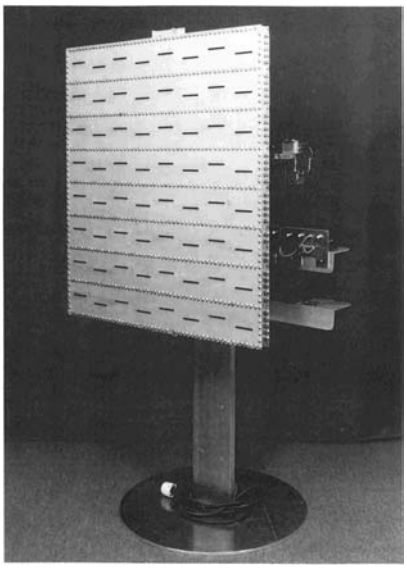

Figure 1. Radiating module composed of a slotted waveguide antenna and a phase-locked, magnetron directional amplifier [From Ref. 2].

2. Rectification

The conversion of microwave power into dc power is the reverse of the microwave power generation process. However, the development of microwave rectifier received relatively little attention, contrary to the microwave generator, for which much research was devoted for a long period of time. In fact, the development of the microwave rectifier was not deemed necessary until application of wireless power transportation stimulated interest in it.

Early experiments in rectifying microwave power focused mainly in running a heat engine. However, even after solution of the many mechanical problems, the overall efficiency was at most 30%.

The first rectifying device was proposed and constructed by W. C. Brown at the Raytheon Spencer Laboratory and Roscoe George at Purdue University in the early 1960's. Brown used thermionic diode rectifiers, whose individual conversion efficiencies were slightly less than 50%. A thermionic diode was an acceptable rectifier with a relatively easy mechanical construction and good efficiency, but its use was limited to frequencies up to 2700 MHz.

George used two point-contact semiconductor diodes in a bridge configuration that had individual conversion efficiencies close to 70%. Tests were performed in an

expanded waveguide arrangement with paraffin liquid to perform as a cooler for the diodes. However, these diodes could not handle high levels of microwave power. Only connecting large numbers of these diodes in series allowed high power rectification. An array of 680 such diodes in series produced 40 W with conversion efficiency close to 50% [Ref. 3].

The first successful experiments in rectifying microwave power motivated the US Air Force to sign contracts for a high altitude platform powered solely by microwave power. Since the proposed platform was a helicopter, a very lightweight rectifier system had to be constructed. Thus, in 1963 the first rectenna (rectifier antenna) was designed and built by W. Brown, to serve as power source for the helicopter [Refs. 4, 5]. As a practical need, the construction was such that the rectenna exhibited no directivity in order to compensate with pointing inaccuracies of the transmitting antenna. Also, since from previous research the low power handling capability of the silicon point contact diodes had been realized, it was recognized that the only feasible use of them was in a bridge configuration rectifier element. The final design was an array consisting of half-wave dipoles spaced a half wave length from each other and a quarter wavelength from a grid reflector. The total efficiency of the rectenna was 50%, and approximately 280 Watts of dc power could be produced. A total of 4480 diodes were used in a two foot square array which had a specific weight of eight pounds per kilowatt. Provision had also been taken for the impedance matching between the diodes and the free space, in order to minimize the reflections. A plane of parallel rods was placed in front of the plane of the diodes with an adjusting capability, solving at the same time both the impedance matching problem as well as the mechanical support problem. This rectenna is illustrated in Figure 2.

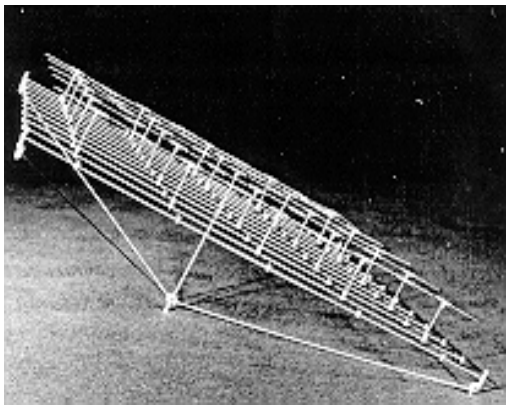

Figure 2. The rectenna constructed by Brown for the microwave-powered helicopter. [from ref. 5]

As the requirement for higher conversion efficiency increased, it was apparent that a more accurate analytical approach was imperative for both, the rectifier element as an entity, as well as for the combination of the rectifying elements in a rectenna array.

In 1975 a computer model for the rectenna element was created by Nahas [Ref. 6]. In this model, each rectifying element consisted of a halfwave dipole, rectifier diode, input low pass filter, output low pass filter, and resistive load, as illustrated in Figure 3.

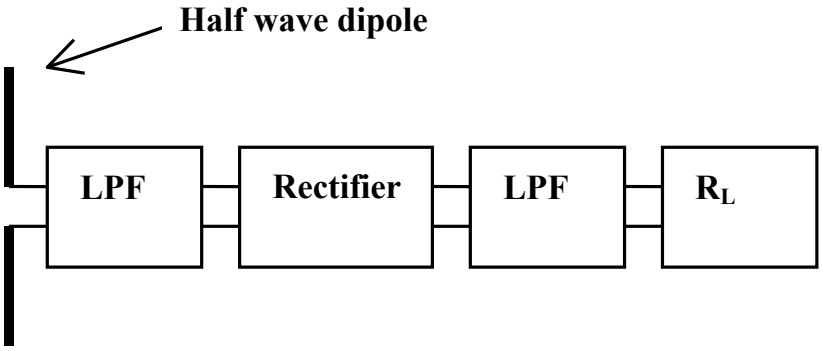

Figure 3. Typical rectenna element.

The input filter was a five section stepped impedance low pass filter with cutoff frequency slightly above the transmission frequency. Thus the harmonic frequencies created by the rectification process were not allowed to reradiate from the dipole to free space. The rectifier was a simple Schottky barrier diode and the output filter was a capacitor which was used to short the microwave energy before the dc line, thus not

allowing the R/F signal to reach the resistive load. The rectenna elements were interconnected in a combination of series and parallel connection, as shown in Figure 4, to reach the desired power limit. The model was computer simulated and the results showed a potential efficiency up to 70%. The simulation also verified that the most important factor for the power losses was the diode series resistance, provided that there were no mismatches between the circuit components.

The first computer model for rectenna elements was followed by another model which computed the interaction of the elements when combined in an array. According to this model which was developed in 1979 by Gutmann and Borego [Ref. 7] the total power produced by an array of identical rectifying elements was less than the sum of the power produced by the individual elements if they operated independently. This is due to the fact that even though the rectifying elements are identical, they do not operate at the exactly the same power levels when receiving a microwave signal. Therefore, since in a rectenna array configuration all the individual elements share the same resistive load, significant power differences are produced due to different power levels of the elements. This difference cannot be neglected especially in very large arrays.

The same computer model also predicted that there is almost the same power degradation in a rectenna independently of the way in which the elements are connected, (in series or in parallel). Additionally, as far as the diode was concerned, the model predicted that in order for the losses to be minimized, a diode with a small forward voltage drop and small series resistance should be used.

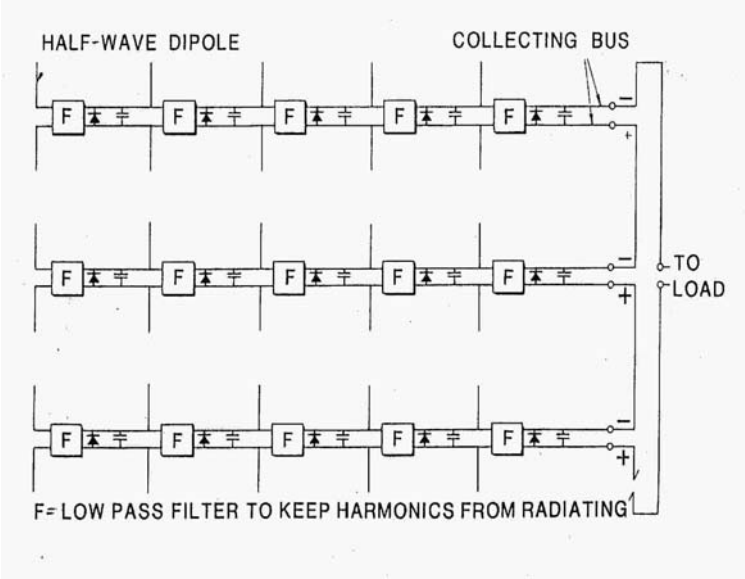

Figure 4. Schematic showing the interconnections between the rectenna elements [From Ref. 8].

In most of the rectenna applications mentioned so far, silicon (Si) Schottky diodes were used. However, gallium arsenide (GaAs) diodes which appeared on the market were considered more appropriate for rectenna applications, since they exhibited conversion efficiencies on the order of 75%. Also their "flip-chip" construction allowed operation at higher operating temperatures than the Si Schottky diodes [Ref. 8]. A drawback in their operation however, was the relatively high value of forward voltage drop, approximately 0.9 Volts.

By the middle seventies the solar power satellite project (SPS) became an important topic as an alternative energy production. Thus, the need for a large scale demonstration of wireless power transmission was imperative. It should be mentioned that with the exception of the microwave power helicopter demonstration by Brown in 1964, only small scale laboratory experiments had been conducted since.

In the summer of 1975 at the JPL Goldstone facility in Mojave Desert California, under the combined efforts of Raytheon Co. and NASA, a large array was constructed for a large scale WPT demonstration [Ref. 9]. The array was mounted approximately half way up a 30 m tower at a distance of 1.54 km from a 26 m parabolic dish reflector. The dish antenna was fed by a 450KW CW power klystron tube. Due to the construction

restrictions, the power impinged on the rectenna array was only 11.3% of the transmitter power. The resistive load which was a combination of bulbs could be varied for efficiency versus load calculations. During the experiments over 30 KW of dc power were transferred with a maximum efficiency of 84%. An important observation was that when the central sub-array was tilted up to an angle of 40°, the total power output of the array remained the same. This was due to the fact that even though there were local areas of enhanced and diminished RF power density of -15% to +10% as a result of a tilted central array, almost all the power scattered from the tilted array was absorbed by neighboring sub-array elements. Another result of great importance was the realization that the forward voltage drop of the diode directly affects the diode's efficiency curve. At low power levels, especially, the diode should have as low a voltage drop as possible for maximum power efficiency. For this reason the gallium arsenide-platinum GaAs-Pt diodes, which exhibited forward voltage drop of 0.9 V, were changed to gallium arsenide-tungsten (GaAs-W) with forward voltage drop of 0.7 V. The efficiency of GaAs-W diodes, is better than this of GaAs-Pt diodes at both low and high power levels.

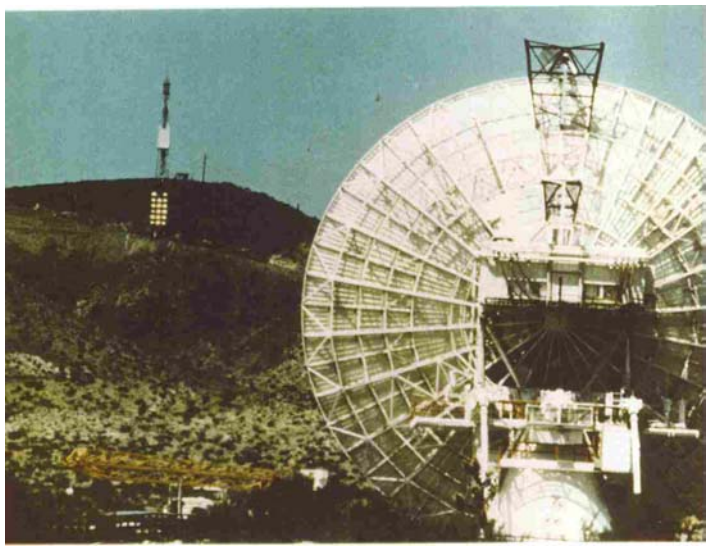

Figure 5. Demonstration of beamed power over one mile distance, at the JPL Goldstone facility in the Mojave desert [From Ref. 9].

Although not extremely high, the weight of any rectenna element in a bar type configuration, was still unacceptable for applications such as microwave powered flight platforms. Thus, a new design approach was introduced by Brown in order to meet the

weight requirements. The new format rectenna was fabricated of a laminated material consisting of a thin film dielectric substrate of suitable electrical and mechanical properties, bonded between two thin sheets of one ounce copper (1.4 mil thick). From a circuit point of view the rectenna resembled the bar type rectennas, retaining the dipole configuration with a single diode and low pass filters placed before and after the diode. However, the efficiency of the rectenna was on the order of 72%, mainly due to losses on the adhesive material used to bond the copper with the thin Mylar film, and also due to losses in the Mylar film itself. The efficiency was greatly improved and reached 85% when the Mylar substrate was substituted with a less lossy Kapton F film. In this case the Teflon used as the copper bonding adhesive, exhibited a low loss tangent at the microwave frequencies of interest. Nevertheless, the mass to weight ratio of this rectenna was extremely good, since each of the elements weighted only 0.2 grams. Considering the power capability of the rectenna this could be translated into a power output to weight ratio of 2.5 kilowatts per kilogram [Refs. 10, 11].

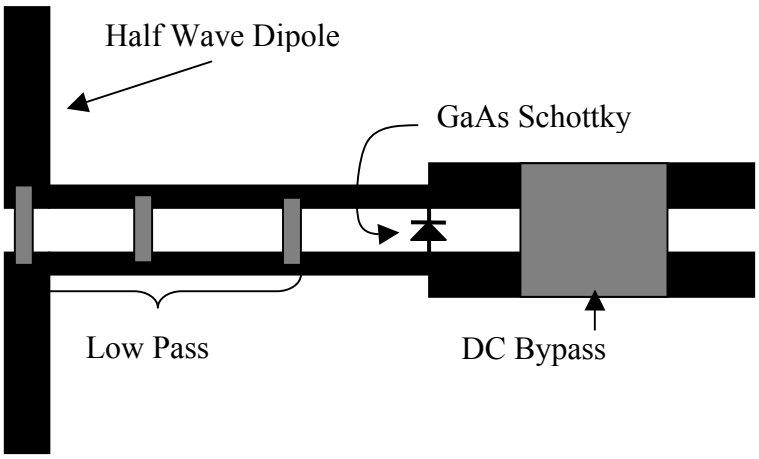

Figure 6. The first thin film Rectenna element printed on mylar and Kapton F substrate [From Ref. 8].

Soon the new design method revealed more advantages. Two identical rectenna foreplanes could be placed one on top of the other in a 90° rotated configuration. In this way dual polarization could be achieved. This approach was followed by a team from Communications research center of Canada in the designing of a rectenna for a high altitude platform application [Ref. 12]. The dual polarized rectenna was developed to

remove the limitations of previous rectennas when used in moving platform applications. Specifically when linear dipoles were used in a single foreplane array, the power beam had to be adjusted every time in order to stay aligned with the linear polarized dipoles. This could be only achieved with some kind of polarization tracking circuitry, a costly and complicated procedure. In the new design, each one of the two foreplanes was collecting power to its corresponding polarization. Thus, both circularly and linearly polarized waves could be used for power transmission.

By the early 90's the interest for the SPS program was almost diminished due to increasing environmental considerations related to the use of the microwave energy. However, another aspect of possible use of WPT had been aroused. This was the feasibility of remote powering actuators in space using microwave power. Thus, in order for the first WPT experiment in space to be conducted, a rectenna built in Texas A&M University, was tested in space. This dual polarized rectenna consisted by two foreplanes of thin film printed dipoles. There were two innovations adopted in the design. The first was the position of the dc capacitor, which acted as low pass filter, after the diode. It was found that placing the capacitor a quarter wavelength away from the diode, the odd harmonics generated from the rectification process appeared at infinite impedance to the diode, where the even harmonics appeared at zero impedance. This way the rectenna dissipated no power through harmonic frequencies and the efficiency was basically a function of diode losses [Refs. 8, 13]. The second innovation in Texas A&M rectenna was the adaptation of a Frequency Selective Surface (FSS), which totally suppressed harmonics created from the rectification process. Since the power operating level of a rectenna is over 30 dB, some of the harmonics could appear at relatively high power levels (-10, -20 dB) even after being filtered out by the input low pass filters. This was highly undesirable, especially in a satellite space environment, where the aforementioned harmonic signals could interfere with mobile and satellite communication links [Ref. 14]. The Texas A&M rectenna used at the Microwave Energy Transmission in Space (METS) experiment is illustrated in Figure 7.

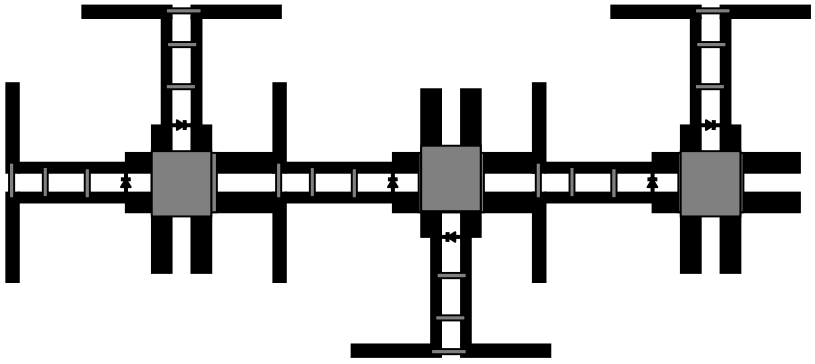

Figure 7. Schematic layout of the Texas A&M university rectenna used in METS experiment [From Ref. 8].

It should be mentioned that until that time almost every rectenna design was implemented at the frequency of 2.45 GHz. Three factors favored the use of 2.45 GHz frequency. The first is the fact that the 2.45 GHz band is one of the allocated ISM (Industrial, Scientific, and Medical) bands. The second is the relatively small atmospheric attenuation of the RF energy in this region of the electromagnetic spectrum. The third reason is the simplicity of manufacturing microwave transmission lines and antennas at the frequency of 2.45 GHz, still retaining at the same time small circuits, absolutely necessary especially in cases where the real estate is limited.

During the last decade of the 20th century, as the need for space applications was increasing, the use of smaller wavelengths in rectenna technology was imperative. Following this need, and in conjunction with the growing literature on patch antenna design, rectenna designers deviated from the traditional dipole rectenna construction [Refs. 15, 16, 17]. In the design by a team from JPL, California Institute of Technology, patch antenna techniques were extensively applied, and the result was a dual polarized rectenna at 8.51 GHz, capable of generating 50 Volts for powering space telescope actuators. Each of the rectangular patches in the rectenna was fed by two slots with 90° difference oriented. The low pass input filters were formed by transmission line lengths residing on the opposite side from the patch, and the diode was connected to the ground

plane through a hole. Chip capacitors were used for shorting the RF energy before the dc lines. In this configuration the antenna and the microstrip feed circuit were isolated from one another. Also, since the diode was placed behind the ground plane, the harmonics generated by the rectification process are not reradiated back to the microstrip patch [Ref. 18]. The JPL patch antenna is illustrated in Figure 8.

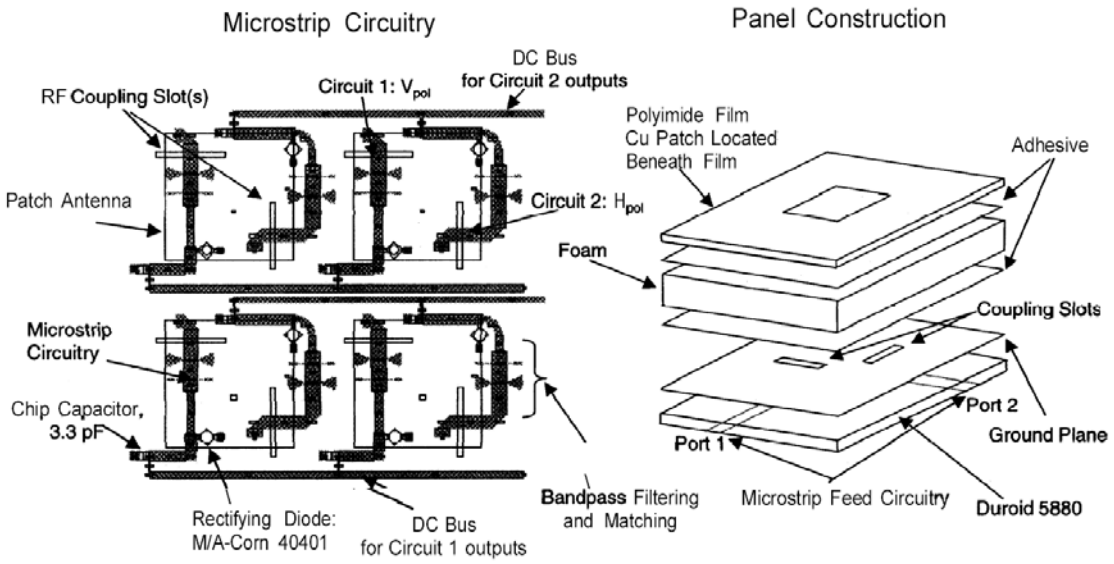

Figure 8. Patch dual polarized rectenna manufactured by a JPL team [From Ref. 18].

Since it was realized that the efficiency was directly dependent on harmonic radiation, various techniques for reducing the undesirable effect of harmonics were investigated. One potential solution to this problem was the adaptation of circular patch instead of the rectangular patch. The use of a circular patch as an antenna element greatly reduced the harmonic generation due to the inherent property of the circular patch to resonate at frequencies that correspond to roots of the Bessel functions, and not to the harmonics. This type of rectenna proposed by a Japanese team for powering a space robot [Refs. 19, 20]. The rectenna which illustrated in Figure 9, consisted of circular patch elements fed by a probe, and a rectifier circuit placed behind the ground plane. The harmonic suppression using the circular patch and a maximally flat response low pass filter combination was on the order of -50 dB. The conversion efficiency of the rectenna was approximately 76%. The same study also proposed a conformal rectenna consisting

of the individual elements described previously, placed in a cylindrical form which conceptually was the body of the space robot. The elements were arranged in line on the cylinder's surface in the azimuth (φ) direction. The number of elements, the inter-element spacing, as well as the cylinder radius, was changed for optimum efficiency.

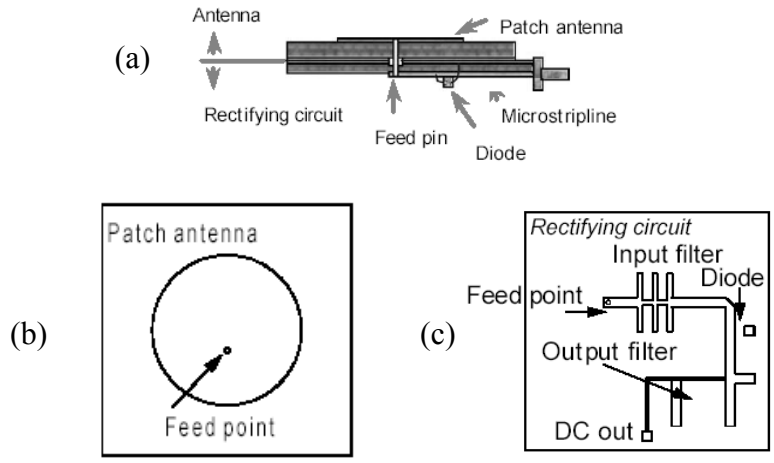

Figure 9. C band circular patch rectenna element. (a) Side view of the rectenna element. (b) Circular patch antenna. (c) Rectifier circuit [From Ref. 19].

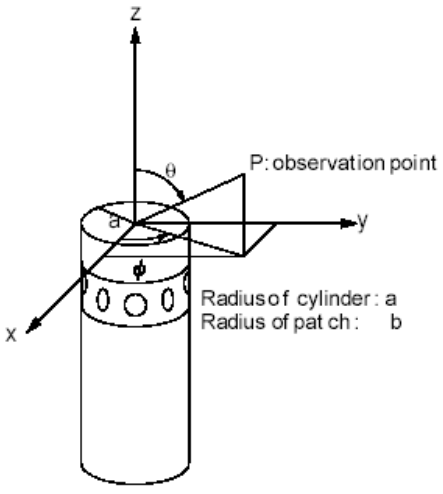

Figure 10. Schematic of the conformal rectenna array proposed in [Ref. 19].

C. MICROWAVE POWERED AIR VEHICLES

As mentioned previously, the use of microwaves for powering air platforms was a very attractive solution to the inherent power limitations of the flight vehicles. A microwave powered vehicle could potentially stay aloft for days or even weeks, since its power source is theoretically undepleted. Furthermore, the adaptation of microwaves as a power source would enhance the payload capabilities of the vehicle, by the means of using the fuel storage space, which now would be available for extra payload.

The first microwave powered air vehicle was the small helicopter manufactured by W. Brown and flown on October 28 1964. It consisted of a six foot diameter rotor, driven by a motor adapted from an ordinary electric drill. A special gearbox employing ball-bearing construction was used to reduce the high shaft speed of the motor to 400 rpm. The rotor power for helicopter takeoff was 0.105 horsepower and the net weight was 5.25 lbs. At the saturation level, the vehicle could support the antenna, the rectifier system plus a payload of 1.5 lbs.

The microwave powered helicopter, shown in Figures 11 and 12, was tethered with a special three wire system above a 9.5 foot parabolic reflector antenna fed by a five kilowatt magnetron oscillator. During the demonstration, the helicopter took off from its support which was located twenty-five feet from the transmitting antenna and climbed to an altitude of fifty feet. In order for an objective of the U. S. Air Force's contract to be fulfilled, the helicopter stayed aloft for a continuous period of 10 hours, without any observable deterioration in its performance.



Figure 11. The microwave powered helicopter built by W. C. Brown in 1964 [From Ref. 5].

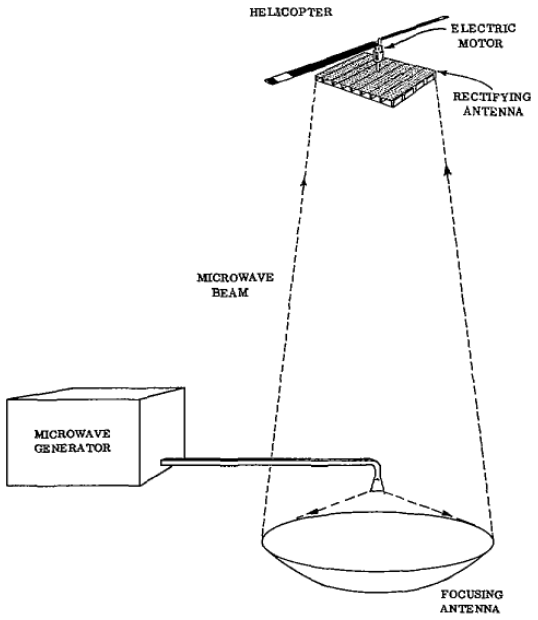

Figure 12. The basic elements microwave powered helicopter system. [From Ref. 5].

Following the success of the tethered version of the microwave powered helicopter, a beam riding model was developed, (Figure 13), motivated by the realization that as long as the helicopter remained a tethered device, its performance was greatly degraded, and its use was limited to experimental demonstrations. In the new design, an unmodulated microwave beam was used as a reference for the stability and position of the helicopter. Since any helicopter has six degrees of freedom, (three in translation and three in rotation), the microwave beam could be used to provide five of these degrees of freedom. The last degree of freedom which could not be beam referenced, was the altitude of the vehicle.

The reference for horizontal displacement was the beam intensity which drops off in a radial direction from the beam center. The phase front of the beam was used for establishing information about the roll and pitch, whereas the polarization of the beam was used for the displacement in yaw [Ref. 3].

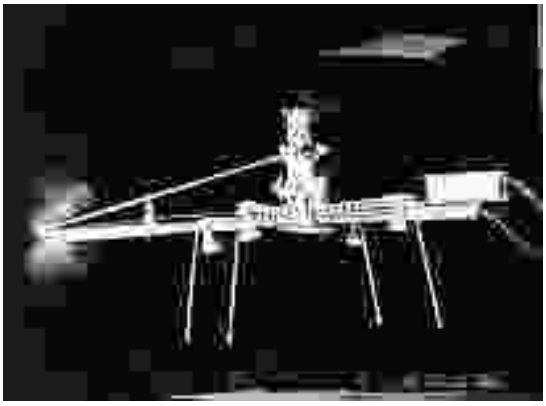

Figure 13. Beam riding microwave power helicopter [from ref. 3].

The next proposed microwave air vehicle was another one by W. Brown, [Refs. 21, 22], in a contract funded by NASA and the Canadian communications research center. It was a streamlined dirigible-shape vehicle, designed to fly at 55,000 ft in order to minimize drag. The airship provided lift by itself, but a large amount of power was required for propulsion purposes. An estimate of the power requirements was about 100 kilowatts of dc power, in order to counteract the drag of the vehicle at higher altitudes. As a result of the relatively simple construction of the airship, the total cost of the system was less by order of magnitude from any other system intended to perform the same mission. However, although promising, the airship never was implemented by NASA, mainly due to environmental considerations related with the use of microwave energy in an uncontrolled space.

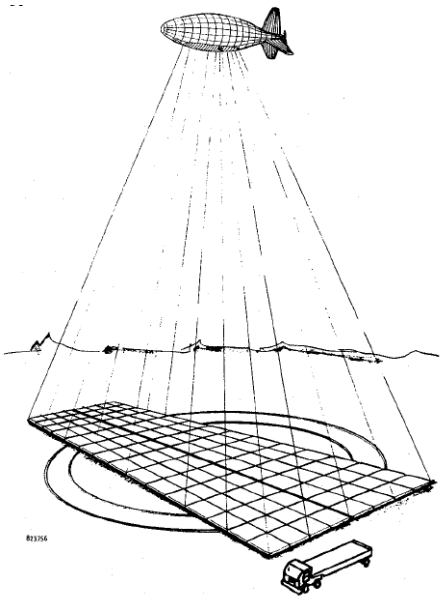

Figure 14. Artist's sketch for a microwave powered airship designed to fly at 70 kft [From Ref. 22].

The Canadian approach for the same project was a microwave power airplane known as the Stationary High Altitude Relay (SHARP) program. The platform was a lightweight airplane designed to fly a circular path at an altitude of 21 km. As illustrated in Figure 15, microwave power would be transmitted from a large array of antennas on the ground, about 85 meters in diameter, to the aircraft where the energy was focused to a spot area with a half power diameter of 30 meters [Ref. 12]. A thin film rectenna would be mounted underneath the airplane covering a 100 m^2 surface. In this configuration 35 kilowatts of power would be delivered, of which 25 kilowatts was used for SHARP's electric motor for propulsion and the remainder for the payload electronics.

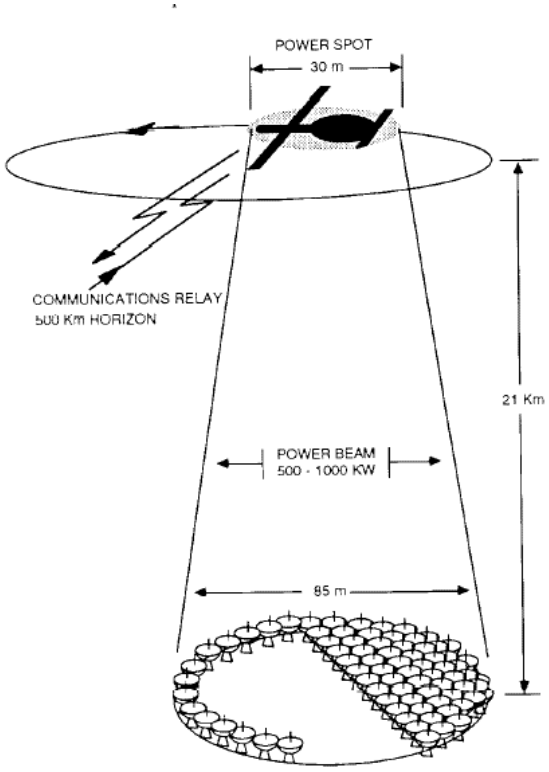

Figure 15. Configuration of the SHARP system [From Ref. 12].

For testing purposes a 1/8 scale model of the SHARP was built and flown for a 20 minute period, on September, 17 1987, (Figure 16). The 4.5 m wingspan remotely controlled airplane was the first microwave powered airplane which was ever flown. It was launched from the hand of a runner as an ordinary glider model, and climbed to an altitude of 150 m using power from an internal battery. At a predetermined point the battery switched off and the microwave beam turned on. The beam was continuously steered to track the aircraft, which was constrained to fly inside a 50 degree cone centered to the transmitter, so that the beam incidence remained near broadside. The microwave beam used to power the model airplane, was formed by a 4.5 m diameter parabolic antenna, fed by a two microwave oven magnetrons, which produced 10 kilowatts of power at 2.45 GHz. The rectenna was mounted in the wing of the airplane as shown in Figure 17.

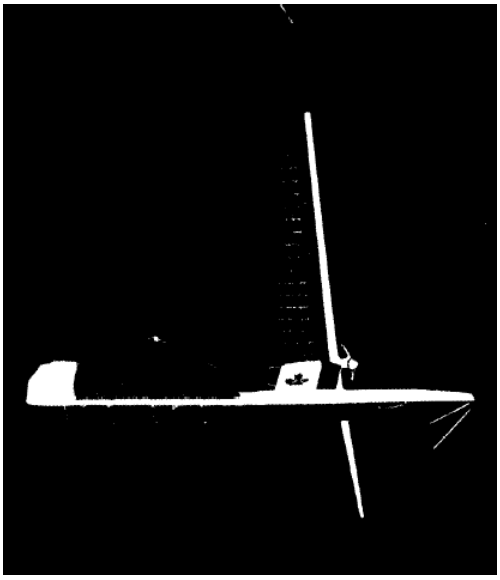

Figure 16. 4.5 m Wingspan microwave powered airplane [From Ref. 12].

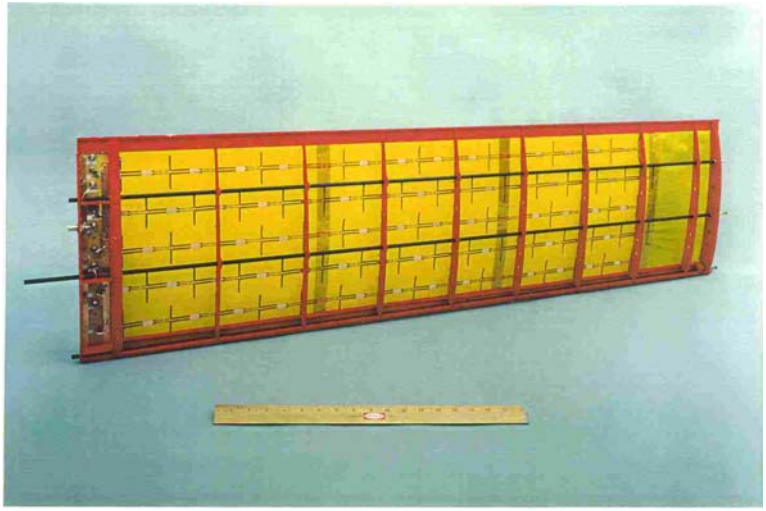

Figure 17. The wing of the 1/8 model of the SHARP airplane with the thin film rectenna mounted [From Ref. 23].

The most recent of microwave powered vehicle was a small airplane, built by ISAS, Japan, [Ref. 8]. The microwave airplane was flown in 1992 to verify a solid-state phased array transmitter. This flight was a part of a series of small demonstrations of WPT technology in Japan.

D. MICRO AIR VEHICLES (MAV)

During the early 90's several studies were done on air vehicles smaller than any previous designs, as a consequence of the radical evolvement of microelectronics, micromechanics and related technologies. These studies were mainly an integration of RAND Corporation's investigation of microsystems and MIT Lincoln Laboratory's early investigations of micro flyers. More recently, in 1995, the Defense Advanced Research Projects Agency (DARPA) defined the various micro air vehicle parameters, in a workshop on Micro Air Vehicle feasibility. According to DARPA, MAVs should be thought of as aerial robots, as six-degree-of-freedom machines whose mobility can deploy a useful micro payload to a remote or otherwise hazardous location where it may perform any of a variety of missions, including reconnaissance and surveillance, targeting, tagging and bio-chemical sensing [Refs. 24, 25, 26]. A typical MAV should be capable of staying aloft for 20 up to 60 minutes, traveling at a distance 10 km from the ground station, at the same time weighting 50 grams at the maximum. Also, according to DARPA's definition, a vehicle is classified as a micro air vehicle, when it is less than 6 inches (or 15 cm) in any dimension.

Although arbitrary, the 6 inch limitation is relatively consistent with both today's technology considerations, as well as future mission requirements. MAVs should be small enough to accomplish missions that traditional vehicles are incapable of, but also their technological requirements should be realizable with the existing technology. A very useful parameter in order to appreciate the scale implications of MAVs is the Reynolds number. The Reynolds number is an aerodynamic scaling function directly related to the size and speed of the vehicle, which characterize the flight environment. Specifically, it can be expressed as the ratio of the inertia force to the viscus force. Figure 18 illustrates a plot of the Reynolds number versus gross weight of the vehicle. In the same plot is also a comparison of the MAV size with the size of other vehicles.

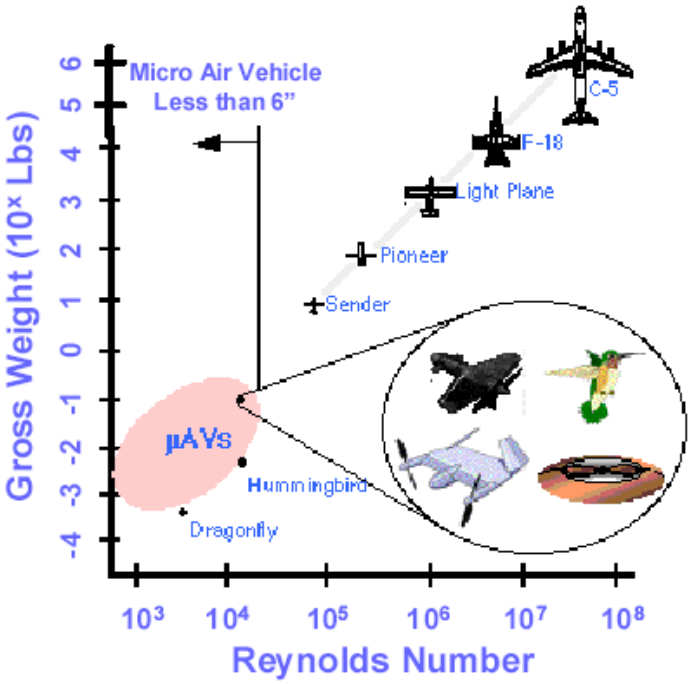

Figure 18. Illustration of the Reynolds's number versus gross weight of various vehicles [From Ref. 24].

As shown in Figure 18, AVs operate at low Reynolds Number (20,000 to 1,000,000) over their entire flight envelope. The airflow over airfoils in this regime is highly complicated due to unsteady aerodynamic phenomena, such as hysteresis stall due to laminar separation bubbles, and is very difficult to model using conventional aerodynamics [Ref. 27]. Therefore, in order to optimize MAVs performance, aerodynamic studies have been focused on insect aerodynamics, since MAVs belong to the flight regime traditionally occupied by very small birds and insects.

Although there is a rich literature related to MAV missions and applications, the MAVs needed to meet these requirements are yet to be implemented. Problems related to microsystems' integration in the limited volume and weight of a MAV has to be overcome. Previous studies [Ref. 28] have revealed that approximately 90% of the available power on a MAV is consumed for flight and control functions, whereas only 10% is available for payload needs. This is primarily due to the inefficiency of the batteries currently in use for electric powered MAV, and to the limited amount of fuel

aboard for an internal combustion engine MAV. The latter does not meet the requirements for low acoustic signature which is imperative in many various MAV applications.

As mentioned previously the idea of powering flying vehicles using microwaves is very attractive and gives a new perspective to the traditional propulsion methods. However, the power limitations of large platforms would require a very large amount of microwave power to be transmitted even if high conversion efficiency was achieved. On the other hand the doctrine of high altitude communication platforms is not valid any more, especially after the evolution of satellites.

Still, the idea of powering micro air vehicles using microwaves seems very promising. Indeed in the case of micro air vehicles a considerable small amount of power would be necessary since the total power requirements of such a vehicle are about 5-10 Watts. Moreover MAVs are not indented to fly long distances or at high altitudes, and therefore the atmospheric attenuation of the powering beam is not severe. Apparently there are two big advantages of the microwave powered MAV. The first one is related to the reduced volume occupied by the power source. This means that the available payload can increase significantly. To argue that the available payload is increased by a magnitude of three is a conservative approach. The second advantage is that a microwave powered MAV could stay aloft for a very large amount of time, at least as much as allowed by the mechanical limitations of the vehicle.

At this time there is no micro air vehicle capable of sustained flight when powered solely by microwaves. Previous studies from B. Vitale [Ref. 29], at Naval Postgraduate School, showed the feasibility of the concept. Vitale proposed a cylindrical type dipole antenna that could potentially be the body of a micro air vehicle and could collect microwave power from a CW radar station. The rectifier was placed away from the antenna inside the vehicle, and consisted of a single diode. However, the power handling capabilities of a single diode is way below the power needs of a MAV.

E. SUMMARY

In this chapter a thorough historical background of Wireless Power Transmission has been presented. Special emphasis has been given to the rectifying antenna (rectenna)

technology as it has evolved over the last 40 years. The shift from bar type rectennas to the printed circuit elements was a result of the need for more compact and lightweight designs.

The major laboratory experiments and airborne platforms powered by microwave power were presented. Key factors in all of these applications are the weight of the design, and achieving a high conversion efficiency.

This chapter also presented the general considerations of micro air vehicles. These new era airborne platforms exhibit unique characteristics and potentially could undertake missions which no existing airborne vehicle can accomplish. Being categorized according to the aerodynamic scale parameter Reynolds number, MAVs belong to the same group as small birds and insects.

The idea of powering micro air vehicles using microwaves appears very attractive, not only because by doing so, the need of a power source onboard is eliminated, but also due to the fact that the endurance of the vehicle could be maximized, and converge with the operational life of the vehicle.

III. RECTIFIED DIODE CHARACTERIZATION

A. INTRODUCTION

The diode is the most important element of the rectenna with regard to efficiency. It was known from earlier work, [Refs. 3, 30], that the following factors enter into the efficiency of rectification of microwave power:

- Recovery time of the diodes.
- Forward resistance of the diodes, which depends on two factors:
  - Spreading or bulk resistance of the semiconductor, which is proportional to the thickness of the material.
  - Barrier resistance as a function of current.
- Reverse resistance of the barrier layer.
- Barrier capacitance and how it varies with back voltage.

The recovery time of the diodes in microwave power rectification has been found experimentally by George that should be less than a quarter cycle of the frequency to be rectified. For example at 2.45 GHz, the recovery time should be less than 0.01 ns, whereas at 10 GHz should be less than 25 ps.

B. THE SCHOTTKY BARRIER DIODE

1. Description

Amongst the various types of diodes currently on the market, the Schottky-barrier diodes (SBD) are considered more appealing due to their high switching capability. This type of diode is formed by bringing metal into contact with a moderate doped n-type semiconductor material, [Ref. 31]. The resulting metal-semiconductor junction behaves like a diode, conducting current from metal anode to the semiconductor cathode. Basically, the current-voltage characteristic of the SBD is very similar to that of pn-junction diode, with two important exceptions [Ref. 32].

(1) In the SBD, current is conducted only by majority carriers – electrons in this case. As a result the minority-carrier charge-storage effect does not appear in the SBD. This has a direct effect in the switching capability of the diode, and in fact a typical SBD can switch from on to off much faster than any pn-junction diode.

(2) The forward voltage drop on a conducting Silicon SBD is typically around 0.3-0.5 V, whereas the forward voltage drop for a pn-junction diode is 0.6-0.8 V. However, gallium arsenide GaAs SBDs, exhibit forward voltage drops of about 0.7 V.

2. Schottky Barrier Diode Characteristics

Schottky barrier diodes [Refs. 33, 34, 35] have evolved into many designs, which can be reduced to two basic categories. The first of those formed on n-type silicon, are characterized by relatively high barrier heights and low values of series resistance, and therefore, are ideal for mixer applications and detectors where dc bias is available. The second type are formed on p-type silicon, and are distinguished by low barrier height, high I_S and high R_S. These diodes were developed for square law detector applications where load resistance is high and dc bias is not available. Since the power level required for a rectenna is generally high (over 30 dB), both types of diodes are considered capable for this application.

Stripped of its package, a Schottky barrier diode chip consists of a metal-semiconductor barrier formed by deposition of a metal layer on a semiconductor. The most common of several different types, the passivated diode, is shown in Figure 19, along with its equivalent circuit.

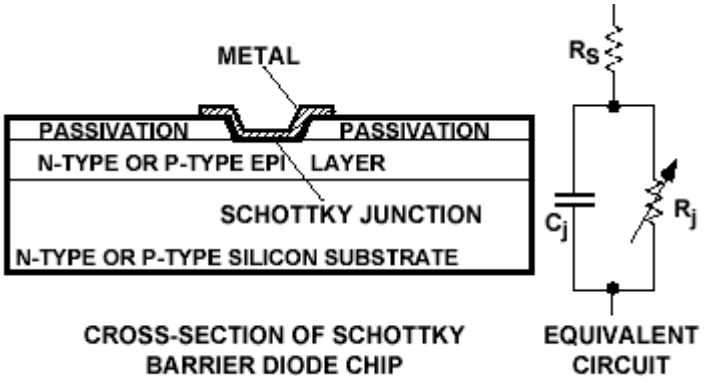

Figure 19. Schematic of passivated type SBD together with its equivalent circuit [From Ref. 36].

The resistance R_S is the parasitic series resistance of the diode, the sum of the bondwire and leadframe resistance, the resistance of the bulk layer of silicon, etc. Electromagnetic energy coupled into R_S is lost as heat – it does not contribute to the rectified output of the diode. Accordingly R_J is the junction resistance of the diode, a

function of the total current flowing through it. For maximum output, all the incoming rf voltage should ideally appear across R_J, with nothing lost in R_S. The equation for junction resistance is

$$R_J = \frac{0.026}{I_T}, \tag{3.1}$$

where

$I_T = I_s + I_b + I_o$, in amperes,

I_s = Diode's saturation current, a function of Schottky barrier height,

I_b = Circulating current generated by the rectification of RF power, and

I_o = External bias current (if any).

The parasitic junction capacitance of the diode, known as C_J, is controlled by the thickness of the epitaxial layer and the diameter of the Schottky contact. The effect of the junction capacitance is to short out the junction resistance, diverting the rf energy into the parasitic series resistance where it does no useful work. However, although at high frequencies and high values of series resistance the junction capacitance has significant effect, experimentally has been found that when the output voltage exceeds 1V, the value of R_j is very small, and the effect of junction capacitance is negligible. Finally L_p is the series inductance and C_p is the shunt capacitance caused by the leads and contacts of the diode package.

3. Forward Voltage Characteristic

A diode is basically a nonlinear resistor, for which a dc V-I characteristic is expressed as

$$I = I_S \left[\exp(\frac{q}{nKT}(V_f - IR_S) - 1 \right], \tag{3.2}$$

where:

q is the charge of the electron 1.602×10^{-19}C,

K is Boltzmann's constant,

T is temperature,

n is the ideality factor of the diode,

IS is the saturation current (10-6 to 10-15 A), and

Vf is the forward voltage of the diode, which is equal to the sum of the total voltage applied on a diode, minus the voltage that dissipated at the parasitic series resistance of the diode RS.

$$V = V_f - IR_S. \tag{3.3}$$

Since I_S is generally very small, Equation (3.2) can be modified to

$$I = I_S\left[\exp\left(\frac{qV}{nKT}\right)\right], \tag{3.4}$$

where also assumed that $V \gg \frac{KT}{q}$. For a diode with an ideality factor n=1 at T=300°K, (3.4) becomes

$$I = I_S(e^{38.69V}). \tag{3.5}$$

It can be seen from the previous equation that the current in the diode becomes zero when *V=0*, approximately equal to $-I_S$ when V is negative, and increases as V takes positive values. The first derivative of (3.4) is evaluated as

$$\frac{dI}{dV} = \frac{qe^{\frac{qV}{nKT}}}{nKT} = G_d = \frac{1}{R_j}, \tag{3.6}$$

where G_d is defined as the dynamic conductance of the diode.

C. HSMS 8101 SCHOTTKY BARRIER DIODE

As known from the basic electromagnetic theory, the antenna dimensions are a function of wavelength and, therefore, frequency of operation. Thus, the relatively high frequency of 10 GHz was selected in the present project, in order to keep the antenna

dimensions as small as possible. Clearly, the diode to be used should be able to operate efficiently at this frequency for best results. The Agillent HSMS 8101 Schottky Barrier diode was selected, due to its unique characteristics

- optimized for use at 10-12 GHz,
- low capacitance,
- low conversion loss,
- low dynamic resistance,
- low cost surface mount plastic package.

This diode is a passivated n-type Schottky diode, and is specifically designed for use at X/Ku bands in down converter and mixer applications. Since it is actually a zero bias detector diode, it requires no bias for high level input power, when it is used for detector applications. Therefore, it is considered adequate for a rectenna application. The electrical characteristics of the HSMS-8101 are listed in Table 1.

Electrical Characteristics of the HSMS-8101 SBD			
Symbol	Parameter	Unit	Value
P_T	Total Power Dissipation	mW	75
P_{IV}	Peak Inverse Voltage	V	4
T_J	Junction Temperature	°C	+150
T_{STG}	Storage Temperature	°C	-65, +150
T_{OP}	Operating Temperature	°C	-65, +150
V_{BR} (I_R 10 μA)	Breakdown Voltage	V	4
C_T V_R=0V, f=1MHz	Total Capacitance	pF	0.26
R_D	Dynamic Resistance	Ω	14
I_S	Saturation Current	A	9×10^{-8}
n	Ideality Factor		1.08
R_S	Parasitic Series Resistance	Ω	4
C_J	Junction Capacitance	pF	0.23
SWR (12 GHz)	Standing Wave Ratio		1.2

Table 1. HSMS 8101 electrical characteristics [From Ref. 36].

The package of the HSMS 8101 is type SOT 23. The obvious advantage of this package type is the Alloy 42 lead frame, which enables the diode to dissipate more power. The package dimensions together with the typical performance of the diode are illustrated in the Figures 20 and 21.

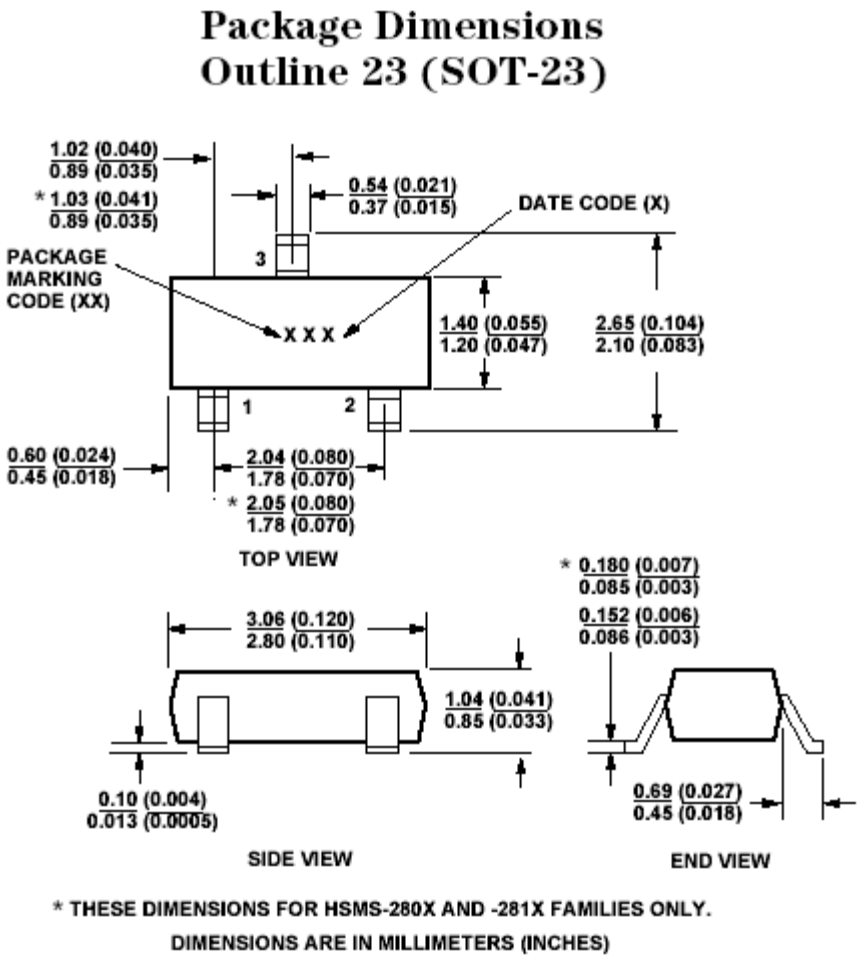

Figure 20. Package dimensions for HSMS 8101 SBD [From Ref. 36].

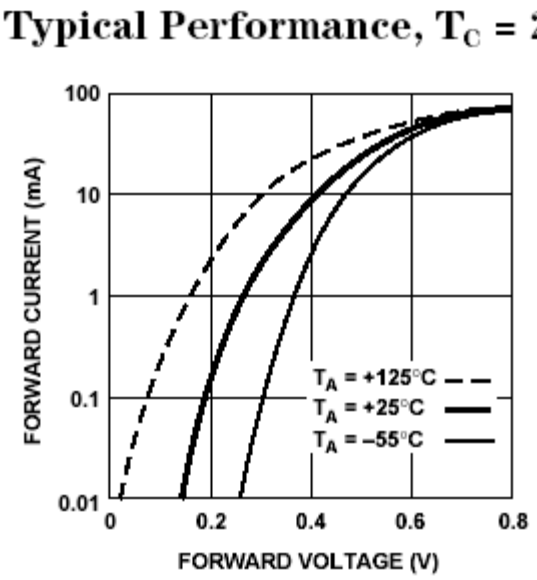

Figure 21. Dc current versus dc voltage curve of the HSMS 8101 SBD for three operational temperatures [From Refs. 35, 36].

As illustrated in Figure 21 the maximum power dissipation of the HSMS 8101 is 75 mW which means that if the power required from a rectenna is 2 Watts then a minimum of 27 diodes are needed, provided that the diodes operate at the upper power limit. For an operation at the 80% of the maximum power dissipation of the diode, approximately 34 diodes are required in order to achieve an output power of 2 Watts.

Some of the diode's electrical characteristics can also be obtained from laboratory measurements. Specifically [Ref. 37] describes a method for obtaining the saturation current I_S, the ideality factor n, and the series resistance of the diode R_S.

Initially the forward voltage V_F of the diode is measured for four values of forward current I_F, I_{F1}=0.010 mA, I_{F2}=100 mA, I_{F3}=4.8 mA and I_{F4}=5.2 mA. For most of the Schottky diodes, the first two points fall on the part of the curve that corresponds to an ideal diode characteristic. Then the ideality factor n of the diode is given by the equation

$$n = \frac{V_{F2} - V_{F1}}{0.0586}. \tag{3.7}$$

Also, the I_S is given by the equation

$$I_S = \frac{0.010}{\exp\left(\frac{V_{F1}}{0.025n}\right)}. \tag{3.8}$$

Similarly, the series resistance R_S is given by

$$R_S = \frac{V_{F3} - V_{F4}}{0.0004}. \tag{3.9}$$

A sample of four diodes was tested in the laboratory in order to verify the manufacturer's data accuracy. The four voltages were measured as V_{F1}= 137mV, V_{F2}=205mV, V_{F3}=353 mV and V_{F4}=355mV. Therefore the values for the three unknown parameters are calculated using (3.7), (3.8) and (3.9) as n=1.16, I_s=8.878×10^{-8}A, R_S=5 Ω.

The measured voltage versus current curve for these diodes is illustrated in Figure 22. As shown in the figure, the barrier voltage of the HSMS 8101 SBD is 0.5715 V. The breakdown voltage is evaluated at 4.1 V when the reverse current is 10 μA. Obviously the values measured in the laboratory are quite close to the manufacturer's value. The only significant deviation was the power dissipation of the diode. Indeed all four diodes could handle up to 1.8 V forward voltage with forward current 140 mA. This translates to a value of 242 mW power dissipation, which is way above the 75 mW maximum power dissipation stated in the manufacturer's data sheet.

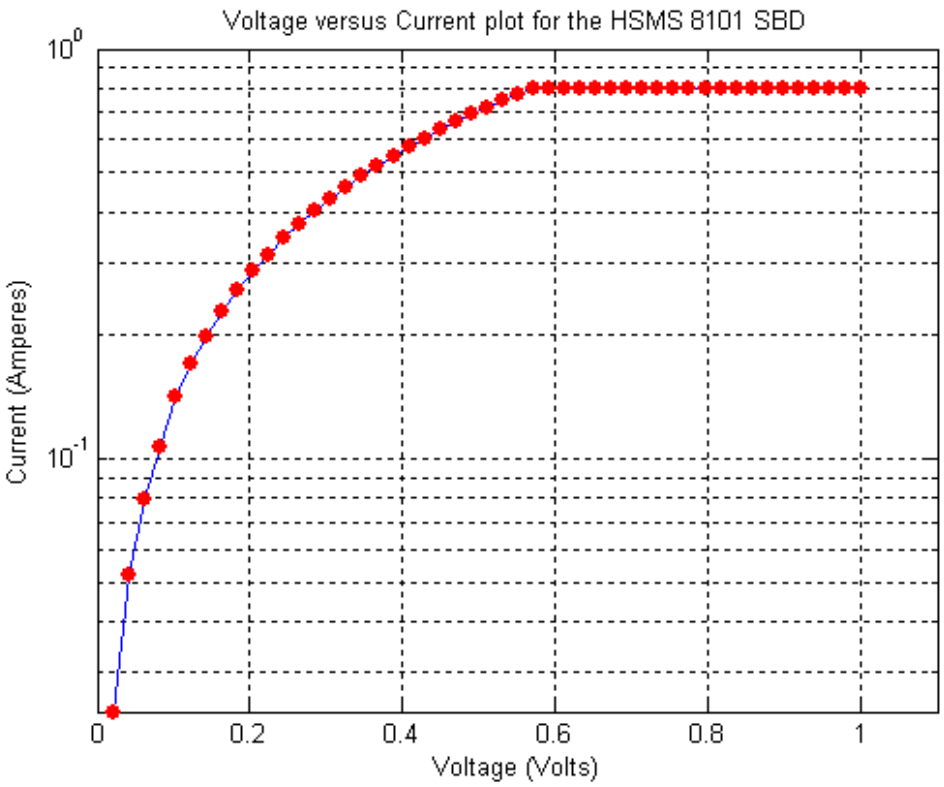

Figure 22. Measured dc voltage versus dc current curve for a sample of four HSMS 8101 diodes.

D. HSMS 8101 DIODE POWER CALCULATIONS

The usual analysis of any diode is based on the study of the truncated power series in which Equation (3.4) can be expanded. However, this analysis is valid only under restrictive conditions and frequently violated in practice. Indeed, Equation (3.4) can be expanded in a Taylor series as long as the power input is low, and the load resistance is considerably high. This condition is not satisfied in a rectenna application where the input power is relatively high and the load resistance is not necessary large. A recent analysis based on Ritz-Galerkin method [Refs. 37, 38] describes the operation of the Schottky barrier diode over the entire range of input power and load resistance, and is not dependent on the truncated power series approximation. In this nonlinear analysis the diode's current is evaluated as zero order Bessel functions and can be expressed by the equation

$$I_o\left(\frac{\Lambda}{n}\sqrt{8R_g P_{inc}}\right) = \left(1+\frac{I_o}{I_s}+\frac{V_o}{R_L I_s}\right)\exp\left\{\left[1+\frac{R_g+R_S}{R_L}\right]\frac{\Lambda}{n}V_o+\frac{\Lambda}{n}R_S I_o\right\} \tag{3.10}$$

where:

I_o = zero order Bessel function,

P_{inc} = incident rf power,

R_g = generator or source impedance,

n = diode ideality factor (emission coefficient),

$\Lambda = q / (kT)$,

q = electronic charge,

k = Boltzmann's constant,

T = temperature in degrees Kelvin,

R_L = output load resistance, and

V_o = output voltage.

In Equation (3.10) the diode package parasitics, the junction capacitance and therefore the operational frequency are not taken into account. [Ref. 37] provides a MATHCAD file for solving (3.10). This file together with the values for n and I_S determined experimentally in the laboratory were used, and the diode's output voltage versus incident power were generated and illustrated in Figure 23.

Analyzing the corresponding plot it can be seen that for an input power of 100 mW a value of 5.5 V output voltage should be expected. Also since the load resistance used for solving (3.10) was 50 Ω, a current of 11 mA should also be measured. This translates to an output power of 60.5 mW. Then, considering that the conversion efficiency can be expressed as the ratio of the output power versus the input power at the diode, the corresponding efficiency for HSMS 8101 SBD can be evaluated as 60.5%.

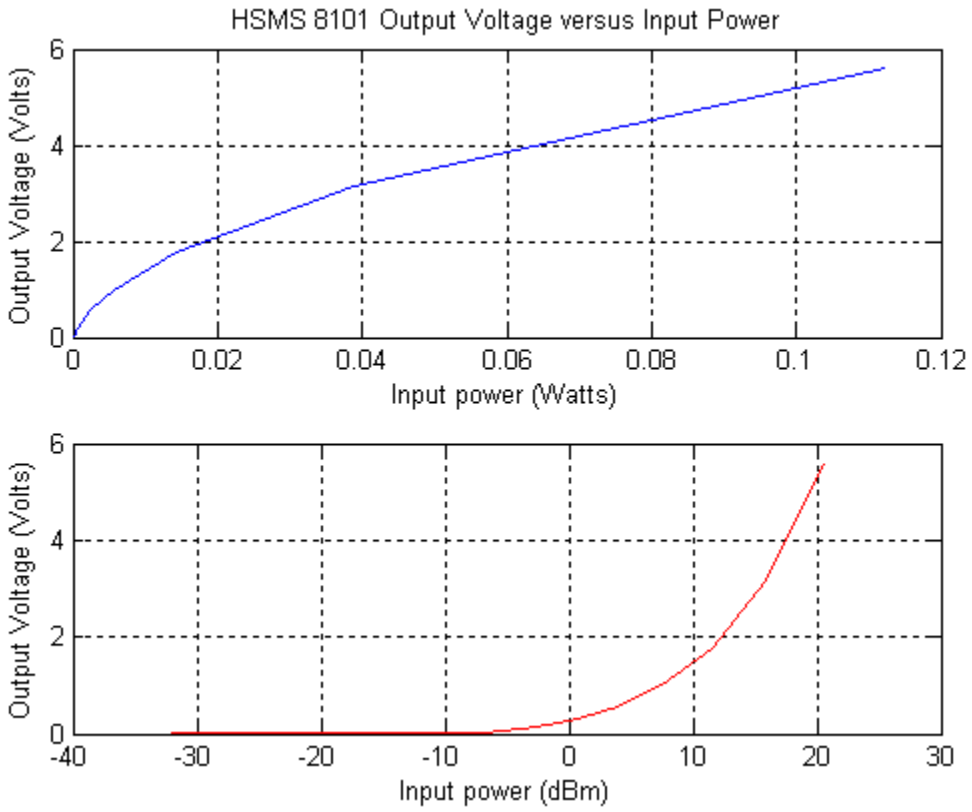

Figure 23. HSMS 8101 Diode Computed Output Voltage Versus Input Power (Computed Using Equation 3.10).

E. IMPEDANCE MATCHING CONSIDERATIONS

When the input impedance of the rectenna is other than the diode impedance, a portion of the received power is reflected back and reradiated from the antenna. Intuitively this condition is undesirable, because it reduces the efficiency of the rectenna. Therefore the impedance matching of the rectenna to the diode, as well as the diode to the load is imperative in order to optimize the efficiency. However, a rectenna circuit configuration with a single diode is highly nonlinear and the diode impedance evaluation is a complicated procedure. Generally, the diode impedance at the fundamental frequency and the various harmonics must be determined. This, approximately, can be evaluated using the typical ac equivalent circuit model for a Schottky diode, which is illustrated in Figure 24 [Ref. 32].

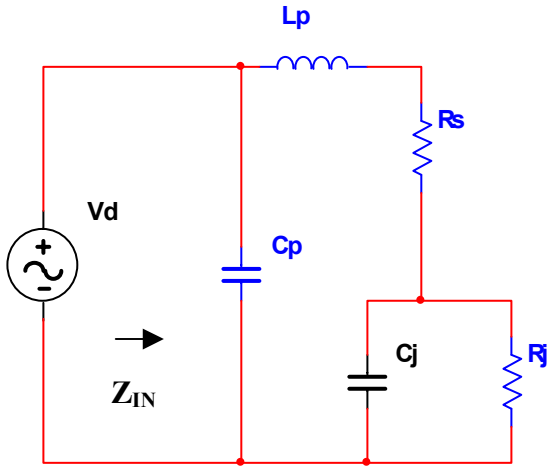

Figure 24. Schottky diode AC equivalent circuit. from [Ref. 20].

As stated previously the junction resistance of the diode is given by Equation (3.6). Then, using the value for I_S which corresponds to HSMS 8101, the junction resistance of the diode can be evaluated for various values of the forward voltage V. The values for R_J are illustrated in Figure 25 as the diode voltage varies from -0.5 to 0.2 V. As shown in the figure the junction resistance becomes smaller and converges to zero as the forward voltage of the diode increases.

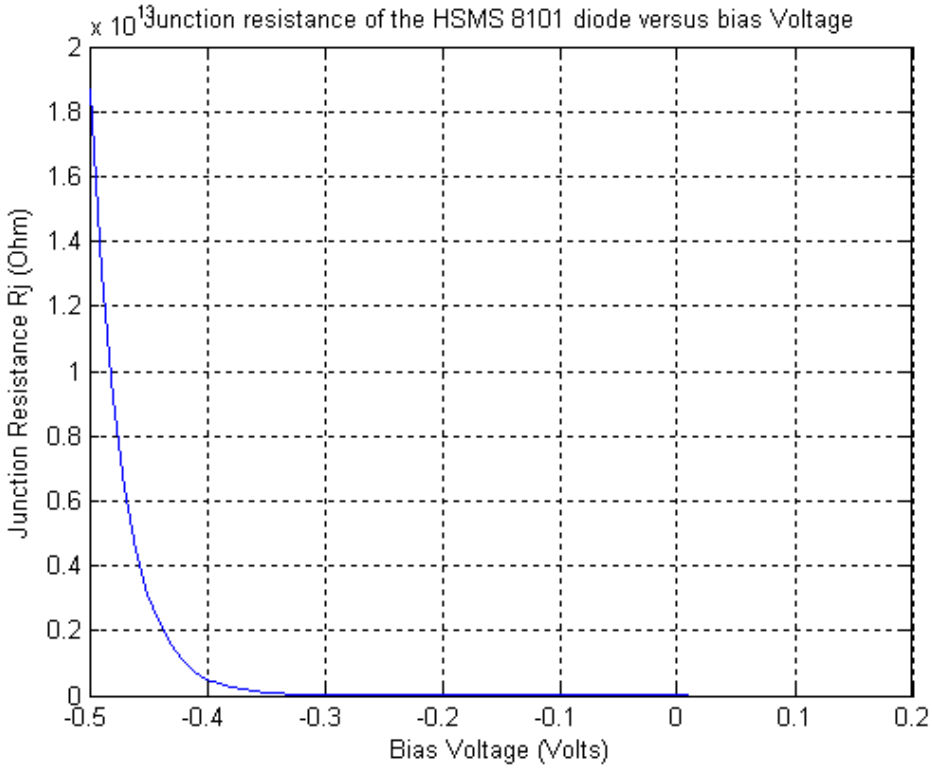

Figure 25. Junction resistance of HSMS 8101 SBD.

From the diode equivalent circuit, the input impedance is evaluated as

$$Z_{IN} = \frac{Z_{CP}(Z_{LP} + R_S + \frac{Z_{CJ}R_J}{Z_{CJ} + R_J})}{Z_{CP} + Z_{LP} + R_S + \frac{Z_{CJ}R_J}{Z_{CJ} + R_J})}, \tag{3.11}$$

where Z_{CP}, Z_{LP}, Z_{CJ} are the impedances for C_P, L_P, and C_J respectively. Using the values for HSMS 8101 Schottky diode given at Table 1, the Z_{IN} is calculated for various frequencies. The results are plotted and tabulated in Figure 26, and Tables 2 and 3. It can be seen that the input impedance of the diode is stabilized at the value of 29.432-j339.55 Ω when the input voltage takes positive values and the frequency is 10 GHz.

It should be mentioned that in the previous approach the change of junction capacitance with the diode current is not being taken into consideration. However, at the

power levels of interest for this project, the diode voltage would be in excess of 1V and the circulating current well above 1 mA. Therefore, the effect of junction capacitance is negligible.

HSMS 8101 Schottky Diode Input Impedance				
	0.1 Volts	**0.25 Volts**	**0.4 Volts**	**0.5 Volts**
10 GHz	8.8733	143.65	30.745	29.432
Fundamental	-j78.56	-j184.18	-j339.4	-j339.55
20 GHz	2.9748	11.68	1.794	1.7173
2nd Harmonic	+j183.75	+j172.51	+ j164.58	+j164.58
30 GHz	0.21589	0.71313	0.19065	0.182
3rd Harmonic	+j81.6	+j81.27	+j80.46	+j80.46
40 GHz	0.0525	0.13264	0.05046	0.04829
4rd Harmonic	+j55.41	+j55.37	+j55.19	+j55.19
50 GHz	0.01928	0.03948	0.01912	0.0183
5th Harmonic	+j42.54	+j42.53	+j42.47	+j42.47

Table 2. Input impedance for HSMS 8101 SBD for the fundamental and harmonics.

HSMS 8101 Schottky Diode Input Impedance Fundamental Frequency	
Voltage (V)	**Impedance (Ω))**
-2	7.792 - j78.625
-1	7.792 - j78.625
0.25	143.65-j184.18
0.6	29.432-j339.55
1	29.432-j339.55
1.4	29.432-j339.55
1.8	29.432-j339.55
2.2	29.432-j339.55
2.6	29.432-j339.55

Table 3. Input impedance of HSMS 8101 at 10 GHz for various voltages.

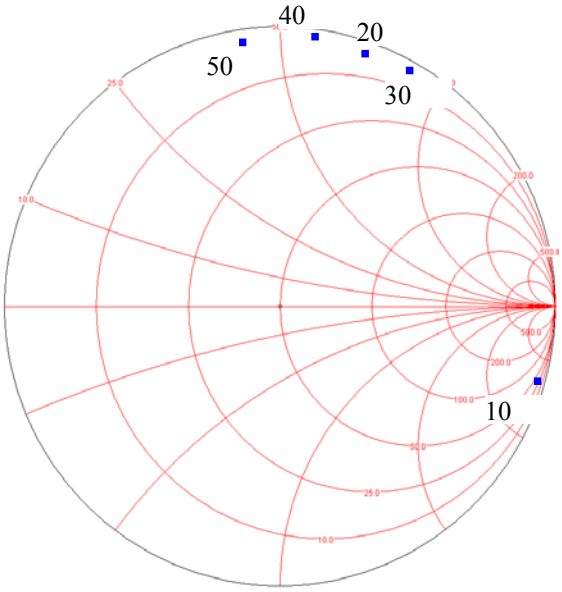

Figure 26. Input impedance of HSMS 8101 for various frequencies and voltage of 1 V.

F. DIODE BURNOUT

Any Schottky diode junction is relatively delicate and can be burned out with excessive rf power. Unfortunately in any rectenna application Schottky diodes found themselves in environments where high power sources are present. In such environments, the Schottky diodes can be protected by a device known as a limiter diode [Refs. 33, 34]. There is a complete line of surface mountable PIN limiter diodes on the market. Most notably, Agilent's HSMP-4820 (SOT-23) or HSMP-482B(SOT-323) can act as a very fast (nanosecond) power-sensitive switch when placed between the antenna and the Schottky diode, shorting out the rf circuit temporarily and reflecting the excessive rf energy back to the antenna. However, although the diodes are protected adding limiter diode before the antenna, the rectenna efficiency drops down due to the increased reflection power. In addition, impedance matching is more complicated when a limiter diode is present.

G. SUMMARY

In this chapter, the various parameters of the Schottky barrier diode have been presented and analyzed. The X/Ku band diode HSMS 8101, which selected for the

implementation of this project, presents attractive characteristics for a rectenna application. However since the power handling capabilities of this diode are relatively small, a large number of diodes is needed for large values of output power.

Using the diode's equivalent circuit, the input impedance at various frequencies was calculated. For the fundamental frequency, this value was evaluated as 29.432-j339.55 Ω.

The output voltage of the diode versus the input power for the entire operational range was evaluated using the rigorous approach of the Ritz-Galerkin method. As a result, conversion efficiency of 60.5% should be expected from the diode when the resistive load is 500 Ω.

IV. MICRO AIR VEHICLE (MAV) DESIGN

A. INTRODUCTION

As mentioned in Chapter II, a typical MAV weighs on the order fifty grams, and its size does not exceed six inches in any dimension. This means that if the electronics used for control purposes and the payload are excluded, the total weight of the remaining parts should be around 10 to 15 grams. Therefore, lightness should be emphasized in the vehicle design and construction. There are various problems associated with the design of very small vehicles. One obvious problem is that as the dimensions go down, the traditional materials such as wood, steel, or plastic become very fragile and difficult to handle. Additionally the motors and sensors for such a small size are extremely inefficient and delicate and make the fabrication process very complicated.

For the purposes of the present project a micro air vehicle was designed and built. Two prototypes were manufactured with different motors in each, in order to study the power requirements of a micro air vehicle. The vehicles were rotorcraft type MAVs with two counter rotating two-blade propellers. A special shaft design using steel tubing allowed the MAV to be tethered for the experiments. This configuration made microwave power level calculations easy, without the need of physically controlling the MAV. On the other hand, by only adding the electronics, the MAV could be transformed to a controlled vehicle retaining the same mechanical parts.

Using the two prototypes, various experiments were conducted and the power requirements for different weight configurations were evaluated. In addition, the rpm for each case was measured, using a stroboscope device.

B. BASIC ROTOR THEORY

As mentioned before, the aerodynamic modeling of a MAV is very complicated and requires extensive aerodynamic study which is beyond the limits of the present project. However, a basic helicopter blade theory is presented for a better understanding of the experimental results. In addition, due to the nature of the experiments only the helicopter hover case is examined.

1. Rotor Blade Airflows

If a single blade is considered as shown in Figure 27, there are two airflows that act on it. The first represented by the vector *BA*, is the rotational airflow V_{rot} which is a result of the rotor rotation, and expressed by the equation

$$V_{rot} = \omega \cdot R, \tag{4.1}$$

where ω is the angular velocity of the rotor, and R the radius. Obviously, V_{rot} is proportional to the rotor rpm, and radius of the rotor. This means that V_{rot} is zero at the root, and takes its maximum value at the tip of the rotor. Also V_{rot} is always parallel with the plane of rotation.

The second airflow applied to the rotor blade, is the induced flow V_i. This is represented by the vector *CB*, and is a result of the air mass that is forced down by the rotor while the helicopter is flying. The vector sum of the induced and rotational airflows is known as relative airflow and is represented by the vector *AC*. As shown in Figure 27, V_i is not parallel to the plane of rotation.

The angular difference between the blade chord line and the direction of V_r is the effective angle of attack of the blade. For a given rotor rpm, the induced flow is inversely proportional with the blade angle of attack.

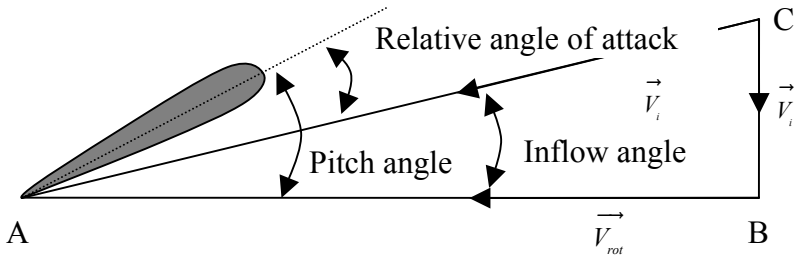

Figure 27. Airflows in a rotor blade [From Ref. 38].

2. Rotor Blade Forces

In a helicopter rotor the aerodynamic force produced must counteract the vehicle weight for hovering. However, as shown in Figure 28 the aerodynamic force is not in line with the weight of the helicopter. Instead, the component which has to be equal the weight of the helicopter is the rotor thrust. The other component of the aerodynamic force

which is parallel to the plane of rotation is the rotor drag, known also as torque. This force acts in a direction opposite to the blade travel and must be overcome by the helicopter's engine, so that the rotor will maintain its rpm.

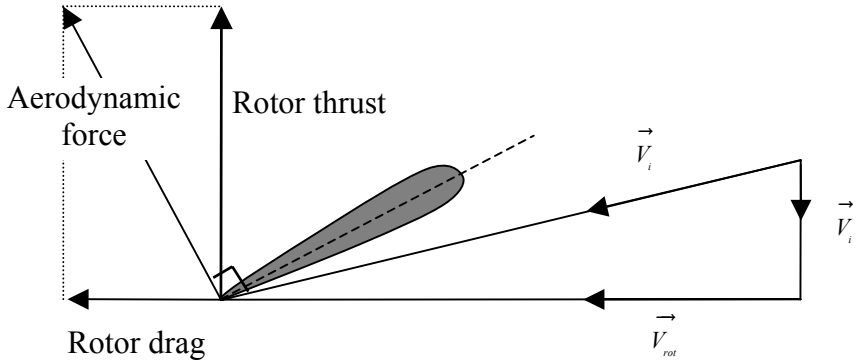

Figure 28. Forces applied in a rotor blade [From Ref. 38].

Obviously the rotor thrust must be as large as possible for better rotor efficiency. This means that the rotor drag should be as low as possible. Therefore, the vector of the aerodynamic force must be as close as possible to the axis of rotation, as shown in Figure 29. Thus, a small angle of attack of the blade produces an aerodynamic force closer to the axis of rotation, whereas a larger one tilts the vector of the total reaction force further back [Ref. 38]. However, a small angle of attack setting produces less lift than a larger one, and therefore, the magnitude of the aerodynamic force becomes smaller. As a result, there is an optimum angle of attack of the blade, which allows the vector of the aerodynamic force to be as close as possible to the axis of rotation, producing at the same time the maximum amount of lift.

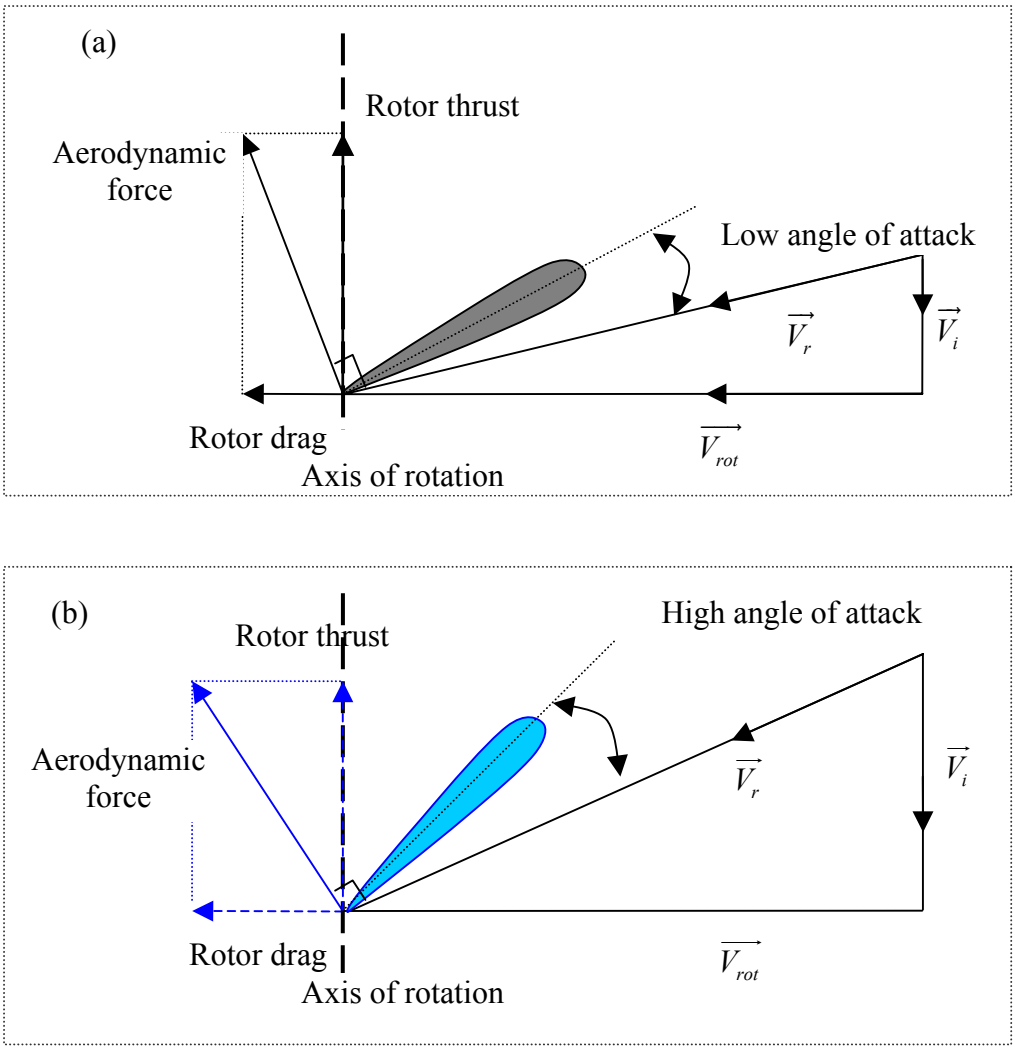

Figure 29. Effects of the angle of attack of the blade to the rotor thrust. (a) Low angle of attack. (b) High angle of attack [From Ref. 38].

3. Rotor Power Calculation

In a simplified form the rotor of a helicopter can be approximated by a stationary disc, while a large mass of air with density ρ and pressure p_o flows through it. As stated by the law of continuity, the mass of the fluid passing through a volume should remain constant all the time, whereas both the velocity and pressure of the fluid alter. Then, if the general case where a helicopter is climbing is considered, using a single axis coordinate system, the rotor velocity is represented as $-V_C$ and its thrust as T, as shown in Figure 30. The single axis is selected with the positive direction coinciding with that of the thrust T and its origin at the center of the disc. Air particles starting with a velocity $-V_C$ far from

the disc are accelerated, and their total velocity at the disc becomes $V = -(V_C + v_C)$. These particles continue to accelerate after passing through the disc up to the point where the induced velocity reaches its ultimate value $-v_u$. The total velocity of the air at that time is $V = -(V_C + v_u)$. These changes of the fluid velocity as it travels through the disc are accompanied with pressure changes too. Thus, if the pressure of the air mass far upstream is represented as p_o, the pressure just before the disc is decreased to p and just past the disc is increased to $p + \Delta p$. Also at the furthermost point of the downstream the pressure returns to its initial value p_o.

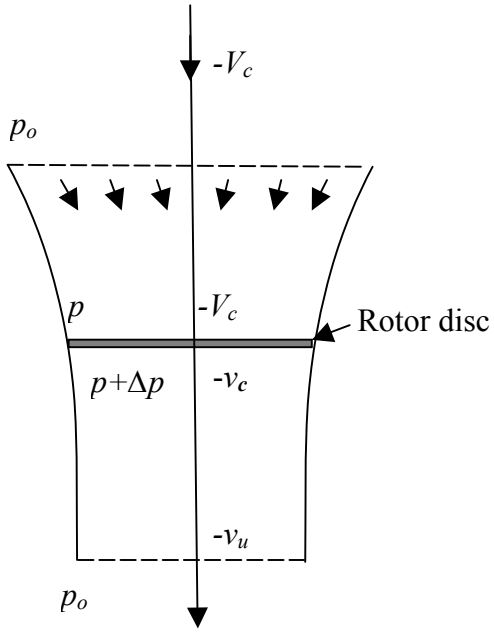

Figure 30. Fluid flow model for a helicopter rotor [From Ref. 39].

In this simple model, the fluid flow is assumed continuous along the slip stream except at the points just before and after the disc where obviously there is a discontinuity of the pressure. Therefore, Bernoulli's equation can be applied separately at the upstream and downstream parts of the flow tube. For the upstream part of the tube the sum of the static and dynamic pressure of the air, satisfies the equation

$$p_0 + \frac{1}{2}\rho V_c^2 = p + \frac{1}{2}\rho (V_c + v_c)^2. \tag{4.2}$$

Similarly for the downstream part of the fluid

$$p + \Delta p + \frac{1}{2}\rho(V_c + v_c)^2 = p_0 + \frac{1}{2}\rho(V_c + v_u)^2. \tag{4.3}$$

Subtracting (4.2) from (4.3) the pressure differential at the rotor is evaluated as

$$\Delta p = \rho(V_c + \frac{1}{2}v_u)v_u. \tag{4.4}$$

The thrust developed by a disc of radius R is expressed as

$$T = \pi \cdot R^2 \cdot \Delta p. \tag{4.5}$$

Therefore, using (4.4) the thrust becomes

$$T = \pi \cdot R^2 \cdot \rho \cdot (V_c + \frac{1}{2}v_u) \cdot v_u. \tag{4.6}$$

But the thrust produced by a helicopter rotor can be expressed as the product of the rate of the fluid mass which passes through the rotor, multiplied with the induced velocity of the air

$$T = \frac{dm}{dt}v_u. \tag{4.7}$$

The rate of mass of the fluid that passes through the disc can be expressed as

$$\frac{dm}{dt} = (V_c + v_c) \cdot A \cdot \rho = (V_c + v_c) \cdot \pi \cdot R^2 \cdot \rho, \tag{4.8}$$

where A is the surface of the rotor. Consequently, the thrust of the rotor is evaluated as

$$T = (V_c + \frac{1}{2}v_u) \cdot \pi \cdot R^2 \cdot \rho \cdot v_u = (V_c + v_c) \cdot \pi \cdot R^2 \cdot \rho \cdot v_u. \tag{4.9}$$

Simplifying

$$v_u = 2v_c, \tag{4.10}$$

which means that the ultimate value of induced velocity is twice the value of the induced velocity at the disc. Substituting the new value for v_c into (4.9) the thrust becomes

$$T = 2(V_c + v_c) \cdot \pi \cdot R^2 \cdot \rho \cdot v_c. \tag{4.11}$$

Rearranging Equation (4.11) we obtain an expression for the induced velocity at the disc

$$v_c = -\frac{1}{2} V_c + \sqrt{\frac{1}{4} V_c^2 + \frac{T}{2\rho \cdot \pi \cdot R^2}}. \tag{4.12}$$

In the case where the helicopter is hovering V_c is zero and therefore (4.12) is simplified as

$$v_{c(hover)} = \frac{1}{R} \sqrt{\frac{T}{2\rho \cdot \pi}}. \tag{4.13}$$

The power applied to the rotor can be evaluated examining the difference in the rate of the kinetic energy of the fluid at the points far upstream and far downstream

$$P_{in} = \frac{dE_{down}}{dt} - \frac{dE_{up}}{dt} = \frac{1}{2}\frac{dm}{dt}(V_c + v_u)^2 - \frac{1}{2}\frac{dm}{dt}(V_c)^2 = \frac{1}{2}\frac{dm}{dt} v_u (2V_c + v_u). \tag{4.14}$$

However, $\frac{dm}{dt} v_u = T,$ hence (4.14) becomes

$$P_{in} == T \cdot V_c + \frac{1}{2} T \cdot v_u. \tag{4.15}$$

Again, if the helicopter is hovering V_c=0, the first term of the right hand side of the (4.15) is zero. Then using (4.10) and (4.13) the power is evaluated as

$$P_{in} = \frac{1}{R} \sqrt{\frac{T^3}{2 \cdot \rho \cdot \pi}}. \tag{4.16}$$

Equation (4.16) holds for a 100% efficient rotor, that is, there are no power losses. However, in order to produce thrust *T*, the energy must be imparted to the slip stream of the rotor, and this conversion is not 100% efficient. Usually the conversion efficiency is referred to *M*, which can be expressed as the ratio of the power imparted to the slip stream to the power generated by the rotor shaft. As stated by [Ref. 5] a typical value of *M* for a tapered and twisted helicopter rotor is 0.75. Taking this into account (4.16) becomes

$$P_{in} = \frac{1}{M \cdot R}\sqrt{\frac{T^3}{2 \cdot \rho \cdot \pi}}. \tag{4.17}$$

The units of thrust T in (4.17) are in Newtons in the basic metric system (SI). Therefore, in order for the thrust to be expressed in kg, it has to be divided by 9.807 m/s2 which correspond to the acceleration of gravity. Equation (4.17) is plotted in Figure 31, and simply states that for a helicopter rotor with radius of 7.5 cm, an input power setting of 1 W generates 30 g of thrust. However, this input power refers only to the rotor of the MAV, and is different from the electrical input power to the motor of the vehicle. Apparently, the electrical input power must be much higher, due to several losses including the motor and the various mechanical parts of the vehicle.

The value of 7.5 cm was used, since it corresponds to the radius of the MAV rotor which was constructed for the present project. Defining the disk loading parameter $D_L = \frac{\text{Weight}}{\text{Rotor Area}}$, and the power loading parameter, $P_L = \frac{\text{Power}}{\text{Weight}}$, the plot of Figure 32 is generated for various values of M and for a rotor having a radius of 7.5 cm.

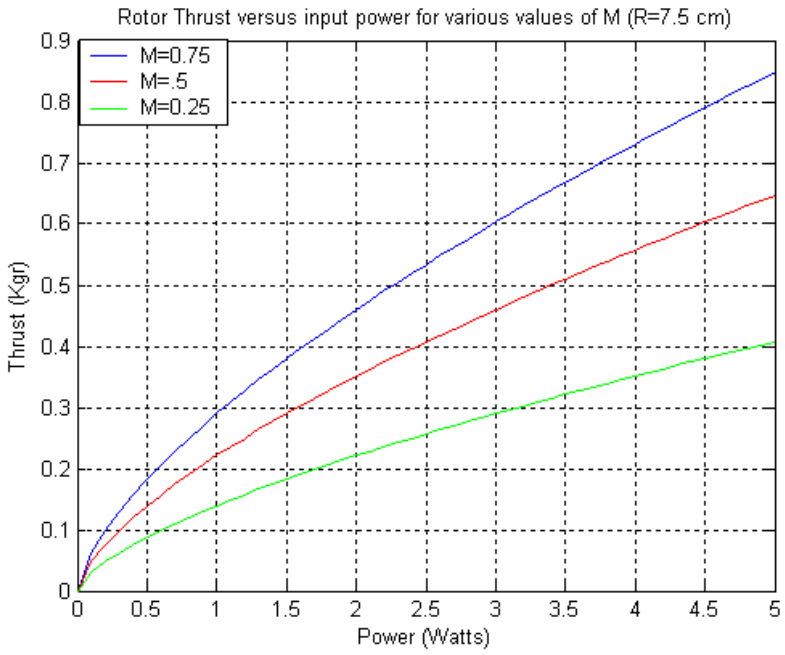

Figure 31. Rotor thrust calculations (R=7.5 cm).

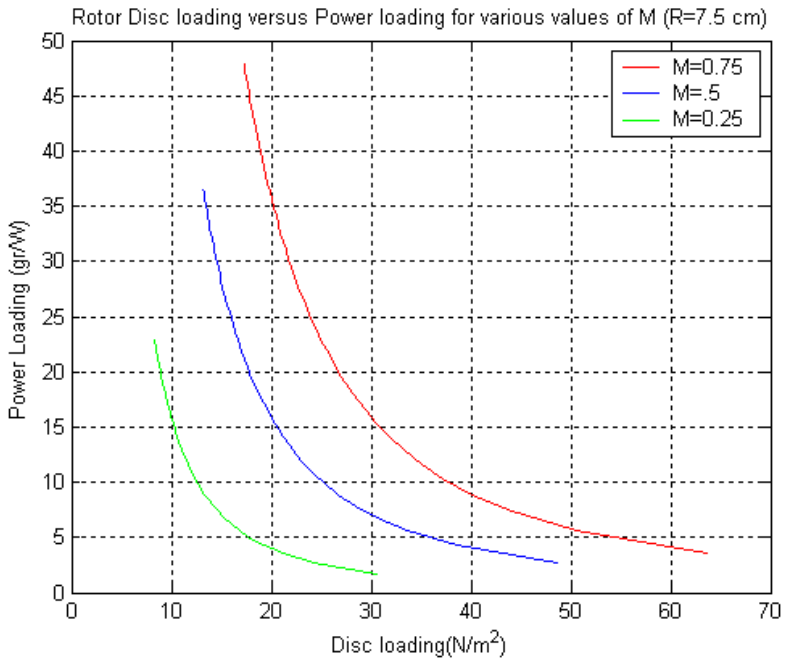

Figure 32. Rotor disc loading versus power loading (*R*=7.5 cm).

C. MAV CONSTRUCTION

A micro air vehicle should be extremely light, since the weight directly affects the performance and power consumption. For this reason, emphasis was applied to the design and construction of the MAV prototypes for the present project. The vehicle was designed to comply with the requirements of a MAV, that is, it has to be no larger than 15 cm in any dimension. It is a coaxial rotor design, where the two rotors are counter rotating. Therefore, the torque generated from one rotor is canceled by the torque generated by the other rotor. This design is more compact than a classical helicopter design with one main rotor at the center of gravity point, and a torque compensating smaller rotor mounted at the tail of the vehicle, and is easier to be implemented in such a small size. Additionally counter rotation provides improved performance because the second rotor recovers the energy lost in the induced rotational velocity imparted by the first rotor, and also the torque compensation provides lift, unlike to a conventional helicopter [Ref. 40].

1. MAV Body Construction

As shown in Figure 33 the main body of the vehicle consists of two cylinders which are constructed from carbon laminate of thickness 0.152 mm. Since the carbon

laminate sustains its maximum strength along the grain, two laminates of thickness 0.076 mm are glued together cross-grain for maximum durability. The inner cylinder serves as housing for the gearbox and the electronics of the vehicle, whereas the outer cylinder forms a duct with four stationary vanes. The vanes were built from balsa wood of 0.5 mm thickness. The inner cylinder is identical for the two prototypes having a diameter of 3.8 cm, and height of 3.6 cm, but the outer cylinder is significantly larger on the second prototype. Specifically, the dimensions of the outer cylinder are 6.7 cm diameter, and 1.6 cm height for the first prototype, and 9.1 cm diameter and 2 cm height on the second prototype. Consequently, the stationary vanes which are mounted between the two carbon cylinders are bigger on the second prototype than on the first. This is because the second prototype is designed to be used as a controlled version and thus bigger vanes are required for effectively controlling the vehicle.

Two types of electric motors were used for propulsion of the two MAVs. A 7 mm diameter coreless motor was used for powering the first prototype. This is a very light but relatively inefficient motor. On the second prototype a 10 mm diameter more was used. Since this motor is indented to be used in precision tool applications, it is a very durable and efficient motor. However, both its power requirement and weight are larger than that of the first prototype motor. The characteristics for both motors are listed in Table 4. In addition, the schematic layouts of the motors are illustrated in Figures 35 and 36.

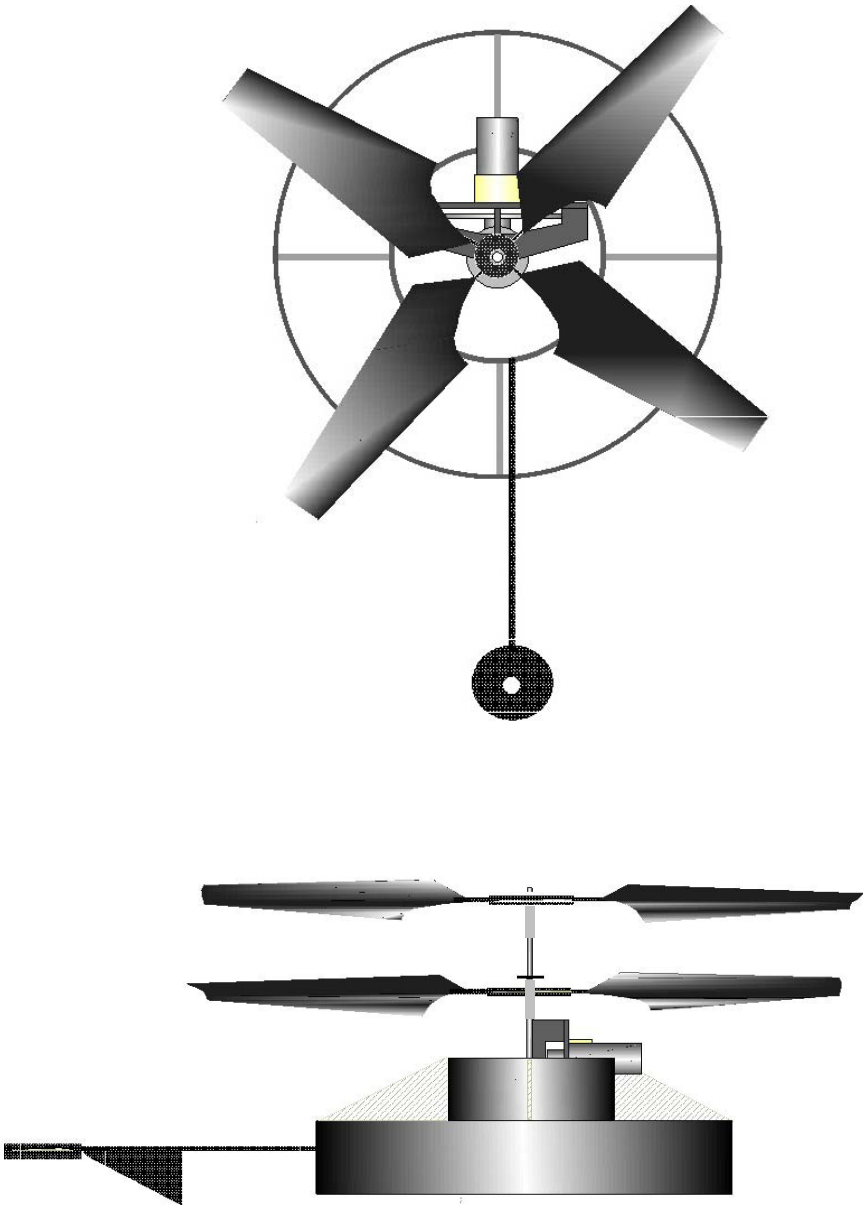

Figure 33. MAV prototype schematic layout.

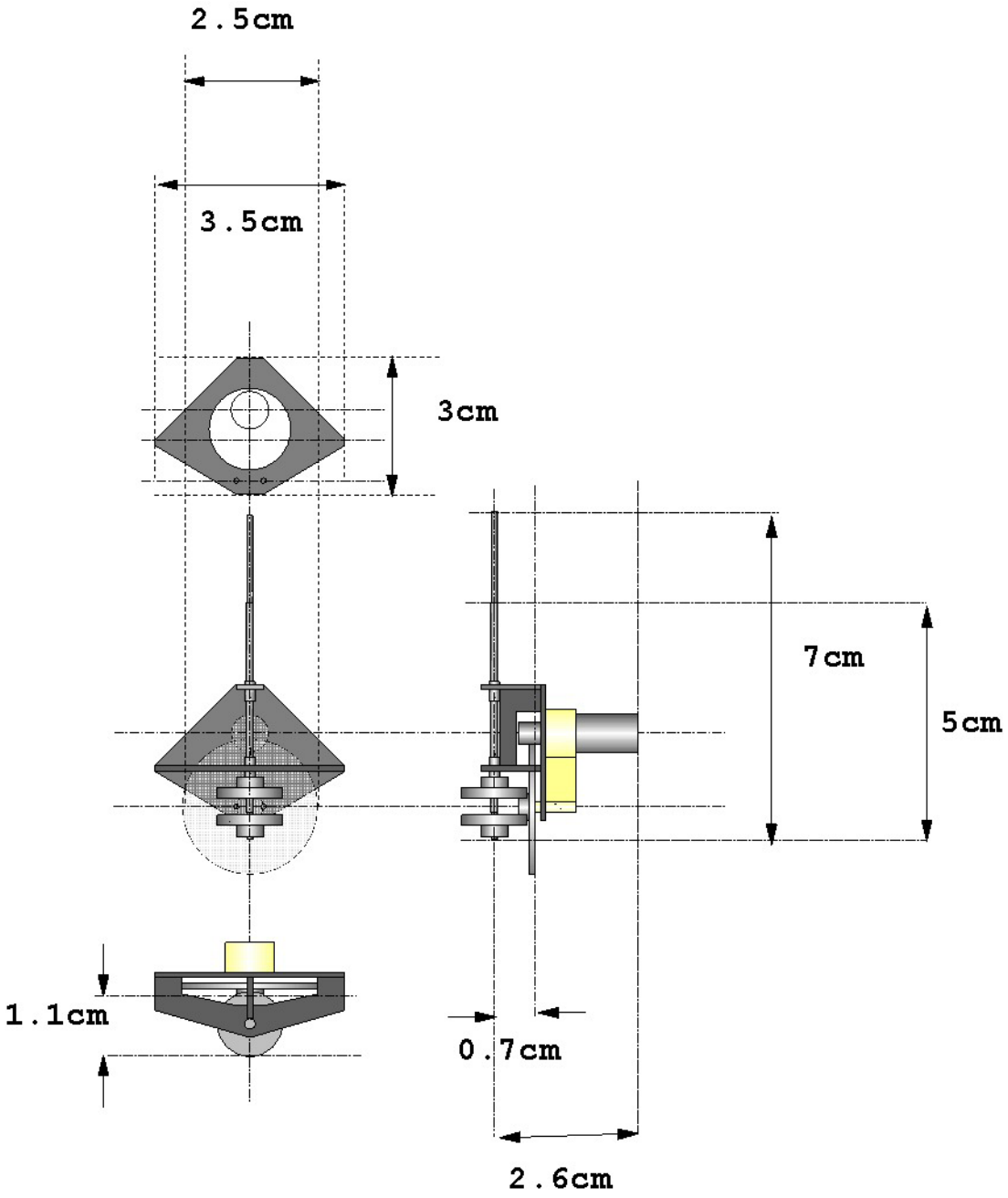

Figure 34. Gearbox schematic layout.

MAV Motor Data		
Code	DIMMK06-10	MAXON 118383
Manufacturer	Didel	Maxon
Diameter	7 mm	10 mm
Length	17 mm	17 mm
Weight	3.2 gr	7 gr
Assigned power rating (Output)	N/A	0.75 W
Nominal voltage	1.2 V	3 V
Resistance	8 Ω	8 Ω
No load speed	N/A	10,200 rpm
Max permissible speed	N/A	19,000 rpm
Max continuous current	N/A	306 mA
Max continuous torque	N/A	0.817 mNm
Efficiency	N/A	60%

Table 4. Characteristics of the MAV motors used for the two prototypes (Manufacturer's DATA).

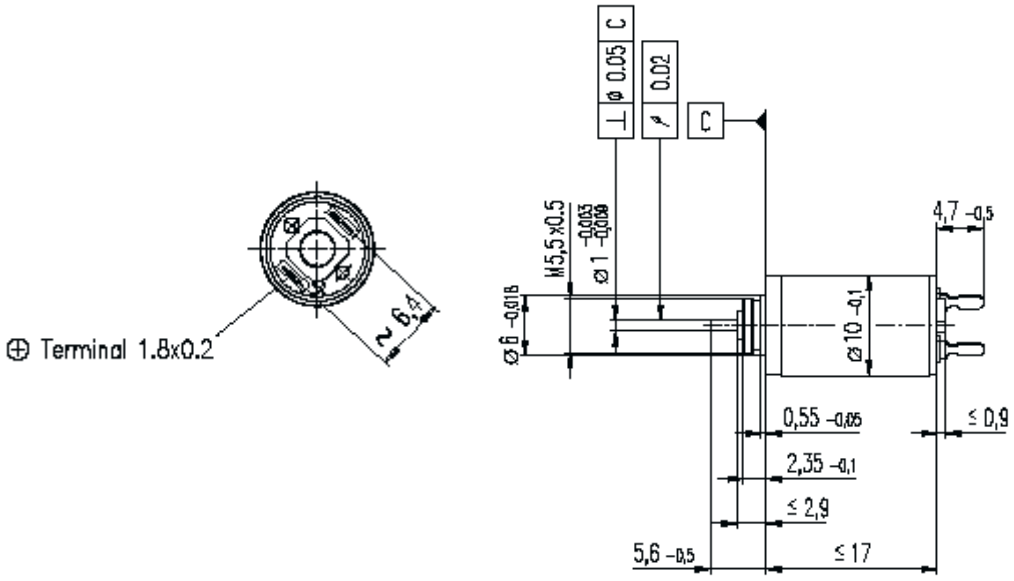

Figure 35. Schematic layout of Maxon 10 mm motor (Manufacturer's DATA).

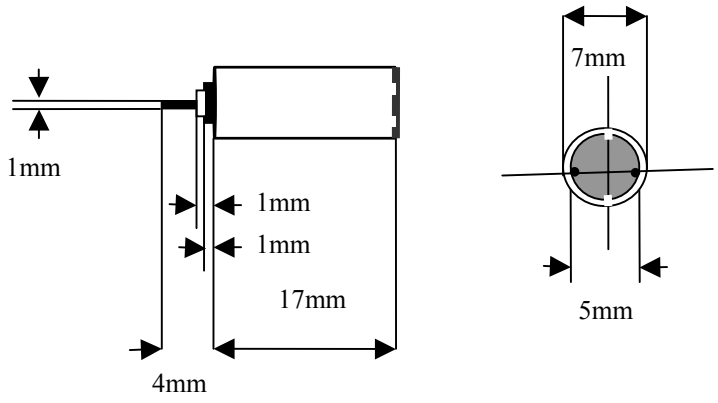

Figure 36. Schematic layout of the 7 mm coreless motor.

A sandwich material made from balsa wood of 0.5 mm thickness and carbon laminate 0.076 mm thick was used for the gearbox chassis. This composite material is extremely durable, being at the same time very light [Ref. 41]. The gearbox consists of an 81 tooth main gear, which in conjunction with the pinion gear in the motor, reduces the motor's rpm to 9:1. The 12 tooth pinion on the main gear is coupled with two 36 tooth crown gears as shown in Figure 34. The final reduction of the motor's rpm is 27:1.

The two crown gears drive the shafts of the vehicle. Specifically, the upper crown gear drives the outer shaft, while the lower drives the inner shaft. Both shafts are built from stainless steel hypodermic tubing. The dimensions of the input shaft are 0.81 mm outer radius, 0.58 mm inner radius and 6.4 cm height. The same dimensions for the outer shaft are 1.27 mm, 1.06 mm and 6 cm. In order to minimize the friction between the two shafts a 1.06 mm outer radius, 0.914 mm inner radius, and 3 mm height steel tube was placed between the two shafts as a bearing. The total weight of the first prototype is 9 g, whereas the same parameter for the second one is 15 g. This difference was mainly due to the heavier motor used for the second prototype, and also to the more robust construction of the second prototype gearbox, which was necessary in order to compensate for the higher loads.

2. MAV Rotor Fabrication

Special attention was given to the rotor blade fabrication. The two rotors cannot exceed six inches (or 15 cm) in diameter; otherwise the vehicle is not categorized as micro air vehicle. Obviously this is disadvantageous because as equation (4.17) states, the bigger the diameter of the helicopter rotor, the more the thrust produced for a given amount of power. Thus, the rotors have to be as efficient as possible in order to compensate for the small diameter. For this reason a full twisted and tapered blade design was implemented using carbon laminates. Again the carbon laminates were glued cross grain for increased strength. The rotor schematic layout is illustrated in Figure 37.

A method proposed by [Ref. 41] was used to construct the blades with the desired amount of twist. According to this method a single carbon laminate was placed along the height of a cylinder at an angle θ with respect to the cylinder centerline. Then a second carbon laminate is glued on top of the first, and the blade is cut to the desired shape as shown in the Figure 38. When the two laminates are glued together they keep the shape of the cylinder even after being removed from it. Thus, the resulting blade is gradually twisted along its length, having a very thin cambered airfoil. The twist of the blade can be adjusted changing the angle θ. If an angle of 20° is used, a blade with length 7 cm exhibits about 20 degrees pitch angle at the root when the tip pitch angle is set to zero.

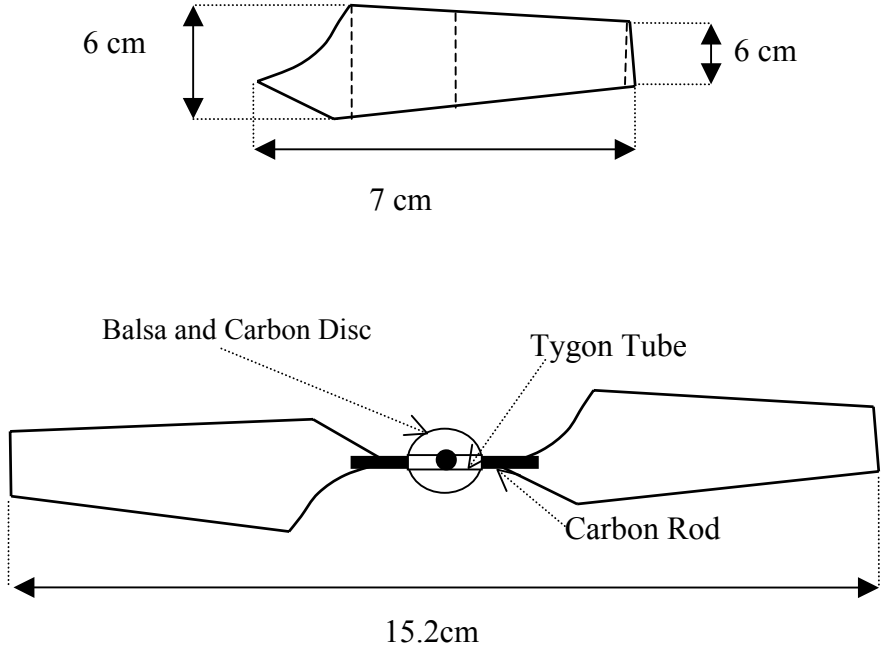

Figure 37. Rotor blade schematic layout.

The camber of the blade is also determined by the angle θ. As shown in Figure 38 when the blade is placed diagonally on the cylinder's surface, its airfoil is generated by a family of ellipses, which can be expressed by the equation:

$$\frac{x^2}{a^2}+\frac{y^2}{b^2}=\frac{x^2}{49}+\frac{y^2\cdot\cos(\theta)^2}{49}=\frac{x^2}{49}+\frac{y^2}{55.49}=1, \tag{4.18}$$

where a=7 cm for the case that the radius of the cylinder is 7 cm, and θ=20°. Then the camber of the airfoil is defined by the local curvature of the ellipse and could be rigorously calculated if the arc length of the ellipse was known. However, since every section of the blade resides at a different part of the same ellipse, the airfoil camber changes along the span. On the other hand, the calculation of the curvature of an ellipse arc length is a complicated procedure, and is not required for the current project. Instead, since the axial ratio of the ellipse generated by a relatively small θ is close to one, the ellipse can be approximated by a circle with radius 7 cm as shown in Figure 39.

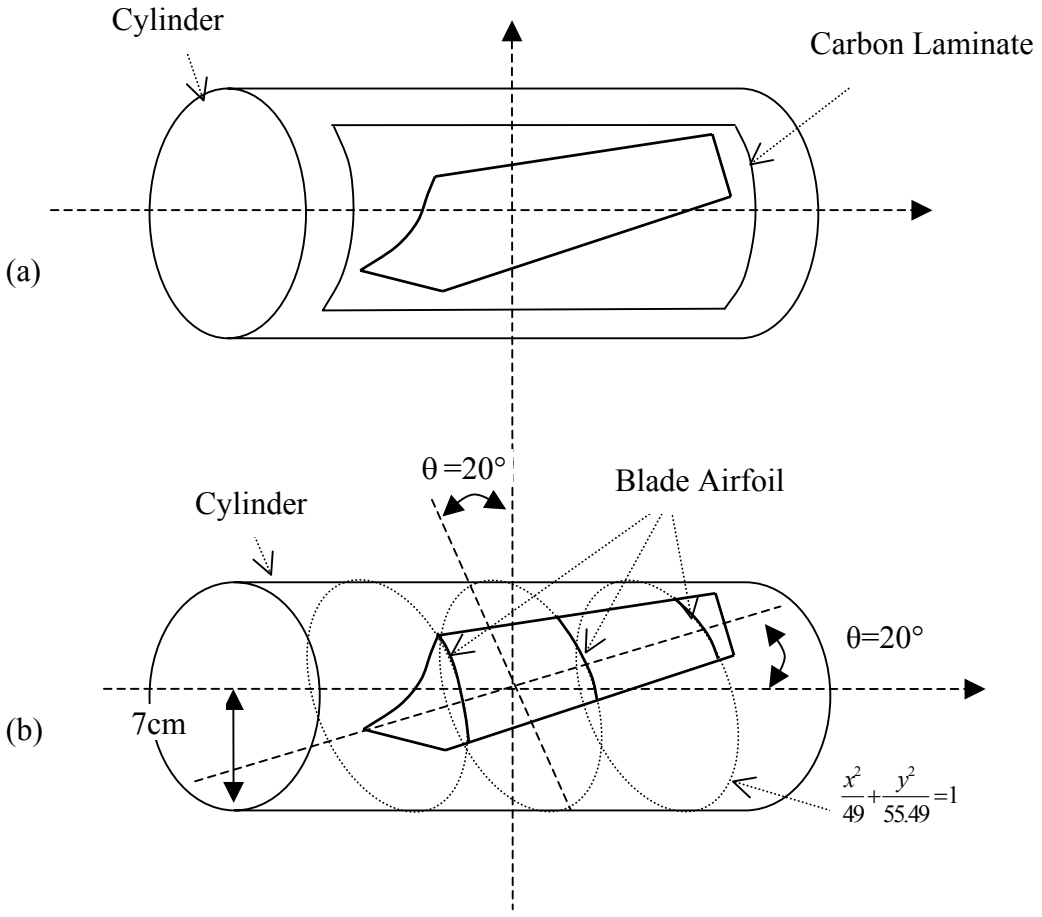

Figure 38. Illustration of the method used for rotor blade fabrication. (a) Carbon laminates on the cylinder. (b) Blade airfoil geometry.

Therefore, the maximum camber of the airfoil is expressed as the ratio $c = CD/AB$, and since the cord length at the widest part of the blade is 2.6 cm the camber is calculated as c=4.6%. Using the same approximation, the airfoil camber for the middle and the tip of the blade is evaluated as 3.58% and 2.8%, since the corresponding arc lengths are 2 cm and 1.6 cm. According to [Ref. 42] for circular arc section airfoils with values of camber 3-6%, the maximum lift coefficient $C_{L,max}$ varies from 0.93 to 1.18, while the minimum drag coefficient $C_{D,min}$ varies form 0.03 to 0.06. For the same values of camber the maximum lift to drag ratio varies from 11.7 to 10.5 at a Reynolds number

2.9×10^3. Additionally, the reference states that for larger values of camber the lift to drag ratio decreases. Therefore, the blade resides close to the optimum lift to drag ratio point for this type of airfoil.

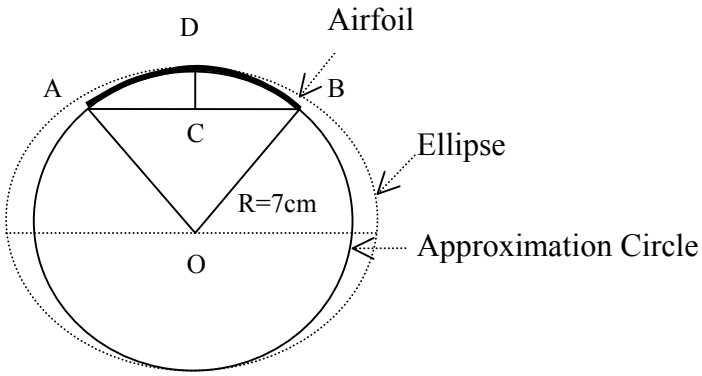

Figure 39. Calculation of the airfoil camber.

A 2 mm diameter carbon rod was glued at the root of each blade, and the two blades mounted at a circular disk, as shown in Figure 37. The disk was built from sandwich material made of balsa and carbon laminate. The blades were secured on the disk with small tygon tubes. These tubes were glued on the disk, but the blade rods were pressure fit in the tubes. This allows the blade pitch angle to be adjusted to optimize performance. The two rotors are identical except for their pitch angles, which are opposite, since they are counter rotating. Each rotor is attached to the corresponding shaft using tygon tubes of different radii.

D. MAV POWER TESTS

Both MAV prototypes were tested in order to evaluate the electrical power required for hover, for various gross weight configurations. The vehicles were tethered in such a way that only vertical movement was allowed. A 0.127 mm thickness stainless steel wire passing through the inner shaft of the MAV, was supported from a mast which in turn was secured to the roof of the laboratory. Due to the slight movement of the vehicle in the yaw axis, a second thin wire was added passing through another point on it, thus precluding the rotation of the body during flight. Small lead balls were used in order

to add weight to the vehicle gradually. The prototypes were tested lifting weights from 5 to 30 g the smaller model, and from 5 to 45 g the bigger model. A voltmeter and an ammeter were connected in the circuit for voltage and current monitoring, respectively. A stroboscope was used to illuminate the rotors for frequency calculation. For easier blade tracking, one of the blades of the upper rotor was painted with light reflecting paint. In Figure 40, the first prototype is shown hovering in the Laboratory.

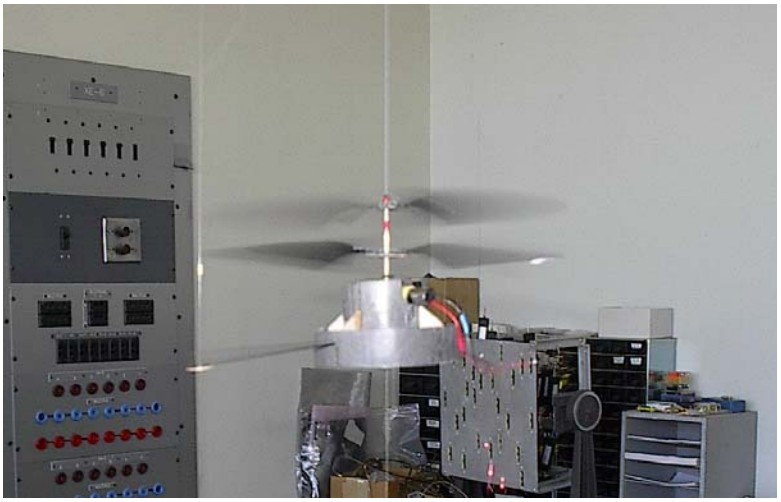

Figure 40. MAV hovering tethered for electrical power calculations.

The results of the measurements are illustrated in Figures 41, 42 and 43, and listed in Tables 5 and 6. It can be seen that the power required for hovering exhibits a relatively steep slope as the gross weight increases. For example the required power for hovering with 5 g extra weight is 0.952 W for the first prototype and 1.43 W for the second, whereas the power required with 15 g extra weight is 2.17 and 2.89 W, respectively. This means that the total weight of the vehicle must be kept as low as possible. There is also a big difference in the power requirements between the two prototypes. The reason for this is the weight difference between the two prototypes, which although small, (only six grams), it turns out to be a big penalty for the total performance.

The operating resistance of the pager motor is relatively stable in the entire operational region, taking values from 44.8 to 54.9 Ω. The variation in operating

resistance of the Maxon motor is larger, and in the range of 72 to 125 Ω. The motor resistance will be the resistive load for the rectenna, and therefore the rectenna design should be optimized to this value of load.

Some useful observations can be made for the range of Reynolds number which corresponds to the operational region of the vehicles. The Reynolds number of any flight platform can be expressed as

$$Re = \frac{L \cdot V \cdot \rho}{\mu}, \tag{4.19}$$

where:

L is a characteristic aerodynamic length of the vehicle,

V is the characteristic velocity,

ρ is the density of the fluid, and

μ is the viscosity of the fluid.

For the standard atmosphere the values of the air density and the viscosity are ρ=1.225 kg/m^3 and μ=1.789x10^{-5} kg/ms. The velocity in this case is the rotational velocity V_{rot} at the tip of the rotor, which is given by (4.1). Then if L=1.5 cm is the length of the airfoil chord at the tip of the blade and R=7.5 cm, the range of Reynolds number can be evaluated from 9,162 to 13,744 for the first prototype, and from 20,615 to 37,500 for the second one.

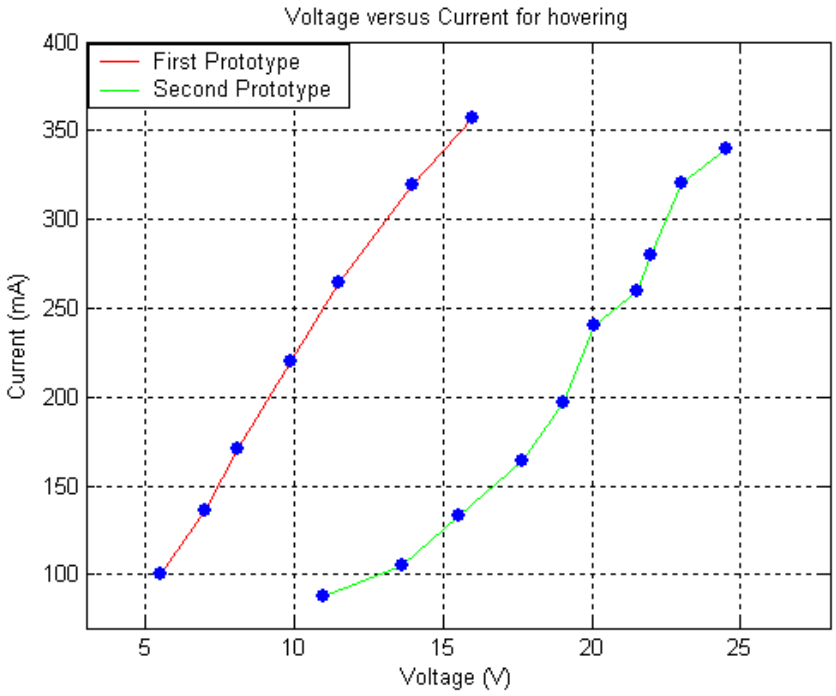

Figure 41. Voltage versus current for hovering.

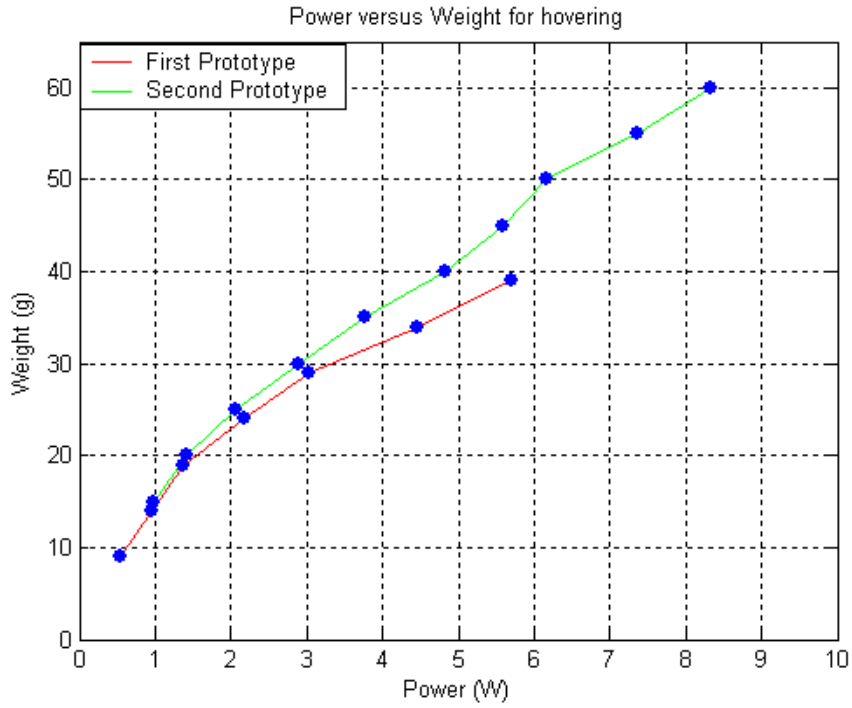

Figure 42. Power versus weight for hovering of the MAV prototypes.

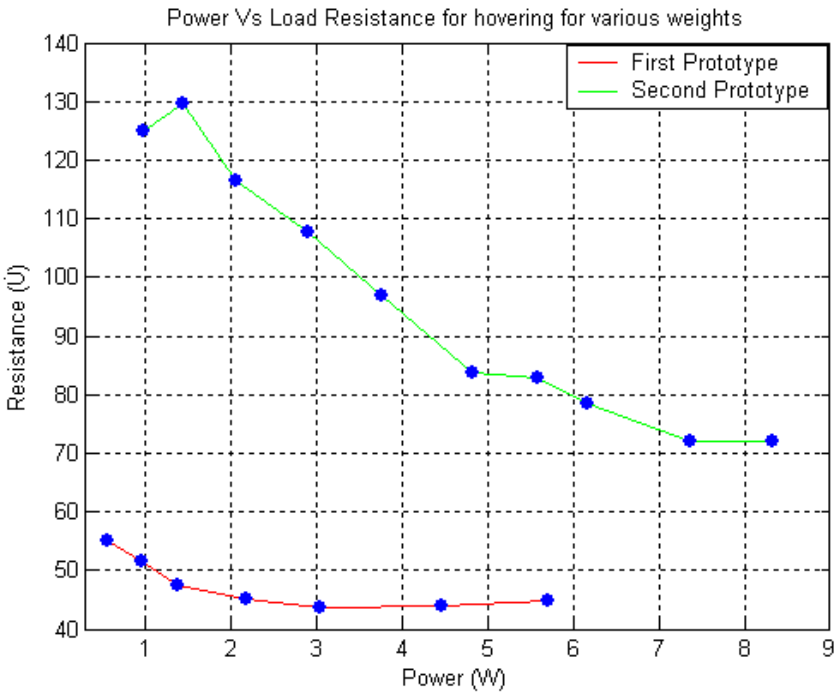

Figure 43. Power versus load resistance for hovering for various weights.

First Prototype							
Weight (g)	net	5	10	15	20	25	30
Voltage (V)	5.5	7	8.1	9.9	11.5	14	16
Current (mA)	0.1	0.136	0.17	0.22	0.264	0.319	0.357
Resistance (Ω)	54.9	51.4	47.4	45	43.5	43.8	44.8
Power (W)	0.55	0.952	1.3817	2.1780	3.0360	4.4660	5.7120
RPM	1200	1440	1620	1740	1770	1800	2100

Table 5. Measured data of the first prototype.

Second Prototype										
Weight (g)	net	5	10	15	20	25	30	35	40	45
Voltage (V)	11	13.6	15.5	17.68	19.07	20.08	21.5	22	23	24.5
Current (mA)	0.08	0.100	0.105	0.133	0.164	0.197	0.24	0.28	0.32	0.34
Resistance (Ω)	125	129.5	116.5	107.8	96.8	83.6	82.6	78.5	71.8	72.0
Power (W)	0.97	1.43	2.06	2.89	3.75	4.81	5.59	6.16	7.36	8.33
RPM	2700	3220	3660	4200	4320	4440	4560	4680	4800	4920

Table 6. Measured data of the second prototype.

E. SUMMARY

In this chapter, the basic aerodynamic considerations of helicopter rotors have been presented. In addition, a complete description of the methods followed for the fabrication of the two MAV prototypes has been presented. Two vehicles weighing 9 and 15 grams correspondingly were tested tethered, and various measurements were taken. Approximately 1.2 W of electrical power was required for hovering when the weight of extra 5 g was added to the vehicle. The results also showed that as the gross weight of the platform increased, the power requirements also increased dramatically and therefore emphasis in minimizing weight should be given in the rectenna design and fabrication.

THIS PAGE INTENTIONALLY LEFT BLANK

V. RECTIFIER ANTENNA (RECTENNA) DESIGN

As mentioned in Chapter II, a rectenna consists of an array of identical elements, where each of them contributes to the power collecting and rectification process. The construction of the rectenna elements is generally based on the same principals, independently of the particular type of array element. Thus, a typical rectenna element is comprised of the antenna, (which collects the microwave power), input low pass filter, diode, and output low pass filter. The purpose of the input low pass filter is to avoid any generated harmonic signals from reradiating by the antenna. Similarly, the output filter isolates the dc line from microwave signals.

Obviously an easy way of implementing a rectenna is using an array of dipoles as described in Chapter II. However, even in its most compact form, (coplanar printed dipoles), the dipole rectenna is not sufficient for being a MAV rectenna. This is mainly because the ground plane should be some distance behind the plane of the dipoles, usually $\lambda/4$, and therefore the resulting rectenna is relatively thick and bulky, and could not be implemented on a thin substrate. On the other hand, when the antenna and the filters reside on the same foreplane, which is the case for the printed dipole rectenna, the radiation pattern of the dipole is altered since the filters also radiate. Moreover, the single foreplane exposes the diodes to the impinging microwave power directly, which is not desirable.

Clearly in a rectenna design which is intended to be used as a MAV power source, special attention should be given in minimizing the weight. Also, since the maximum dimension of a MAV is six inches, the rectenna should be physically small. Therefore the rf frequency should be high enough, so that the antenna element dimensions can be minimized, yet still be substantial in terms of wavelength. For this reason the frequency of 10 GHz selected as most appropriate.

A circular patch rectenna was selected for implementation in the present project, since it presents the most attractive solution for a MAV application. Since both the circular patch and the low pass filters could be implemented in a very thin substrate, the rectenna element is very light and compact. As mentioned in Chapter II, the inherent

capability of the circular patch antenna to resonate at frequencies which correspond to roots of Bessel functions, and not to multiples of the fundamental frequency, greatly reduces the reradiation of the harmonics.

The feed probe of the patch antenna was designed to be at the 30 Ω impedance point in order to match with the input low pass filter, which in turn matches with the impedance of the diode. Accordingly the output low pass filter designed to have 30 Ω input and output impedance.

A. CIRCULAR PATCH ANTENNA

1. Theory

The theoretical analysis of a circular patch antenna resembles the common analysis of a rectangular patch, where the patch, the ground plane, and the microwave substrate are treated as a cavity [Refs. 43, 44]. The only difference is that the circular patch is treated as a circular cavity and therefore cylindrical coordinates are used. Similarly the modes that are supported for a circular patch antenna are TM^z modes, provided that the substrate height is much smaller than the effective wavelength of the microstrip. The schematic layout of a circular patch antenna is illustrated in Figure 44.

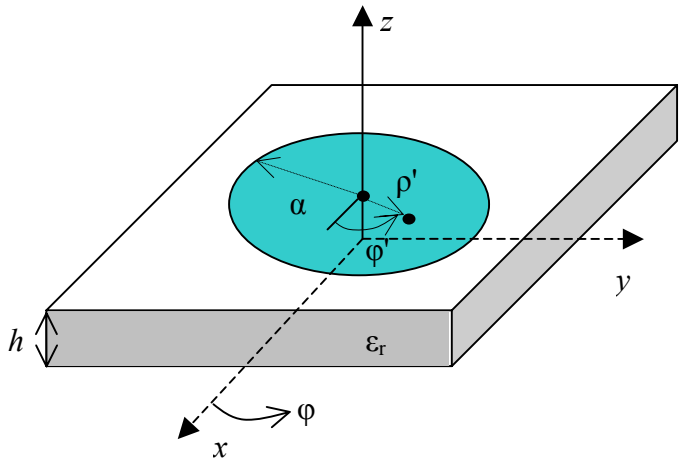

Figure 44. Schematic of the circular microstrip patch antenna [From Ref. 44].

If the vector potential approach is used, the magnetic vector potential A_z must satisfy the homogeneous wave equation

$$\nabla^2 A_Z(\rho,\phi,z) + k^2 A_Z(\rho,\phi,z) = 0. \tag{5.1}$$

Also, for the TM^z modes the electric and magnetic fields are related to the vector potential with the following equations:

$$\begin{aligned} E_\rho &= -j\frac{1}{\omega\cdot\mu\cdot\varepsilon}\frac{\partial^2 A_Z}{\partial\rho\partial Z}, \\ E_\phi &= -j\frac{1}{\omega\cdot\mu\cdot\varepsilon}\frac{\partial^2 A_Z}{\partial\phi\partial Z}, \\ E_z &= -j\frac{1}{\omega\cdot\mu\cdot\varepsilon}\left(\frac{\partial^2}{\partial z^2}+k^2\right)A_z, \end{aligned} \tag{5.2}$$

$$\begin{aligned} H_\rho &= \frac{1}{\mu}\frac{1}{\rho}\frac{\partial A_z}{\partial\phi}, \\ H_\rho &= \frac{1}{\mu}\frac{\partial A_z}{\partial\rho}, \\ H_z &= 0, \end{aligned} \tag{5.3}$$

where the corresponding boundary conditions are

$$\begin{aligned} &E_\rho(0\le\rho'\le\alpha,\ 0\le\phi'\le 2\pi,\ z'=0)=0, \\ &E_\rho(0\le\rho'\le\alpha,\ 0\le\phi'\le 2\pi,\ z'=h)=0, \\ &H_\phi(\rho'=\alpha,\ 0\le\phi'\le 2\pi,\ z'\le h)=0. \end{aligned} \tag{5.4}$$

The primed cylindrical coordinates ρ',φ',z', are used to represent the fields inside the cavity. Using the Bessel function of first kind $J_m(x)$, with order m, the magnetic vector potential can be expressed as

$$A_z = B_{mnp}J_m(k_p\rho')\left[A_2\cos(m\varphi')+B_2\sin(m\varphi')\right]\cos(k_z z'), \tag{5.5}$$

with the constraint equation

$$\left(k_\rho\right)^2+\left(k_z\right)^2 = k_r^2 = \omega_r^2\mu\cdot\varepsilon, \tag{5.6}$$

where:

$$k_\rho = \frac{\chi'_{mn}}{\alpha},$$
$$k_z = \frac{\rho \cdot \pi}{h},$$

$$m, p = 0,1,2,...$$
$$n = 1,2,3,...$$

The factor χ'_{mn} in the previous equation represents the zeros of the derivative of the Bessel function $J_m(x)$, and determine the order of the resonant frequencies. The first four values of χ'_{mn} are

$$\begin{aligned} \chi'_{11} &= 1.8412, \\ \chi'_{21} &= 3.0542, \\ \chi'_{01} &= 3.8318, \\ \chi'_{31} &= 4.2012. \end{aligned} \tag{5.7}$$

If the substrate height is very small compared to wavelength, which is usually the case for the microstrip patch antenna, then p=0 and k_z=0, and the resonant frequencies can be found using Equations (5.5), (5.6) and (5.7). Thus, the resonant frequencies of the cavity for the TM^z_{mn0} modes are

$$\left(f_r\right)_{mn0} = \frac{1}{2\pi\sqrt{\mu \cdot \varepsilon}}\left(\frac{\chi'_{mn}}{\alpha}\right). \tag{5.8}$$

Therefore, using the values of (5.8) the dominant mode TM^z_{110}, is expressed as

$$\left(f_r\right)_{mn0} = \frac{1}{2\pi\sqrt{\mu \cdot \varepsilon}}\left(\frac{\chi'_{mn}}{\alpha}\right) = \frac{1.8412c}{2\pi \cdot \alpha\sqrt{\varepsilon_r}}, \tag{5.9}$$

where c is the speed of light in the free space and ε_r the dielectric constant of the substrate material.

However, the Equation (5.9) does not account for the fringing effect. Since the fringing makes the patch look electrically larger, the corrective factor of effective radius can be used, which compensates for the fringing. The effective radius can be calculated

$$\alpha_e = \alpha\left\{1+\frac{2h}{\pi\cdot\alpha\cdot\varepsilon_r}\left[\ln\left(\frac{\pi\cdot a}{2h}\right)+1.7726\right]\right\}^{1/2}, \tag{5.10}$$

and therefore,

$$\left(f_r\right)_{mn0} = \frac{\chi'_{mn}c}{2\pi\cdot\alpha_e\sqrt{\varepsilon_r}}. \tag{5.11}$$

The radius of the patch can be calculated solving the equation (5.10). Following the procedure of [Ref. 44] (5.10) can be rearranged as follows

$$\alpha = \frac{F}{\left\{1+\frac{2h}{\pi\cdot F\cdot\varepsilon_r}\left[\ln\left(\frac{\pi\cdot F}{2h}\right)+1.7726\right]\right\}^{1/2}}, \tag{5.12}$$

where $F = \frac{8.971\times10^9}{f_r\sqrt{\varepsilon_r}}$, f_r is given in Hz, and h is given in cm. The radiation patterns of the circular patch antenna as given by [Ref. 44] are as follows

1. $E-\text{plane}\ \ \left(\phi = 0°,\ 0°\le\theta\le 90°\right)$

$$E_\varphi = 0, \tag{5.13}$$

$$E_\theta = j\frac{k_0\alpha_e V_o e^{-jk_0 r}}{2r}\left[J_0\left(k_0\alpha_e\sin\theta\right)-J_2\left(k_0\alpha_e\sin\theta\right)\right],$$

2. $H-\text{plane}\ \ \left(\phi = 90°, 270°,\ 0°\le\theta\le 90°\right)$

$$E_\theta = 0, \tag{5.14}$$

$$E_\phi = j\frac{k_0\alpha_e V_o e^{-jk_0 r}}{2r}\left\{\cos\theta\left[J_0\left(k_0\alpha_e\sin\theta\right)+J_2\left(k_0\alpha_e\sin\theta\right)\right]\right\}.$$

The conductance due to the radiated power and directivity of the circular patch antenna can be evaluated using the formula of the radiated power.

$$P_{rad} = \left|V_0\right|^2\frac{k_0\alpha_e}{960}\int_0^{2\pi}\left[J'^2_{02}+\cos^2(\theta)J^2_{02}\right]\sin\theta d\theta, \tag{5.15}$$

where:

$J'^{2}_{02} = J_0\left(k_0\alpha_e \sin\theta\right) - J_2\left(k_0\alpha_e \sin\theta\right)$, and

$J_{02} = J_0\left(k_0\alpha_e \sin\theta\right) + J_2\left(k_0\alpha_e \sin\theta\right)$.

Using (5.16), the conductance across the gap between the patch and the ground plane at $\phi' = 0$ can be evaluated as

$$P_{rad} = \frac{(k_0\alpha_e)^2}{480}\int_0^{\pi/2}\left[J'^{2}_{02} + \cos^2(\theta)J^2_{02}\right]\sin\theta d\theta. \tag{5.16}$$

The conductance of the patch for the TM^z_{110} mode as presented by [Ref. 44], is illustrated in Figure 45.

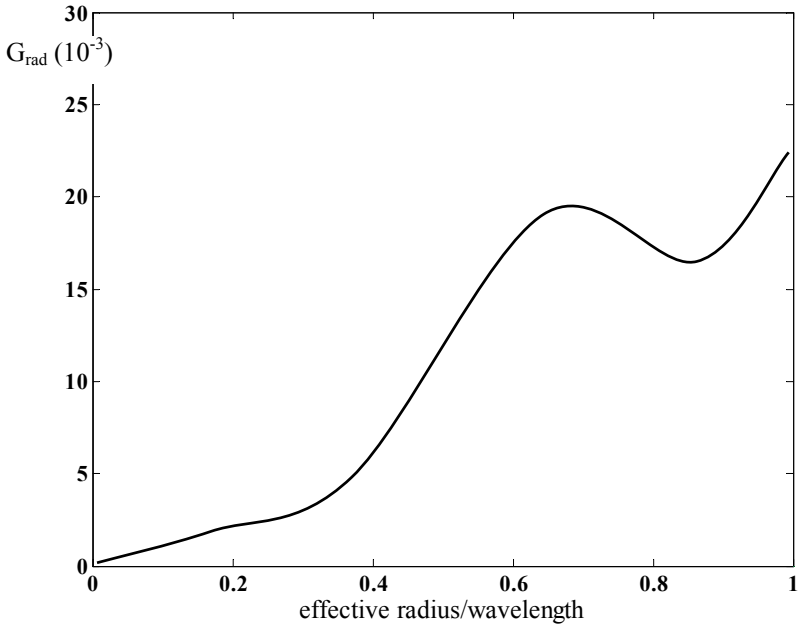

Figure 45. Radiation conductance of the circular patch antenna [From Ref. 44].

Equation (5.16) does not take into account ohmic losses of the patch and dielectric losses, but only losses due to radiation. Ohmic and dielectric losses for TM^z_{110} modes, are expressed correspondingly by the equations

$$G_c = \frac{\pi\left(\pi\cdot\mu_0\cdot f_r\right)^{-3/2}}{4h^2\sqrt{\sigma}}\left[\left(k\cdot\alpha_e\right)^2 - 1\right], \tag{5.17}$$

and

$$G_d = \frac{\pi \tan\delta}{4\mu_0 h^2 f_r}\left[\left(k\cdot\alpha_e\right)^2 - 1\right]. \tag{5.18}$$

Therefore, the total conductance can be expressed as the sum

$$G_t = G_{\text{rad}} + G_c + G_d. \tag{5.19}$$

The radiation efficiency of the antenna is given as

$$eff_r = \frac{G_{rad}}{G_{rad} + G_c + G_d}. \tag{5.20}$$

The resonant input impedance of the circular patch is real and depends on the feed position of the patch. The feed is usually a probe placed at some distance from the center. The resonant input impedance of the patch is given as

$$R_{in}\left(\rho' = \rho_0\right) = \frac{1}{G_t}\frac{J_0^2(k\cdot\rho_0)}{J_0^2(k\cdot\alpha_e)}, \tag{5.21}$$

where the reference of the feed is taken at $\phi' = 0,$ and $\rho' = \rho_0$ is any radial distance from the patch center.

The directivity of the patch can be evaluated if the radiation conductance is known, since it is expressed by the equation

$$D_0 = \frac{\left(k_0\alpha_e\right)^2}{120 G_{\text{rad}}}. \tag{5.22}$$

2. Design and Fabrication

The design of the circular patch antenna was based upon the theoretical analysis which was presented previously. In order to minimize the weight of each element as much as possible, a very thin substrate was selected. The type of the dielectric material was RO3003 manufactured by Rogers Corporation. This material exhibits a relatively small dielectric constant, ε_r=3, and a very low loss tangent, $\tan\delta$=0.0012 at 10 GHz. The substrate height used was 0.127 mm. The substrate has electrodeposited ½ oz copper on both sides. Based on the characteristics of the substrate and Equation (5.13), the radius of the patch is calculated as α=0.510 cm. Similarly the effective radius from equation (5.11)

is $\alpha_e = 0.517$ cm, and using Figure 45 the conductance at the peripheral of the patch is G_{rad}=2×10^{-3} Siemens. Therefore, using (5.21) the directivity of the patch is evaluated as D0=6.88 dB.

Using Equations (5.7) and (5.8) the resonant frequencies of the antenna can be calculated as follows

$$\begin{aligned} (f_r)_{110} &= \frac{1.8412c}{2\pi\cdot\alpha_e\sqrt{\varepsilon_r}} = 9.952 \quad \text{GHz}, \\ (f_r)_{210} &= 16.5 \quad \text{GHz}, \\ (f_r)_{010} &= 20.7 \quad \text{GHz}, \\ (f_r)_{310} &= 22.7 \quad \text{GHz}. \end{aligned} \tag{5.23}$$

Equation (5.22) simply states that the circular patch antenna does not resonate at the harmonics of the fundamental frequency, which is 10 GHz. Thus, the radiation of the harmonics generated by the rectification process is greatly reduced.

The antenna radiation efficiency can be calculated using Equations (5.17, 5.18, 5.19 and 5.20). Thus substituting the values for $(f_r)_{110}$ and α_e computed before the conductance due to conductor loss is evaluated as $G_c = 3.25\times10^{-5}$ Siemens and the conductance due to dielectric loss $G_d = 1.41\times10^{-4}$ Siemens. Thus the total conductance is $G_t = 2.17\times10^{-3}$ Siemens, and the radiation efficiency is $eff_r = 91.99\%$.

The circular patch antenna was optimized using the program PATCHD presented in [Ref. 45]. Using the data for frequency and substrate material, PATCHD evaluates the radius of the patch as $\alpha = 0.503$ cm. The output of the program is given in Table 7. The computer software CST Microwave Studio was also used to simulate the patch. The various plots generated are presented in Figures 46 through 50.

PATCHD.V50 10-05-2003 14:08:44	
Frequency	9.9992 GHz
Substrate Height	0.0127 cm
Substrate Relative Dielectric Constant	3.00
Substrate Loss Tangent	0.0012
Conductor Relative Conductivity	1.000
Patch Radius	0.503 cm
Feed Location	0.115 cm
Input Resistance	28.72 Ohms
Patch Total Q	82.479
Efficiency	97.45%
Patch Bandwidth (SWR2:1)	0.86%

Table 7. Patch data as evaluated using the PATCHD program [From Ref. 45].

The results of the PATCHD.V50 and the Microwave studio together with the theoretical calculated are in agreement between them as can be seen in table 8.

	CST Microwave Studio	PATCHD.V50	Theoretical results
Frequency	9. 997 GHz	9.9992 GHz	9.952 GHz
Patch Bandwidth (SWR2:1)	0.86%	0.4%	0.56%
Input Impedance	30.02+j0.4846 Ohms	28.72 Ohms	30 Ohms
Radiation efficiency	91.91%	97.45%	91.99%

Table 8. Summarized computational data of patch antenna.

The patch antenna was fabricated on a 23×20 mm brick of dielectric material. The feed probe was mounted at the 30 Ω impedance point in order to match the 30 Ω input impedance of the input low pass filter.

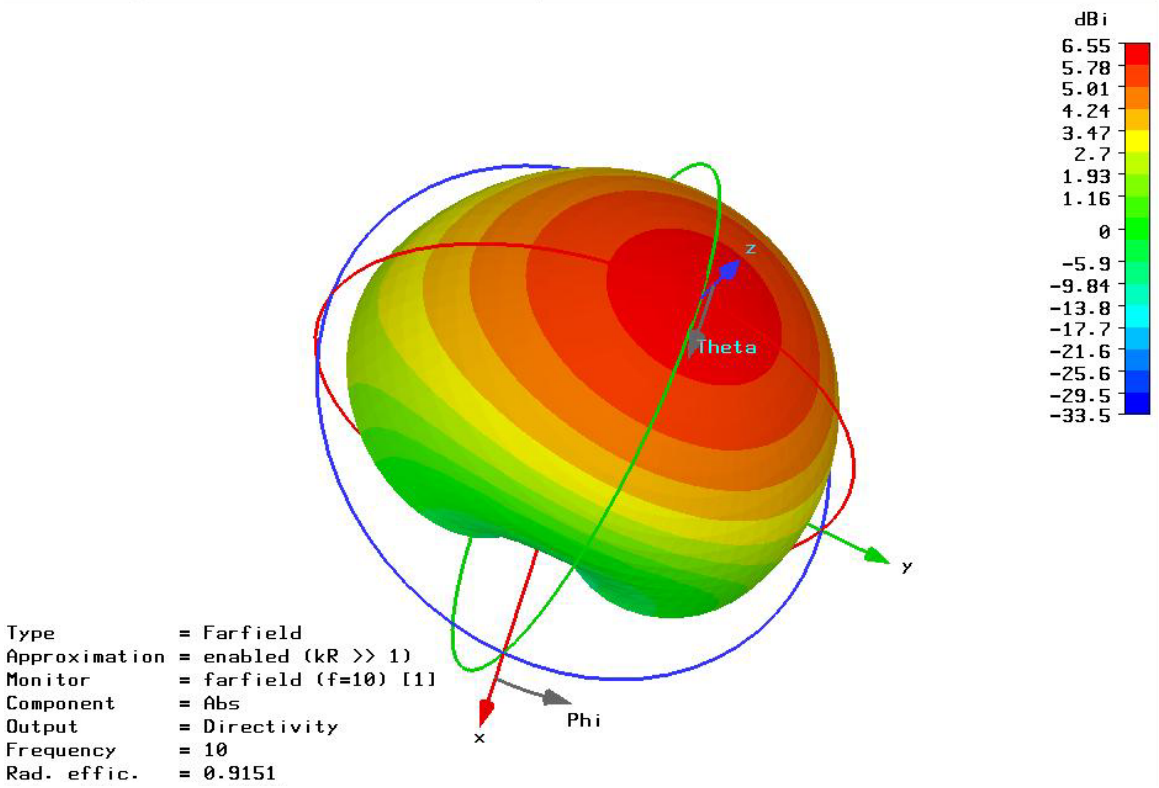

Figure 46. Computed three-dimensional radiation pattern of the circular patch antenna at 10 GHz (Microwave Studio simulation).

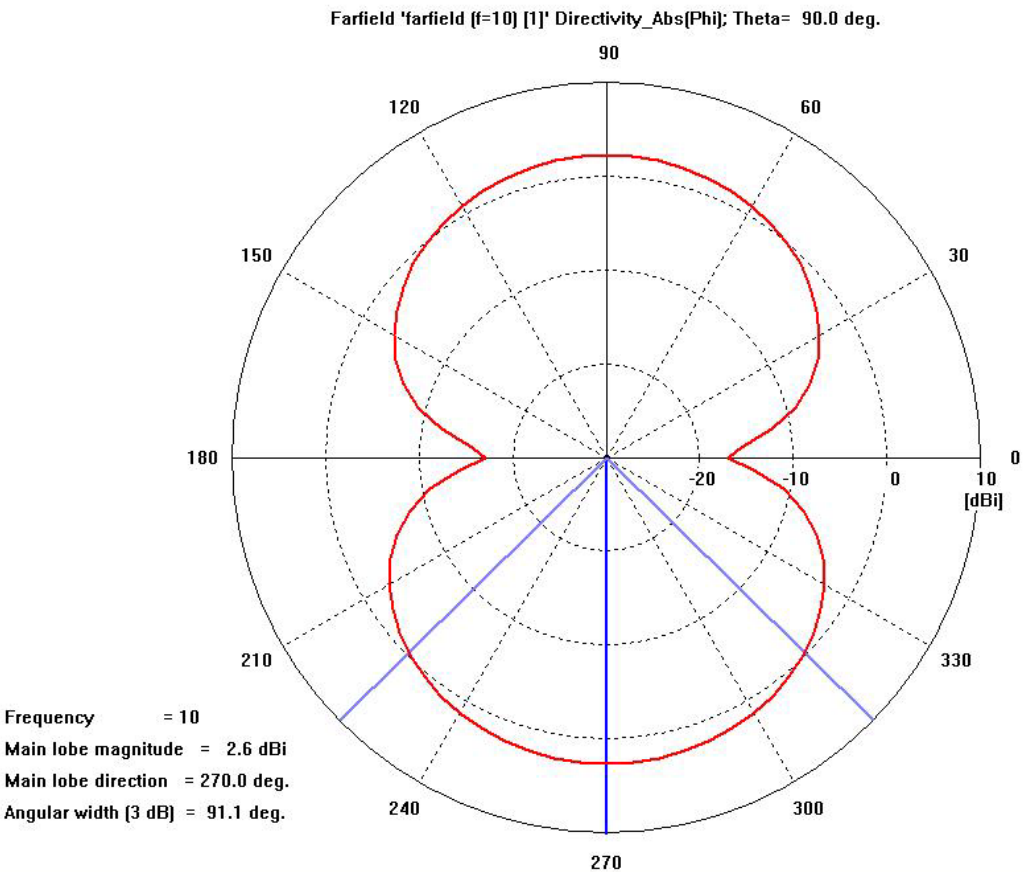

Figure 47. Computed radiation pattern of circular patch antenna (φ-component). (Microwave Studio simulation).

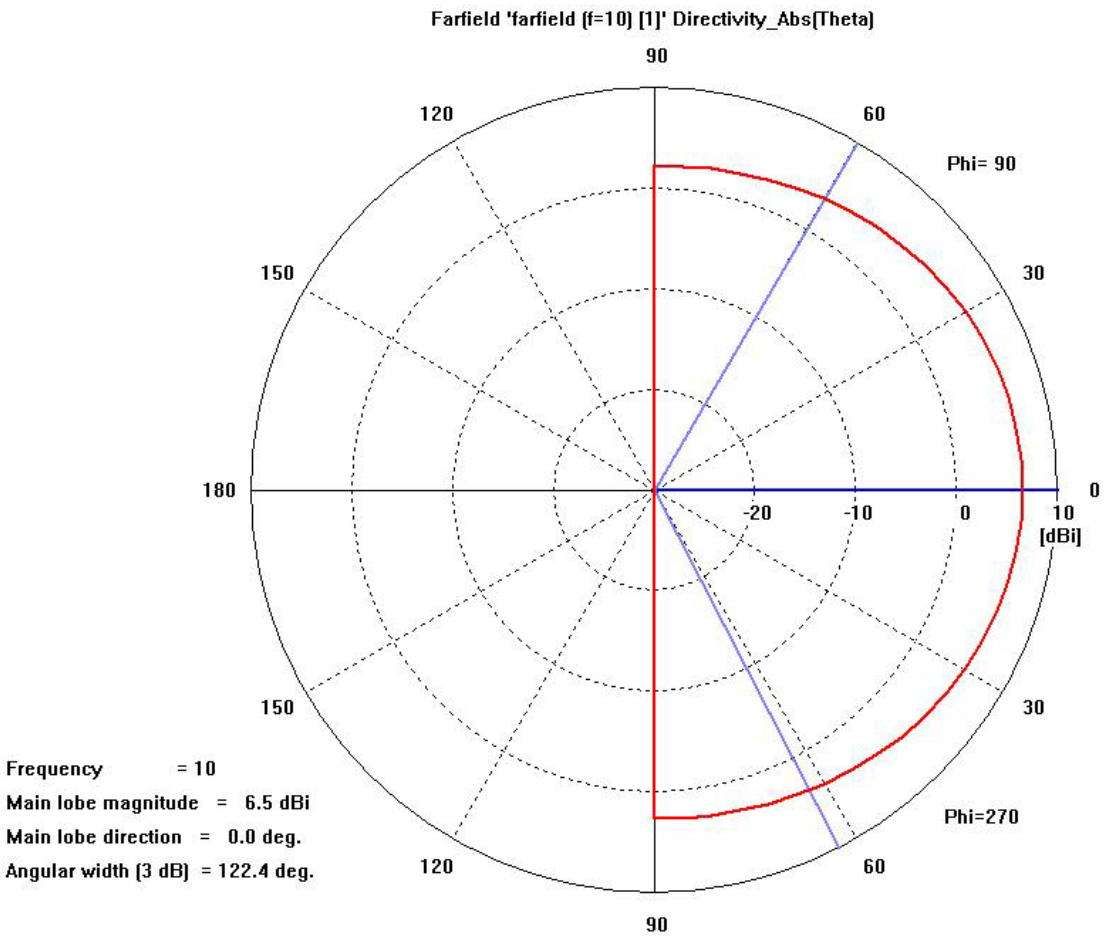

Figure 48. Computed radiation pattern of circular patch antenna (θ-component). (Microwave Studio simulation).

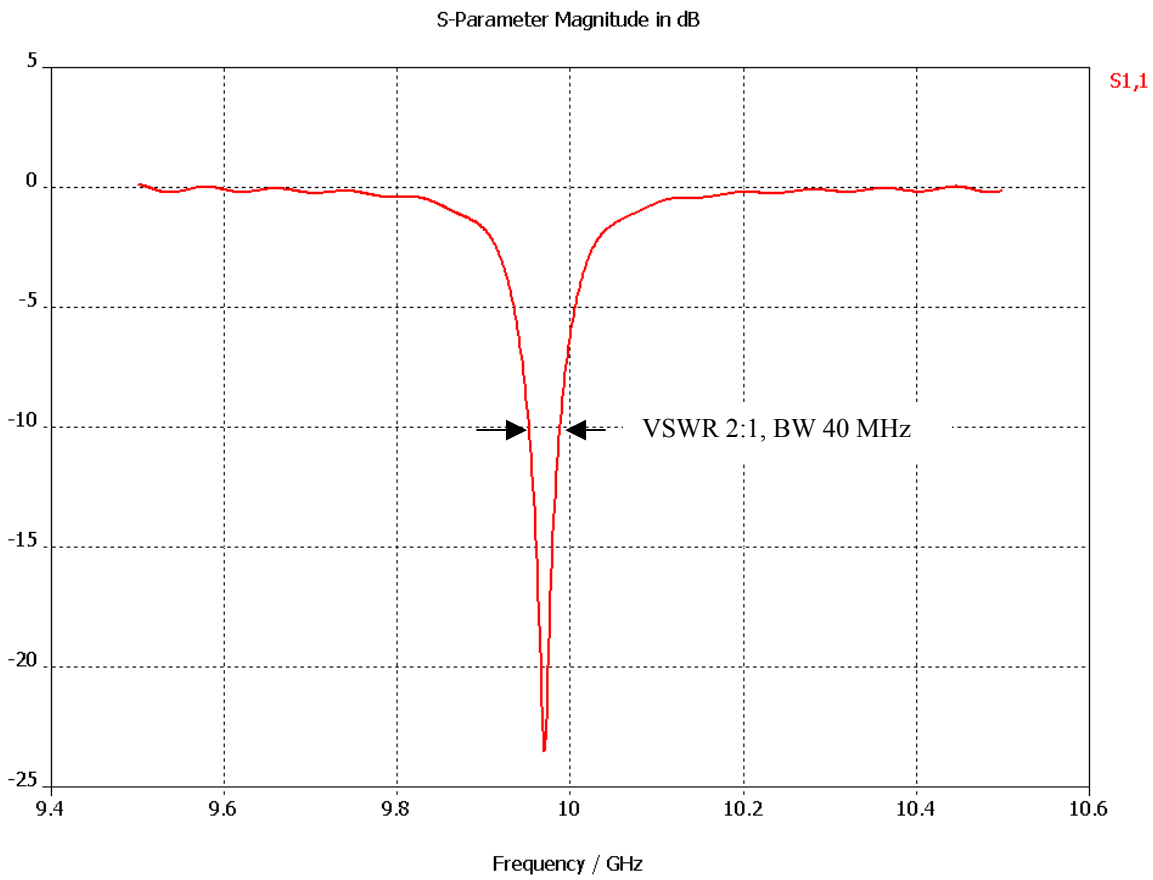

Figure 49. Computed return loss of the circular patch antenna normalized to 50 Ω. (Microwave Studio simulation).

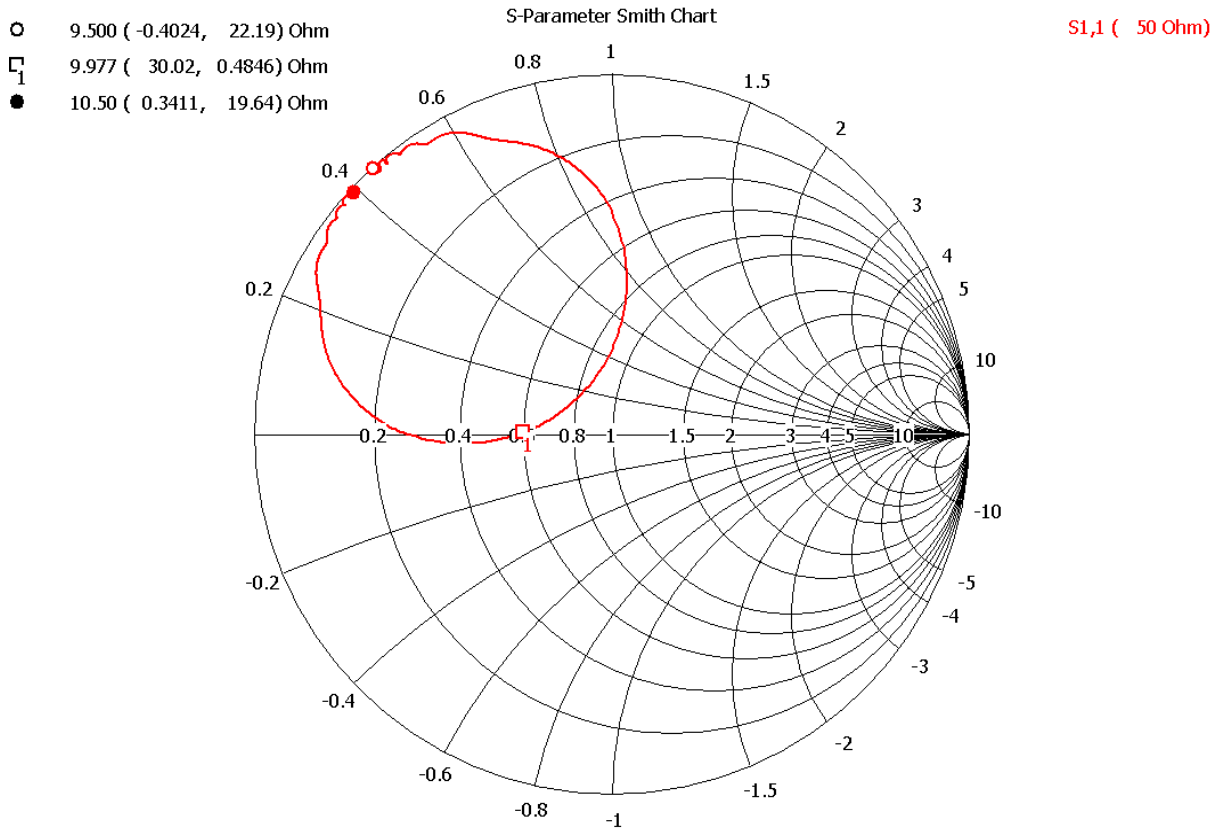

Figure 50. Smith chart plot of the computed input impedance of the circular patch antenna (Microwave Studio simulation).

B. INPUT AND OUTPUT LOW PASS FILTERS

1. Theory

The two Low Pass Filters (LPFs) implemented for each rectenna element were maximally flat response stepped impedance filters. This type of filter is characterized by the insertion loss method, that is, the filter response is defined by its insertion loss, or power loss ratio $P_{LR.}$ [Ref. 32]. The power loss ratio can be expressed as

$$P_{LR} = \frac{\text{Power available from source}}{\text{Power delivered to the load}} = \frac{1}{1-\left|\Gamma(\omega)\right|^2}. \tag{5.24}$$

This quantity is the reciprocal of $\left|S_{12}\right|^2$, provided that both load and source are matched. The insertion loss (IL) in dB is given by

$$IL = 10\log P_{LR}. \tag{5.25}$$

The factor $\left|\Gamma(\omega)\right|^2$ is an even function of ω [Ref. 28]; therefore it can be expressed as a polynomial in ω^2.

The maximally flat filter response, known also as the binomial or Butterworth response is an optimum filter response in the sense that it provides the flattest possible passband response for a given filter order. The power loss ratio of a maximally flat LPF can be expressed as follows

$$P_{LR} = 1 + k^2 \left(\frac{\omega}{\omega_c} \right)^{2N}, \tag{5.26}$$

where N is the order of the filter and ω_c is the cutoff frequency. The passband extends from $\omega = 0$ to $\omega = \omega_c$. At the band edge the power loss ratio is $1+k^2$. For k=1 this point corresponds to -3 dB point. For $\omega > \omega_c$, the attenuation increases monotonically with frequency as shown in Figure 51. For $\omega \gg \omega_c$, $P_{LR} \simeq k^2 \left(\omega/\omega_c\right)^{2N}$, which means that the insertion loss increases as the rate of 20N dB/decade.

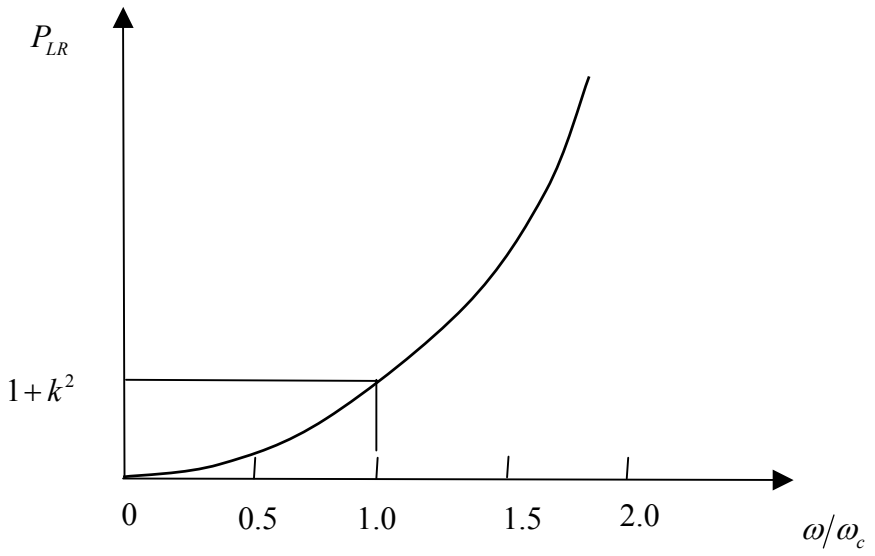

Figure 51. Maximally flat low-pass filter response for N=3 [From Ref. 32].

If the two-element low-pass filter is as shown in Figure 52, Equation (5.24) can be used to determine the values of the normalized elements L and C. For example if $N=2$, the normalized element values of the filter are $L = C = \sqrt{2}$. A table with the normalized element values for N = 1 to 10 can be found in [Ref. 32]. These data are used for ladder circuits where the element values are numbered from g_0 at the generator impedance, to g_{N+1} at the load impedance, for the filter having N reactive elements.

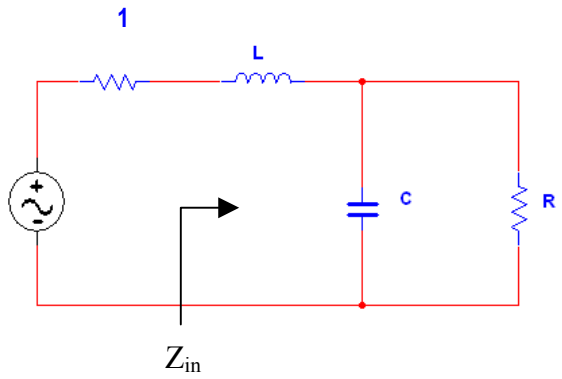

Figure 52. Low-pass filter prototype N=2 [From Ref. 32].

The implementation of a maximally flat low-pass filter using microstrip lines, can be realized by using alternate sections of high and low impedance lines. This type of filter is known as stepped impedance filter. A stepped impedance filter takes up less space than similar response low pass filters, which can be implemented using stubs. This is obviously an advantage for the present project since the design should be as small as possible, in order to reduce the weight.

The Z parameters of a transmission line of length ℓ and characteristic impedance Z_0, can be expressed as

$$\begin{aligned} Z_{11} &= Z_{22} = -jZ_0 \cot \beta\ell, \\ Z_{12} &= Z_{21} = -jZ_0 \csc \beta\ell. \end{aligned} \tag{5.27}$$

The equivalent circuits for a short section of transmission lines having either very small or very large characteristic impedance are illustrated in Figure 60. The series elements of the T-equivalent circuit are

$$Z_{11} - Z_{12} = -jZ_0 \left[\frac{\cos(\beta\ell) - 1}{\sin \beta\ell} \right] = jZ_0 \tan\left(\frac{\beta\ell}{2} \right), \tag{5.28}$$

while the shunt elements of the *T*-equivalent circuit is Z_{12}. This means that if $\beta\ell < \pi/2$, the series elements have a positive reactance (inductors), whereas the shunt elements have negative reactance (capacitors). Using the equivalent circuits of Figure 53, the electrical lengths of the inductor and capacitor sections are given by [Ref. 32] as

$$\begin{aligned} \beta\ell &= \frac{LR_0}{Z_h} \quad \text{inductor,} \\ \beta\ell &= \frac{CZ_l}{R_0} \quad \text{capacitor,} \end{aligned} \tag{5.29}$$

where:

Z_h is transmission line with high impedance,
Z_l is transmission line with low impedance, and
R_0 is the characteristic impedance of the filter.

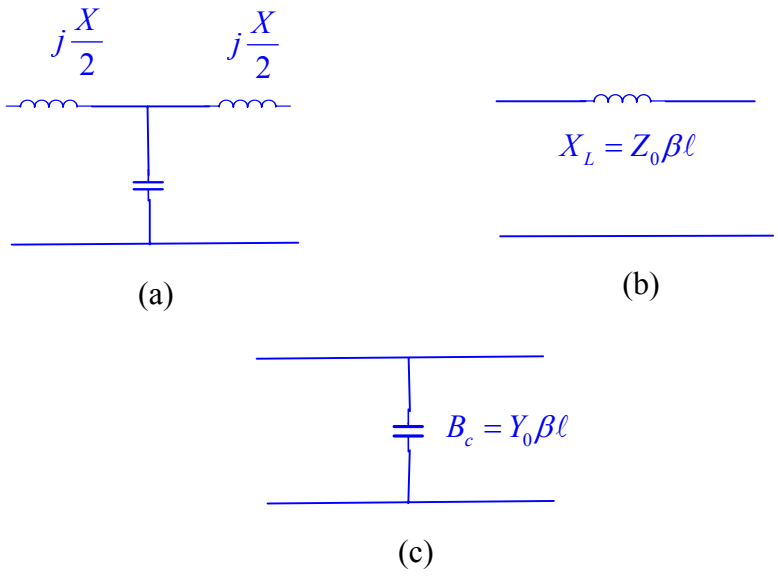

Figure 53. Approximate circuits for short sections of transmission lines. (a) T-equivalent circuit for a line having $\beta\ell \ll \pi/2$. (b) Equivalent circuit for small $\beta\ell$ and large Z_0. (c) Equivalent circuit for small $\beta\ell$ and small Z_0 [From Ref. 32].

2. Design and Fabrication

The input and output low pass filters were designed following the theoretical analysis presented in the previous section. The two filters were etched on the same substrate. The input impedance was designed to be 30 Ω, in order to match the calculated input impedance of the diode. The material used is RT Duroid® 5870, manufactured by Rogers Corporation. It exhibits dielectric constant ε_r =2.33, and loss tangent $\tan\delta$ = 0.0012 at 10 Ghz. The thickness of the substrate is 0.127 mm, and both sides are electrodeposited with ½ oz copper. Since the substrate is extremely thin, the transmission lines etched were restricted to have very small width, especially for high impedance. Thus, the highest line impedance realizable is 100 Ω, which corresponds to the high impedance section, Z_h of the filter. Similarly, a line impedance of 10 Ω corresponds to the low impedance section Z_l.

The characteristic impedance of a microstrip line is given by [Ref. 32]

$$Z_0 = \begin{Bmatrix} \dfrac{60}{\sqrt{\varepsilon_e}} \ln\left(\dfrac{8d}{W} + \dfrac{W}{4d}\right) & \text{for } W/d \le 1 \\ \dfrac{120\pi}{\sqrt{\varepsilon_e}\left[W/d + 1.393 + 0.667\ln\left(W/d + 1.444\right)\right]} & \text{for } W/d \ge 1, \end{Bmatrix} \tag{5.30}$$

where:

W is the width of the transmission line,

d is the height of the substrate, and

ε_e is the effective dielectric constant of the substrate.

For a given characteristic impedance Z_0, and dielectric constant ε_r, the W/d ratio is expressed as

$$\frac{W}{d} = \begin{Bmatrix} \dfrac{8e^A}{e^{2A} - 2} & \text{for } W/d \le 2 \\ \dfrac{2}{\pi}\left[B - 1 - \ln\left(2B - 1\right) + \dfrac{\varepsilon_r - 1}{2\varepsilon_r}\left\{\ln\left(B - 1\right) + 0.39 - \dfrac{0.61}{\varepsilon_r}\right\}\right] & \text{for } W/d > 2, \end{Bmatrix} \tag{5.31}$$

where

$$A = \frac{Z}{60}\sqrt{\frac{\varepsilon_r + 1}{2}} + \frac{\varepsilon_r - 1}{\varepsilon_r + 1}\left(0.23 + \frac{0.11}{\varepsilon_r}\right), \text{ and } B = \frac{377\pi}{2Z_0\sqrt{\varepsilon_r}}.$$

The effective dielectric constant of the line is given by

$$\varepsilon_e = \frac{\varepsilon_r + 1}{2} + \frac{\varepsilon_r - 1}{2}\frac{1}{\sqrt{1 + 12\,d/W}}. \tag{5.32}$$

Similarly, the effective wavelength can be expressed as

$$\lambda_e = \frac{c}{f\sqrt{\varepsilon_e}}, \tag{5.33}$$

where f is the cutoff frequency of the filter.

From (5.30), (5.31) and (5.32) the width d, effective dielectric constant ε_e, and effective wavelength λ_e, were calculated as follows

$$Z_0 = 30\ \Omega \rightarrow W = 0.74\ \text{mm} \rightarrow \varepsilon_e = 2.035 \rightarrow \lambda_e = 0.0175\ \text{m},$$
$$Z_l = 10\ \Omega \rightarrow W = 2.7\ \text{mm} \rightarrow \varepsilon_e = 2.198 \rightarrow \lambda_e = 0.01686\ \text{m},$$
$$Z_h = 100\ \Omega \rightarrow W = 0.085\ \text{mm} \rightarrow \varepsilon_e = 1.775 \rightarrow \lambda_e = 0.0187\text{m}.$$

The input low pass filter is a four section, (N=4), maximally flat response filter. Since its purpose is to avoid harmonic generated signals to reradiate back to the patch antenna, its cutoff frequency selected to be 12 GHz. Then, for the frequency of 20 GHz, $\left|\frac{\omega}{\omega_c}\right| - 1 = \frac{20}{12} - 1 = 0.66.$ Therefore, the attenuation given by Figure 54 for n=4 is 15 dB.

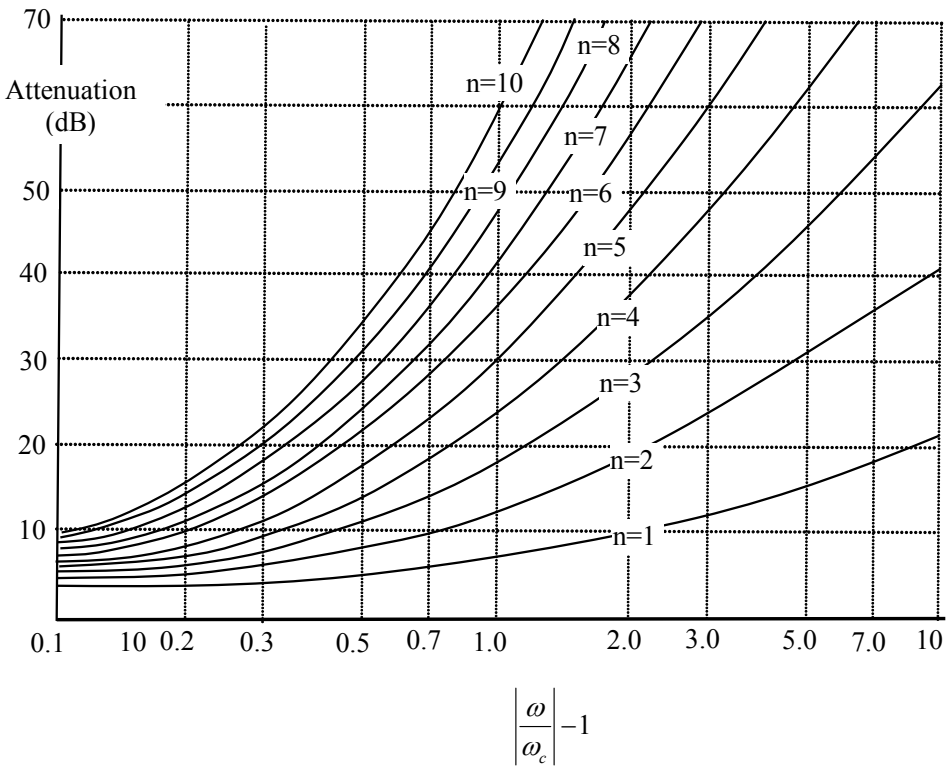

Figure 54. Attenuation versus normalized frequency for maximally flat filter prototypes [From Ref. 32].

The low pass prototype values are as follows

$$g_1 = 0.7654,$$
$$g_2 = 1.8478,$$
$$g_3 = 1.8478,$$
$$g_4 = 0.7654,$$
$$g_5 = 1.000.$$

Using the normalized values for the maximally flat prototype the prototype low pass filter can be realized as shown in Figure 55.

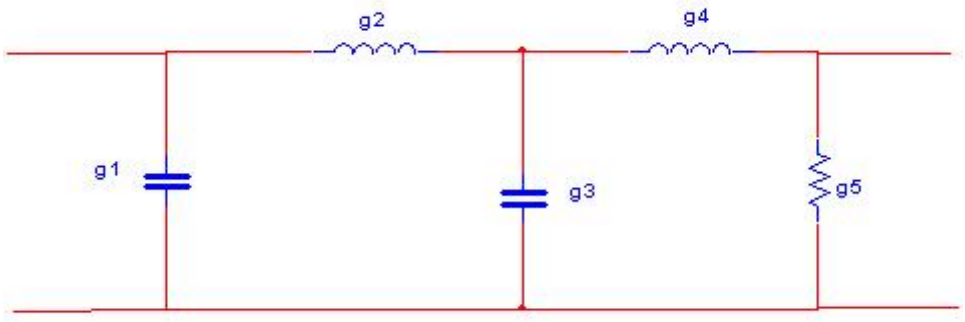

Figure 55. Schematic layout of the input low pass filter realized by the normalized element values.

The electrical lengths of the lines which correspond to the filter sections can be calculated as follows:

$$\begin{aligned}
\beta\ell_1 &= g_1 \frac{Z_l}{R_0} = \frac{0.7654\times 10}{30} = 0.259 \quad \text{rad},\\
\beta\ell_2 &= g_2 \frac{R_0}{Z_h} = \frac{1.8478\times 30}{100} = 0.551 \quad \text{rad},\\
\beta\ell_3 &= g_3 \frac{Z_l}{R_0} = \frac{1.8478\times 10}{30} = 0.625 \quad \text{rad},\\
\beta\ell_4 &= g_4 \frac{R_0}{Z_h} = \frac{0.7654\times 30}{100} = 0.551 \quad \text{rad},\\
\beta\ell_5 &= g_5 = 1 \quad \text{rad}.
\end{aligned} \tag{5.34}$$

The actual lengths of the transmission line sections can be evaluated if (5.33) is solved with respect to ℓ. Thus using the values for the width of the lines, the effective wavelength, and the effective dielectric constant, which were calculated previously, the lengths of the filter sections can be calculated as

$$\ell_1 = \frac{\lambda_{e(l)} \times 0.259}{2\pi} = \frac{0.0168 \times 0.259}{2\pi} = 0.692 \text{ mm} \rightarrow 27.244 \text{ mils}$$
$$\ell_2 = \frac{\lambda_{e(h)} \times 0.551}{2\pi} = \frac{0.0187 \times 0.551}{2\pi} = 1.639 \text{ mm} \rightarrow 64.527 \text{ mils}$$
$$\ell_3 = \frac{\lambda_{e(l)} \times 0.625}{2\pi} = \frac{0.0168 \times 0.625}{2\pi} = 1.67 \text{ mm} \rightarrow 65.747 \text{ mils} \qquad (5.35)$$
$$\ell_4 = \frac{\lambda_{e(h)} \times 0.230}{2\pi} = \frac{0.0187 \times 0.230}{2\pi} = 0.687 \text{ mm} \rightarrow 27.047 \text{ mils}$$
$$\ell_5 = \frac{\lambda_{e(0)}}{2\pi} = \frac{0.0175}{2\pi} = 2.785 \text{ mm} \rightarrow 109.645 \text{ mils}$$

The input low pass filter was simulated in the Advance Design System (ADS) software, and its response is illustrated in Figure 56. As shown in the figure the attenuation at the second harmonic of 20 GHz is -14 dB.

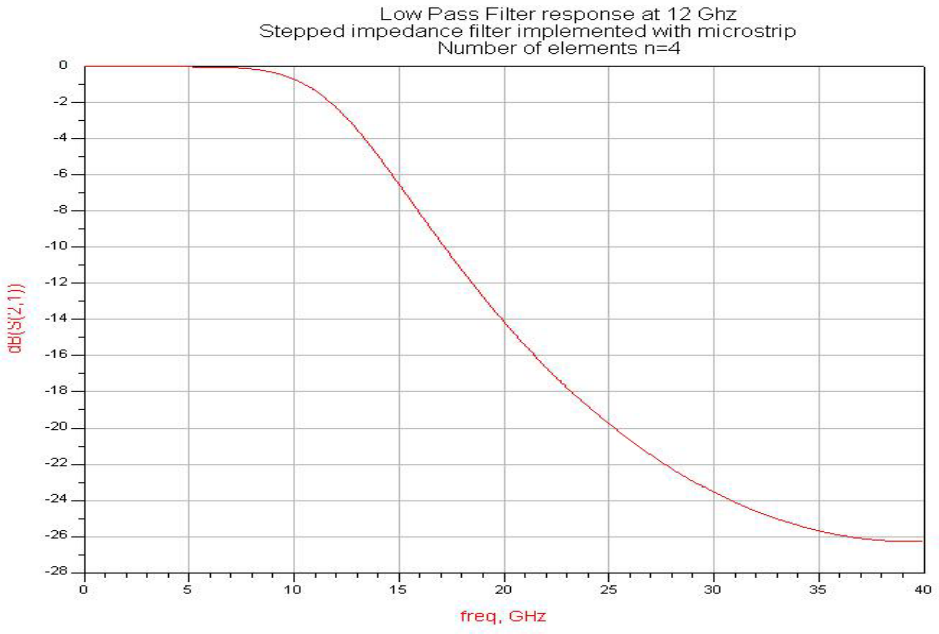

Figure 56. Computed input low pass filter response. (Advance Design System simulation)

The same procedure was followed in the design of the output LPF. The purpose of the output LPF is to avoid microwave frequencies passing through the dc line. Thus,

this filter is designed to have a cutoff frequency of 2 GHz. Since the first microwave frequency to be rejected by the filter is the fundamental frequency, the transition region of the filter is large and therefore, a relatively simple filter is adequate.

For a filter with cutoff frequency of 2 GHz the attenuation at 10 GHz is evaluated as

$$\left|\frac{\omega}{\omega_c}\right| - 1 = \frac{10}{2} - 1 = 4. \tag{5.36}$$

Thus, using Figure 54 for n=2 the attenuation at 10 GHz is more than 25 dB. Using same impedance values for Z_h, Z_l and Z_0, the lengths of the microstrip line sections are evaluated as

$$\begin{aligned} \beta\ell_1 &= g_1 \frac{Z_0}{Z_h} = \frac{1.4142 \times 30}{100} = 0.424 \quad \text{rad}, \\ \beta\ell_2 &= g_2 \frac{Z_l}{Z_0} = \frac{1.4142 \times 10}{30} = 0.471 \quad \text{rad}, \end{aligned} \tag{5.37}$$

and the actual lengths of the filter sections are

$$\begin{aligned} \ell_1 &= \frac{\lambda_{e(h)} \times 0.424}{2\pi} = \frac{0.0187 \times 0.424}{2\pi} = 7.6 \text{ mm} \rightarrow 299.21 \text{ mils}, \\ \ell_2 &= \frac{\lambda_{e(l)} \times 0.471}{2\pi} = \frac{0.0168 \times 0.471}{2\pi} = 7.57 \text{ mm} \rightarrow 298.03 \text{ mils}. \end{aligned} \tag{5.38}$$

The output low pass filter was also simulated using the Advance Design System and the response as is illustrated in Figure 57.

The low pass filters were etched on a substrate brick of 23 by 20 mm. The input filter is connected through the feed probe with the patch antenna. Thus, microwave energy received by the antenna is fed to the input filter. The rectifying diode is connected between the last section of the input filter and the ground plane using via hole. The output filter starts just after the diode and prevents the microwave frequencies from reaching the dc line.

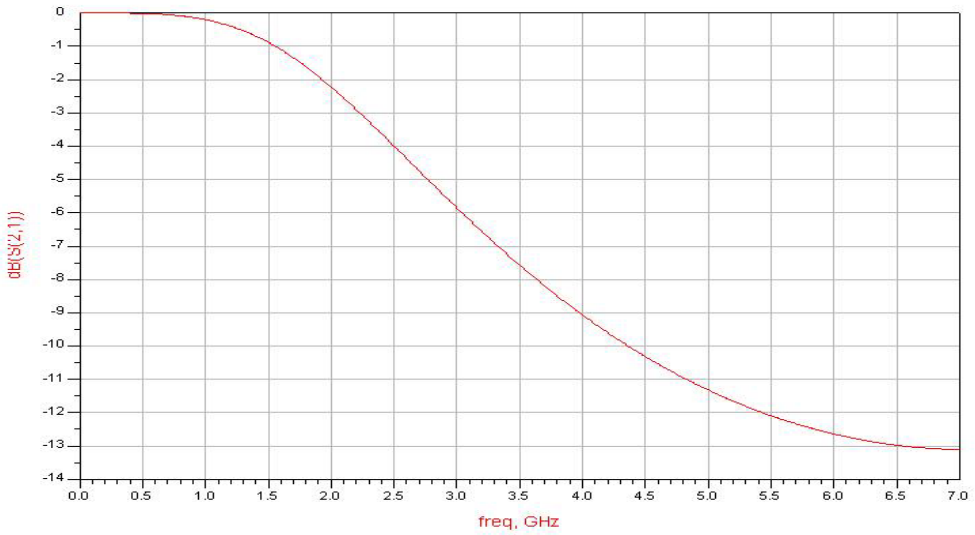

Figure 57. Computed output low pass filter response. (Advance Design System simulation)

C. SUMMARY

In this chapter the basic theory of a circular patch antenna has been presented. The circular patch antenna was selected for the rectenna element due to its inherent property of not resonating with harmonic frequencies. The return loss of the designed patch is -23 dB at 9.952 GHz, as predicted by CST Microwave Studio. PATCHD was also used for estimating the 30 Ω impedance point of the patch, where the antenna feed probe was attached.

A detailed analysis has been presented for the input and output low pass filter design. Both filters are maximally flat response stepped impedance filters, and optimized using Advance Design System. The attenuation of the input LPF is 15 dB at 20 GHz, while the attenuation of the output LPF is 25 dB at 2 GHz.

VI. RECTENNA FABRICATION AND TESTING

A. RECTENNA ELEMENT FABRICATION

Each rectenna element was built using the substrate bricks of the patch antenna and the low pass filters, which were described in Chapter V. The two boards have the same dimensions and therefore, are perfectly aligned when placed one on top of the other. For each element a piece of balsa wood was glued between the two microwave substrates for rigidity. A 0.25 mm diameter soldered probe connected the patch antenna with the low pass input filter. An HSMS 8101 diode was soldered at the end of the input filter and to the ground plane through a plated hole as shown in Figure 58. The dc line was connected at the end of the low pass output filter. The layout of the rectifier element is illustrated in Figure 59. A total of 20 rectenna elements were fabricated. The weight of each element was 0.41 g.

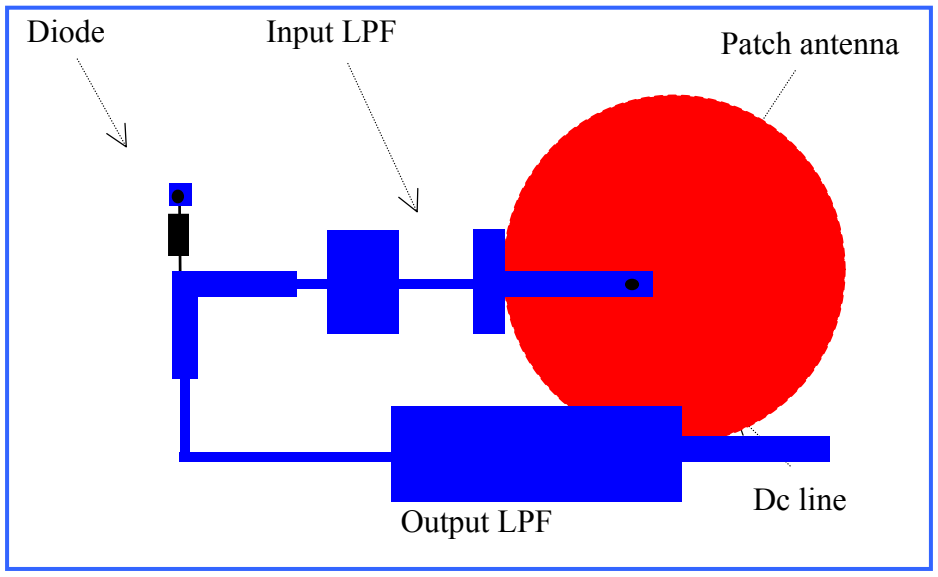

Figure 58. Schematic layout of the rectenna element.

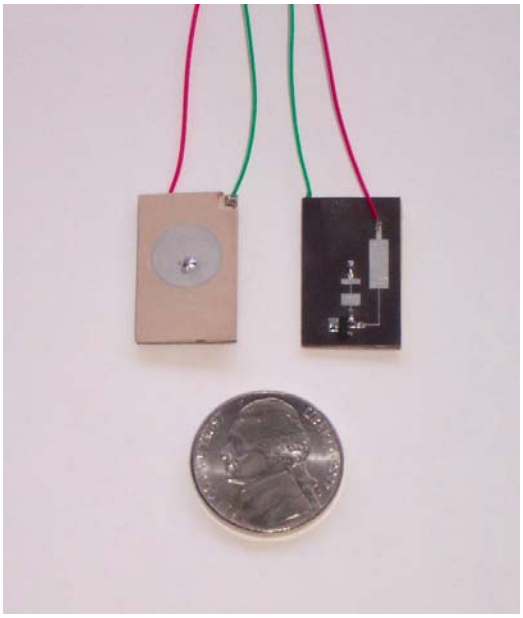

Figure 59. Rectenna element.

B. RECTENNA ELEMENT MEASUREMENT

As mentioned in Chapter II the overall efficiency of a rectenna element is defined as the total dc output power at the load in proportion to the incident power. Thus, any power that is reflected by the circuitry is not converted into dc power and decreases the overall efficiency [Ref. 18]. Using the Friis link equation the efficiency of the rectifier can be expressed as

$$n = \frac{P_{dc}}{P_{rec}} = \frac{4\pi R^2 P_{dc}}{P_{trans} G_{trans} A^{eff}}, \tag{6.1}$$

where:

G_{trans} is the gain of the transmitting antenna,

P_{trans} is the transmitted power,

R is the distance from the transmitting antenna, and

A^{eff} is the effective area of the receiving antenna.

The effective area of the patch is

$$A^{eff} = G_{rec} \frac{\lambda^2}{4\pi}, \tag{6.2}$$

where G_{rec} is the gain of the patch. For the current circular patch antenna design, the effective area is calculated as 3.23 cm^2, where the computed gain of 6.54 dB was used.

Each rectenna element was measured in the laboratory for efficiency. An HP8530B microwave oscillator was used as power source for a 10 GHz microwave signal. The signal was passed through a Hughes 1277 H03F amplifier and fed to a Narda 20 dB horn antenna. The output from the amplifier was measured with a HP435A power meter. The rectenna element was mounted on a mast opposite from the transmitting antenna at a distance of 70 cm. A decade resistance box was used for varying the load at the element. A digital voltmeter together with an ammeter was used for current and voltage monitoring at the load. Also a TDS 3012B oscilloscope was used to verify that the output from the rectenna element was dc current. The block diagram of the measurement system is illustrated in Figure 60.

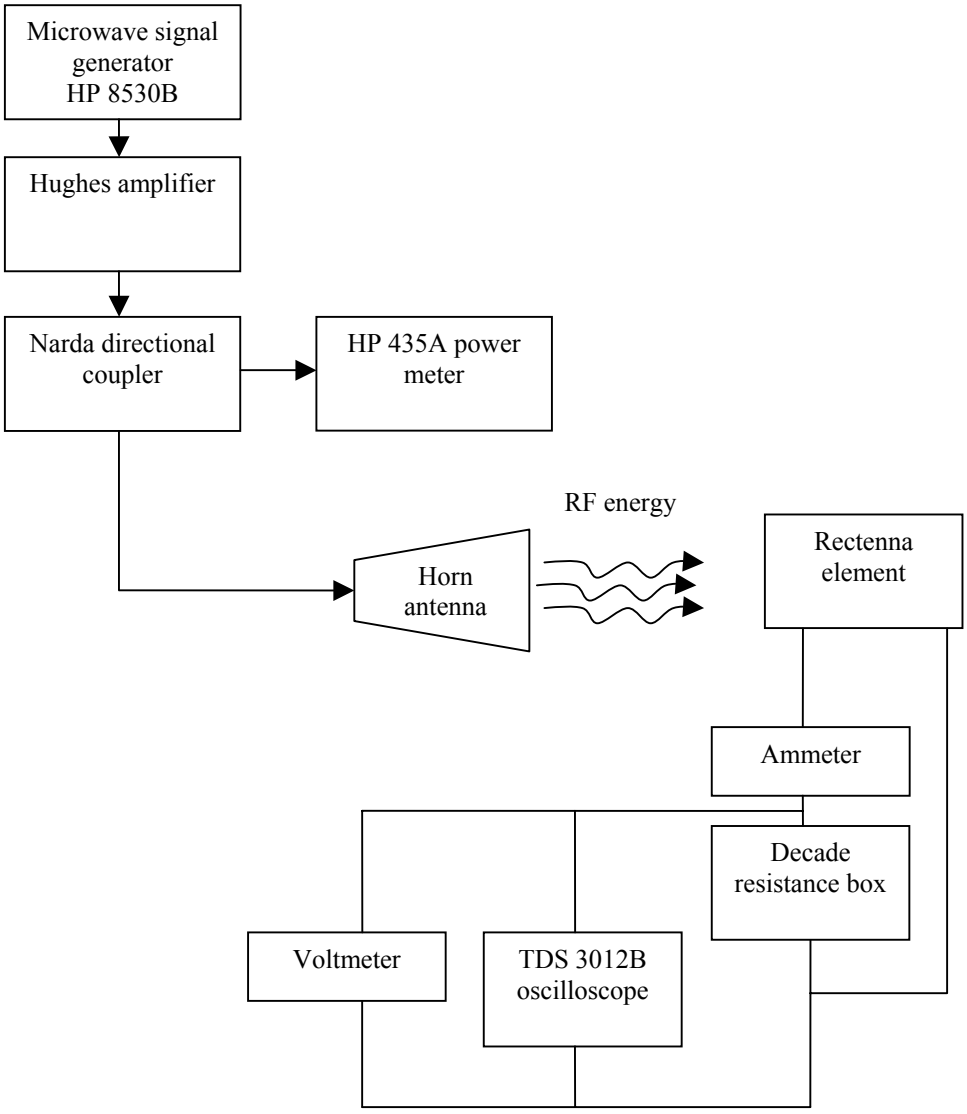

Figure 60. Block diagram of the rectenna element measurement system.

Each of the 20 rectenna elements was measured separately for different values of resistive load. Initially 1 W output microwave amplifier was used for signal amplification. However, for an effective measurement, the diodes on the rectenna elements have to be biased at a relatively high power level [Ref. 18]. For this reason the measurement was repeated using the 20 W output amplifier, where the output power was varied from 1 to 18 W.

Although the elements were theoretically identical, the measured dc output power was slightly different on each of them. This difference can be attributed to impedance mismatches introduced by soldering irregularities of the patch antenna feed probe and the diode. This can also be verified from the fact that the resonant frequency for each element was different by a factor of 30 MHz. The resonant frequency of the elements was estimated as 9.75 ± 0.015 GHz. The efficiency of the elements was calculated using Equations (6.1) and (6.2) and found to be 10.3%. The low efficiency value is mainly a result of the aforementioned mismatches. The very thin substrate used for the antenna and rectifier manufacturing was also responsible for losses which reduce the overall system efficiency. However, as mentioned in Chapter V, the selection of a very thin substrate was imperative in order to keep the weight of the rectenna as low as possible. The voltage versus current for three elements, when the resistive load was varied, is presented in Tables 8, 9 and 10 and Figure 61. As shown in Figure 62, where the dc output power versus the resistive load is illustrated, for all three elements the maximum dc output power occurs when the resistive load takes values from 250 to 1500 Ω. The output power when the load is 50 Ω varies from 4 to 5 mW, which corresponds to an efficiency of 4.5% as illustrated in Figure 63.

Element 1			
Current (mA)	Voltage (V)	dc Power (mW)	Load (Ω)
10.02	0.505	5.0601	50
8.88	0.9	7.992	100
6.71	1.65	11.0715	250
4.71	2.374	11.1627	500
2.27	3.4	7.718	1,500
0.39	4.39	1.7121	10,000
0.02	4.71	0.0942	10^6

Table 9. Measured data for the first rectenna element ($f = 9.975$ GHz).

Element 2			
Current (mA)	Voltage (V)	dc Power (mW)	Load (Ω)
10.00	0.500	5	50
7.88	0.91	7.098	100
6.75	1.62	10.935	250
4.9	2.3	11.27	500
2.2	3.45	7.59	1,500
0.4	4.3	1.72	10,000
0.02	4.7	0.094	10^6

Table 10. Measured data for the second rectenna element $(f = 9.971 \text{ GHz})$.

Element 3			
Current (mA)	Voltage (V)	dc Power (mW)	Load (Ω)
8.45	0.426	3.5997	50
7.25	0.635	4.60375	100
5.93	1.384	8.20712	250
4.43	2.151	9.52893	500
2.32	3.44	7.9808	1,500
0.39	4.41	1.7199	10,000
0.04	4.46	0.1784	10^6

Table 11. Measured data for the third rectenna element $(f = 9.968 \text{ GHz})$.

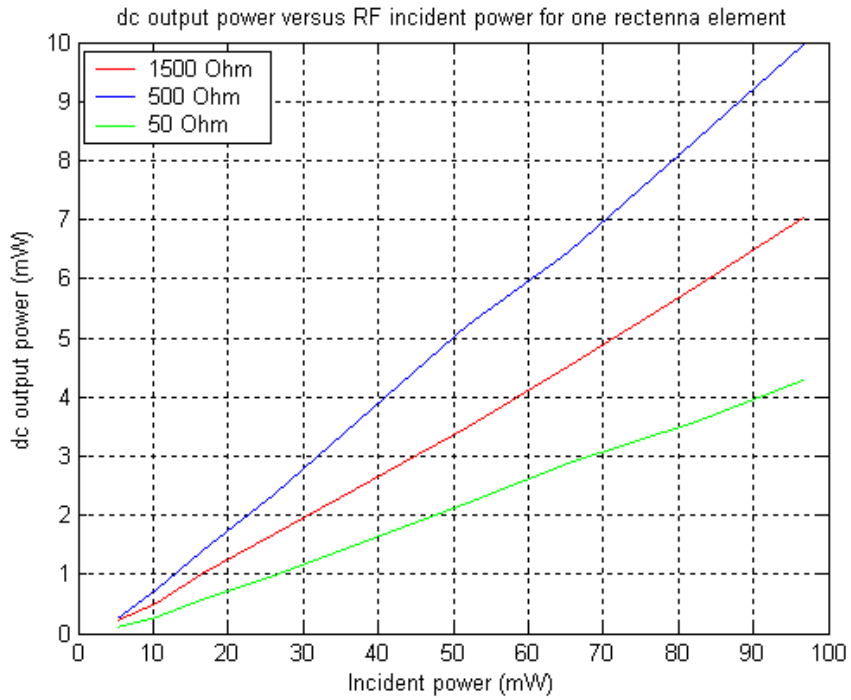

Figure 61. Dc output power versus microwave received (P_{rec}) for one rectenna element ($f = 9.975$ GHz).

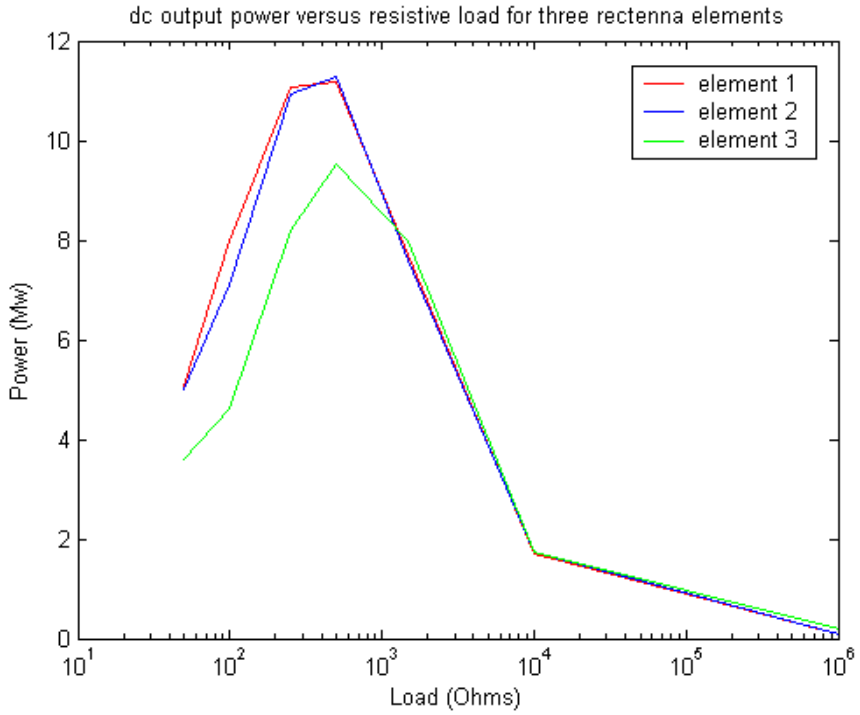

Figure 62. Dc output power versus resistive load for three rectenna elements.

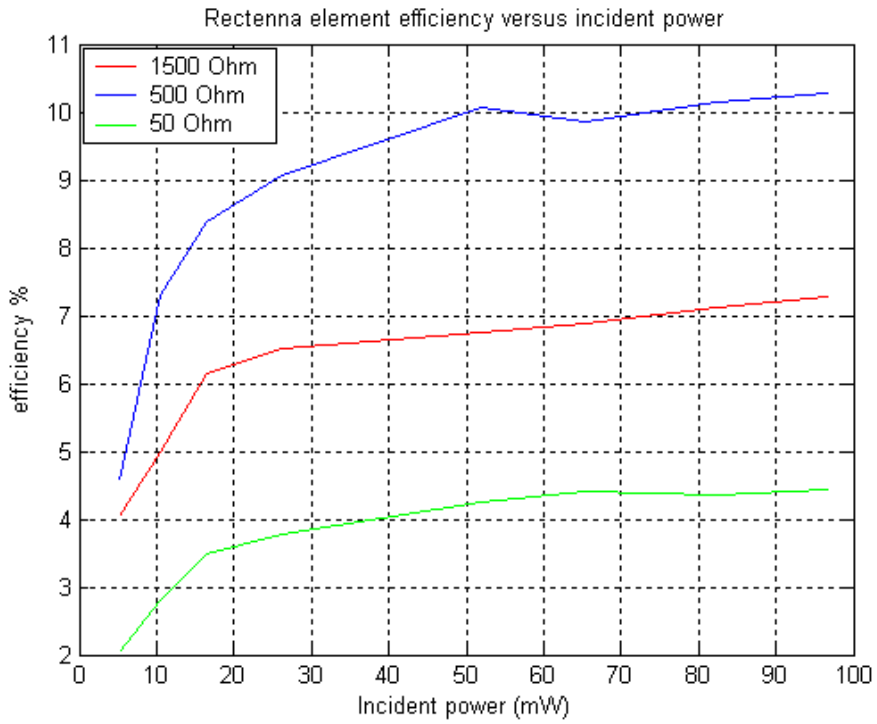

Figure 63. Rectenna efficiency measurement ($f = 9.975$ GHz).

C. RECTENNA TESTING

The individual rectenna element was used as building block for the rectenna array. A total of sixteen elements were attached together using very thin carbon rods. The result was an array 8 by 11 cm weighting 9 g, which is shown in Figure 64. To reduce mutual coupling, the elements were placed 0.6 cm apart from each other. This resulted in a distance of 2 cm between the centers of the patches. To achieve the voltage and current parameters corresponding to the MAV's motor when this is used as load for the rectenna, various element interconnections were tested. The same measurement system as for the individual elements was used for measuring the rectenna array (Figure 65). The results from the measurement are illustrated in Figures 66 to 73. As can be seen the rectenna efficiency depends on the resistive load and the type of element connection. Thus, the maximum efficiency of 8.2% was achieved when a series combination of the elements of the two top and the two bottom rows were connected in parallel and the resistive load was 1500 Ω. The efficiency of this configuration was 6% and 1.2% when the resistive load was 500 and 50 Ω correspondingly. The maximum efficiency of the parallel connection was 4.3% for a resistive load of 50 Ω, while the values for 500 and 1500 Ω were 1.3%

and 0.5% correspondingly. Accordingly the maximum efficiency for series element connection was 4.5%, 6.5% and 2.8% for the resistive loads of 1500, 500 and 50 Ω. The dc output power from the rectenna was below the power required for the MAV to fly when the transmitted power was 18.6 W. A maximum of 450 RPM of the MAV rotors was obtained when a parallel connection of the elements was used. With 18.6 W of transmitting power, 84% conversion efficiency is required for dc output power of 1.3 W (as much as required for the MAV to hover when it carriers the weight of the rectenna) provided that all the other parameters of the rectenna remain the same.

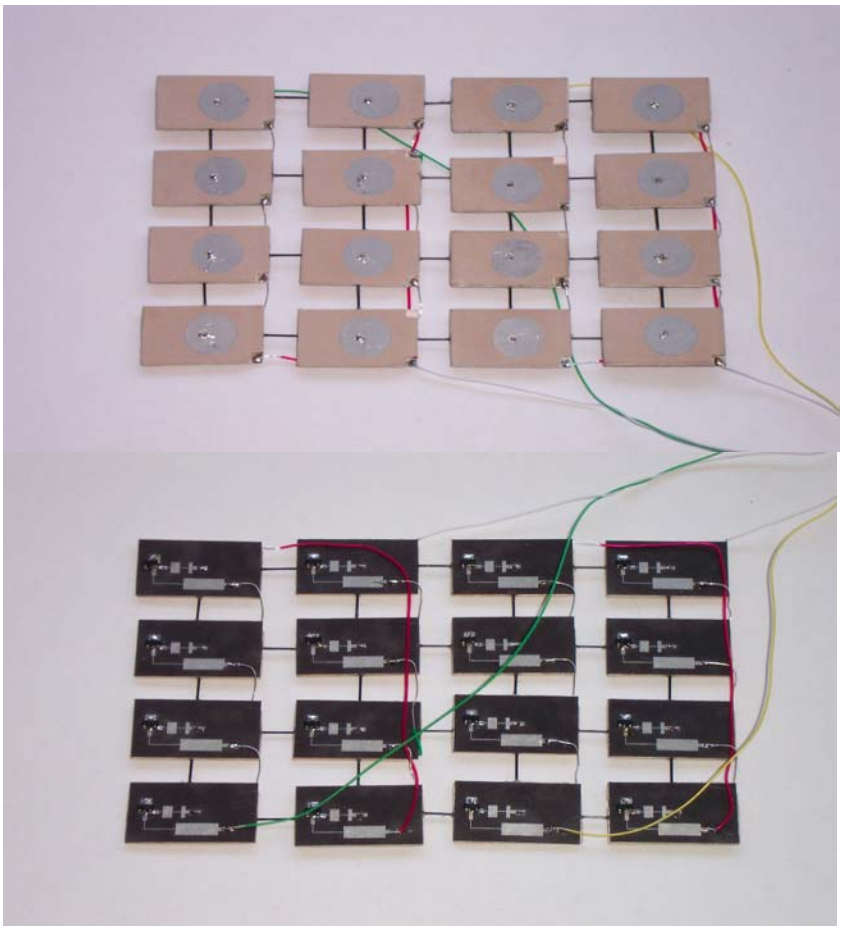

Figure 64. Rectenna array in mixed connection configuration. (a) Front view, (b) Rear view.

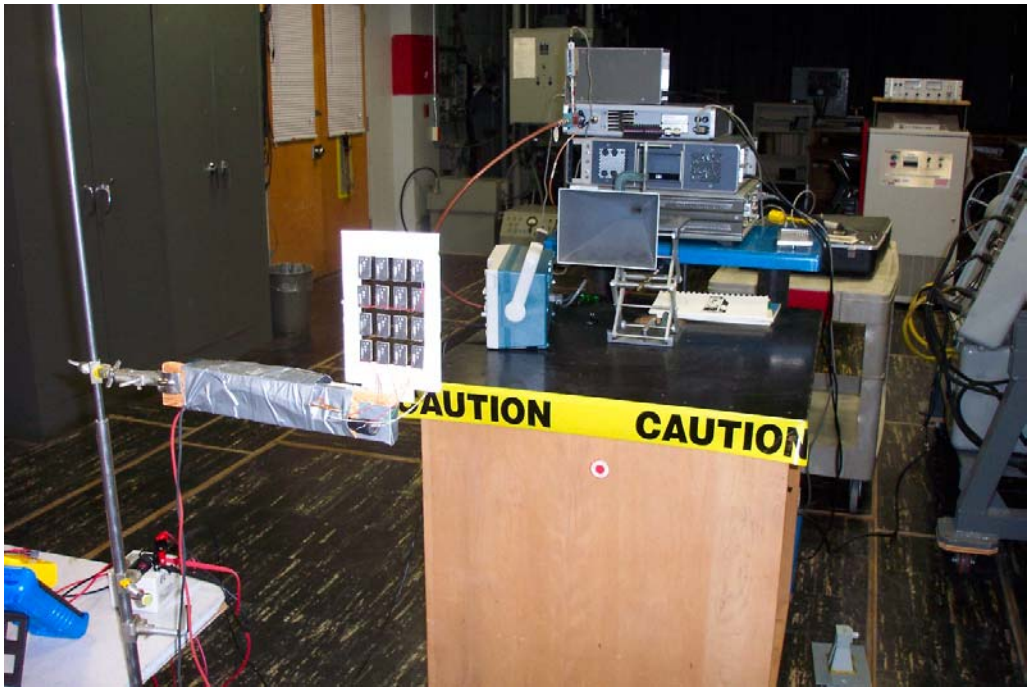

Figure 65. Rectenna measurement system.

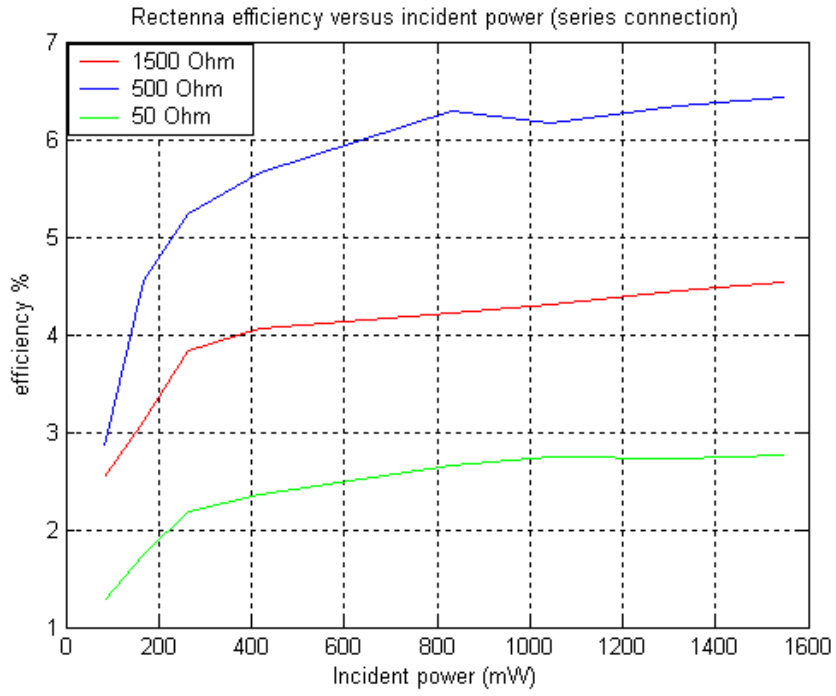

Figure 66. Rectenna efficiency when the elements are connected in series ($f = 9.975$ GHz).

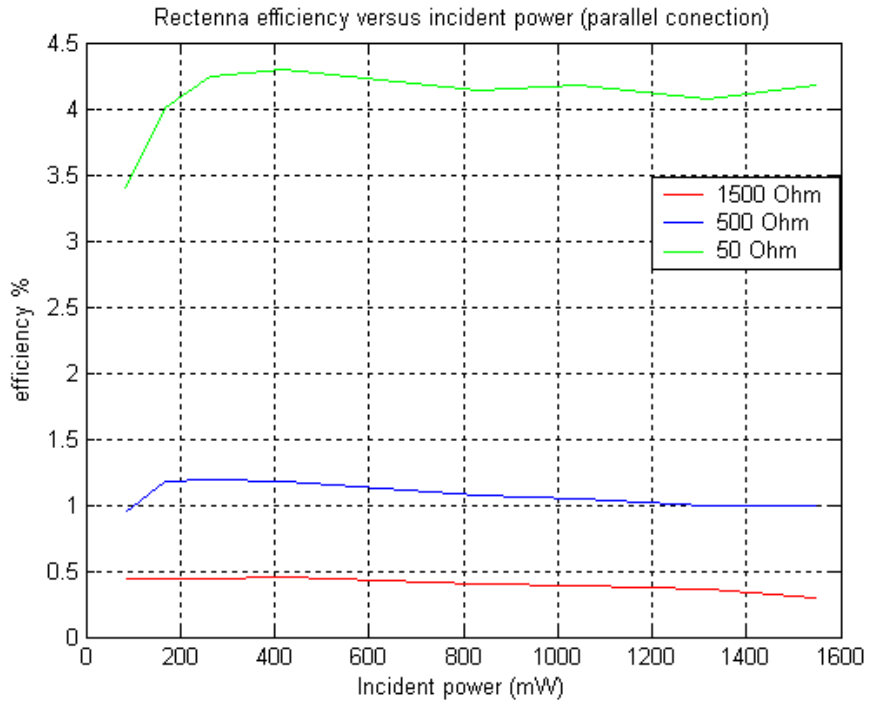

Figure 67. Rectenna efficiency when the elements are connected in parallel ($f = 9.975$ GHz).

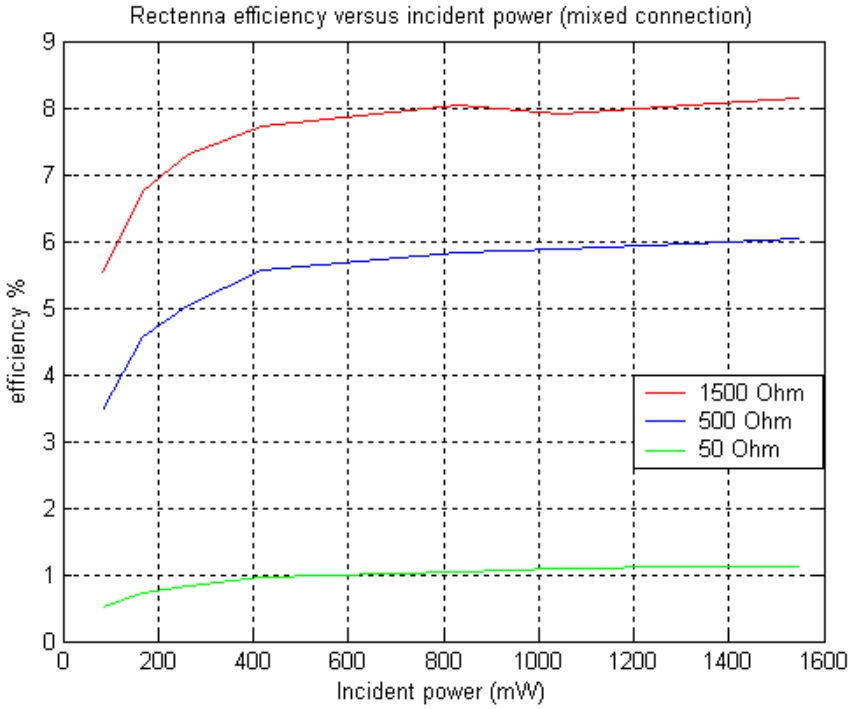

Figure 68. Rectenna efficiency when two series combinations of elements are connected in parallel ($f = 9.975$ GHz).

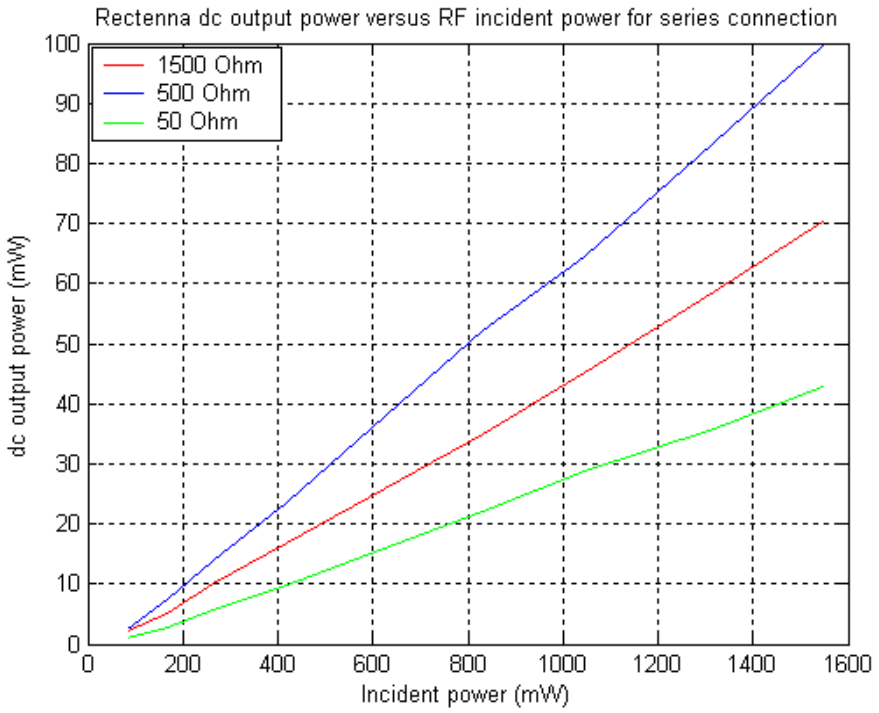

Figure 69. Rectenna dc output power versus incident power for series element connection ($f = 9.975$ GHz).

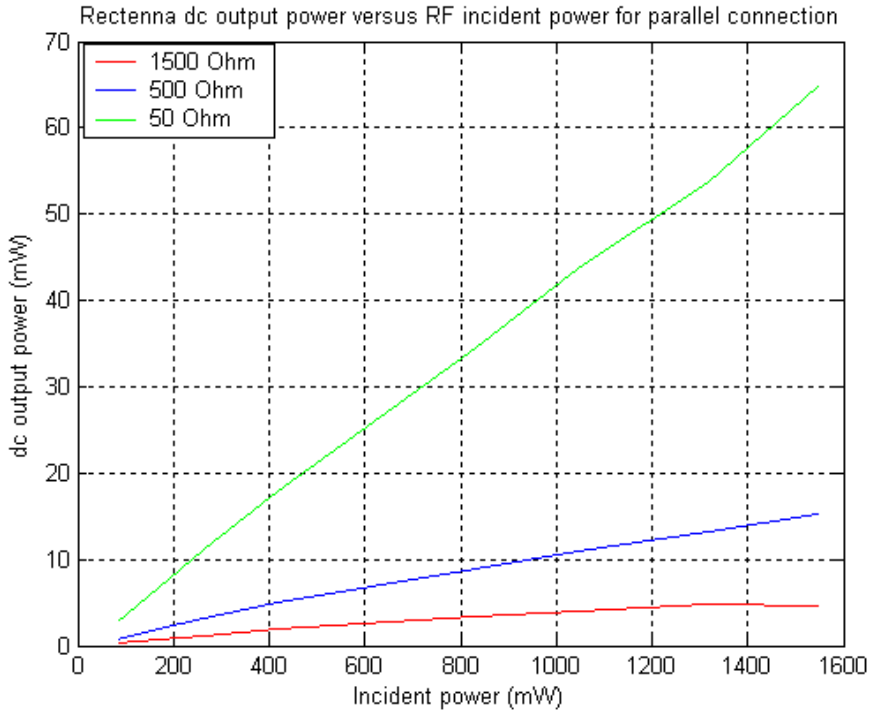

Figure 70. Rectenna dc output power versus incident power for parallel element connection ($f = 9.975$ GHz).

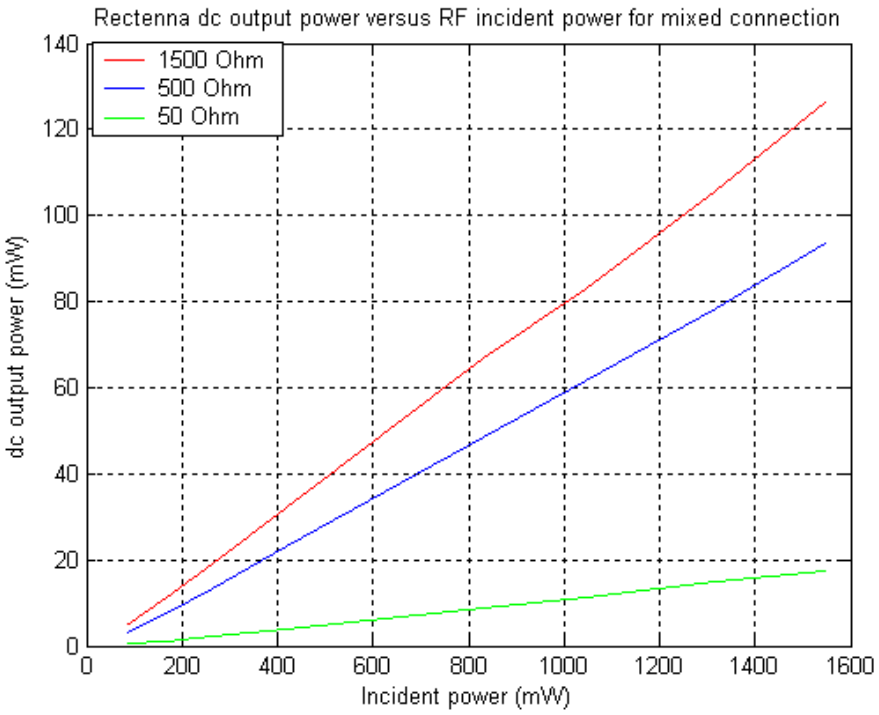

Figure 71. Rectenna dc output power versus incident power when two series combinations of elements are connected in parallel ($f = 9.975$ GHz).

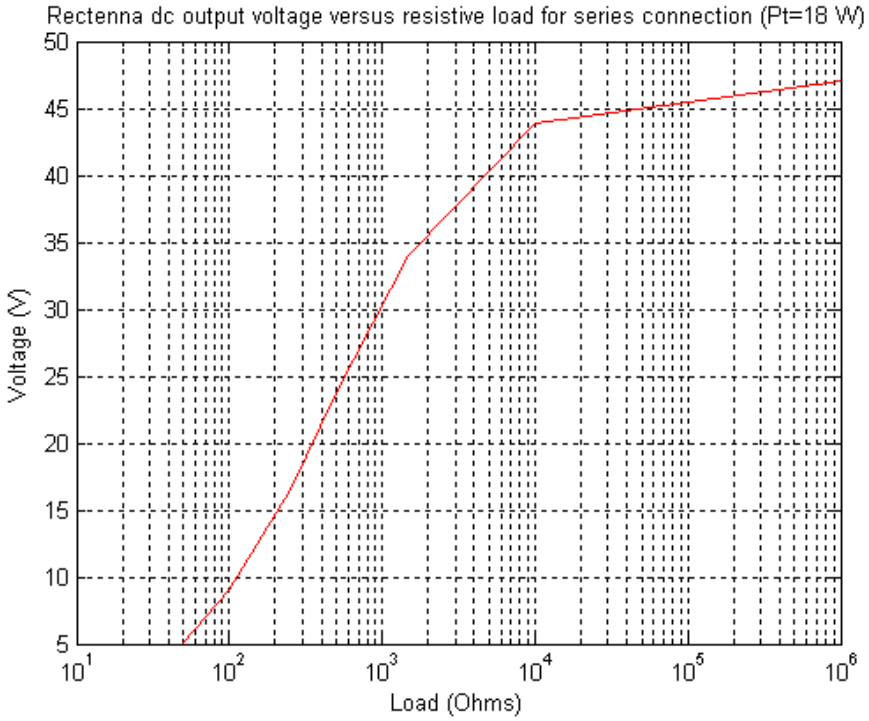

Figure 72. Rectenna dc output voltage versus resistive load for series connection ($f = 9.975$ GHz).

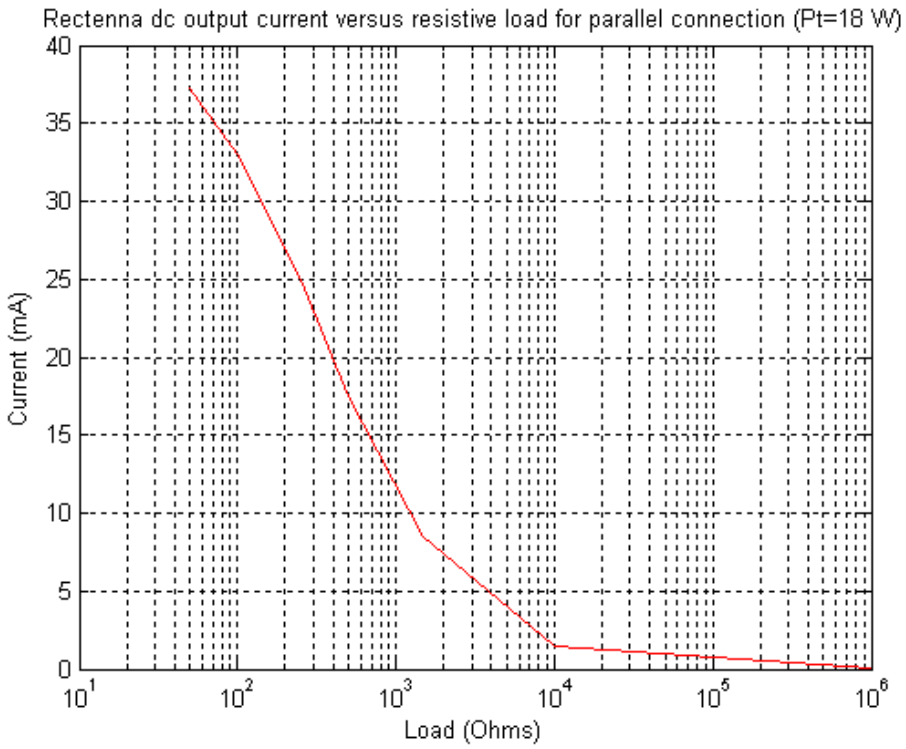

Figure 73. Rectenna dc output current versus resistive load for parallel connection ($f = 9.975$ GHz).

D. SUMMARY

In Chapter VI a detailed description of the rectenna element fabrication was given, together with the testing procedure. A total of 20 elements were tested in the laboratory for various power densities and load resistances at a distance of 70 cm away from the transmitter antenna. A relatively poor efficiency was achieved from the elements, which at best case was 10.3%. Moreover, the rectenna elements found to resonate in frequencies which were different by ± 15 MHz. These discrepancies are attributed to impedance mismatches introduced by soldering irregularities of the antenna probe feed and the diode.

A rectenna array was manufactured using sixteen elements. Various element interconnections were attempted to identify the best arrangement when the resistive load is 50 Ω (equal to the MAV's motor resistance). A parallel connection was found to be the most sufficient, since the output current is maximized. The maximum efficiency of this type of connection was 4.3%. The efficiency of the rectenna was maximized to 8.2% when two combinations of series connected elements, were connected in parallel.

The dc output power of the rectenna was below the minimum required for the MAV to fly. A maximum of 450 RPM of the MAV rotors was achieved when the parallel element connection was used.

THIS PAGE INTENTIONALLY LEFT BLANK

VII. CONCLUSION AND RECOMMENDATIONS

A. CONCLUSION

In this thesis the feasibility of powering a micro air vehicle using microwave energy has been studied both theoretically and experimentally. In Chapter II, the rich history of rectenna development has been presented together with the various experiments and demonstrations. The bar type dipole rectenna array first suggested by Brown was the basis for most of the rectenna designs. This initial design evolved to more efficient ones, since was well understood that the impedance mismatching of the circuit and the reradiation of the harmonics were the primary factors which reduced the rectenna efficiency. Thus, microwave input and output filters were added to maximize the efficiency. The progress continued further ahead with the adaptation of microstrip patch rectennas, introduced to alleviate the inherent bulkiness problem of the dipole rectennas.

An efficient implementation of a rectenna array suggests careful selection of the microwave diode used as rectifier. The Schottky barrier diode is considered to be the most sufficient for this purpose, due to its high frequency switching capability. For this reason the HSMS 8101 Schottky diode was selected since its operation is optimized at 10 GHz. In Chapter III, the various parameters of the HSMS 8101 diode have been investigated. The diode's input impedance at microwave frequencies was calculated using the AC equivalent model.

In order to investigate the feasibility of powering a micro air vehicle using microwaves, the power requirements of a MAV must be known. Thus, two prototypes of a counter rotating helicopter type MAV were manufactured and tested, as thoroughly presented in Chapter IV. The results show that a minimum of 1.3 W of dc power is required for hovering of a 10 g MAV when it carries 10 g of load.

As the most critical component of the microwave power transmission system, the rectenna array must be designed and manufactured in a manner which the total efficiency is maximized. A circular patch antenna was selected as the most appropriate to alleviate the harmonic reradiation problem which is interwoven with any rectenna design. As explained in Chapter V, the inherent capability of the circular patch to resonate at roots of

Bessel functions and not at multiples of the fundamental frequency, makes it the best candidate for rectenna applications. The theory of the maximally flat response stepped impedance filters, which were designed as input, and output low pass filters for the rectifier circuit, has also been presented. For both the antenna and filter applications very thin microwave substrates were used in an effort to keep the weight down.

Finally, in Chapter VI the assembly process of the rectenna elements, as well as that of the rectenna array has been presented. Each of the elements consists of two individual circuit boards, one for the patch antenna and the other for the rectifier system. A feed probe was soldered to connect the antenna with the input low pass filter, while the Schottky barrier diode was connected via a hole to the rectifier ground plane. A total of twenty rectenna elements were manufactured and tested for various load resistances and incident power levels. The results show a relatively poor circuit efficiency of 10.3% which is lower than the expected value. This discrepancy is mostly attributed to impedance mismatches of the circuit. The efficiency of the array which was made by attaching the elements with thin carbon rods was lower (8.2%). This was due to the fact that the resonant frequency of the elements was different by a factor of ± 15 MHz, which precluded operating all elements at the optimum frequency. The rectenna output power was not sufficient for the first MAV prototype to fly when the transmitted power was 18.6 W. With this power level the maximum rotor RPM achieved was 450.

B. RECOMMENDATIONS FOR FUTURE WORK

The results of this thesis show that in order to make a micro air vehicle fly using microwave power, the research has to be focused in two major areas. The first one is towards the weight of the design. The weight of the vehicle as well as the payload must be minimized. The weight of the vehicle can be minimized using composite materials which allow a very light structure without jeopardizing the rigidity. Similarly, the weight of the payload can be reduced using integrated microelectronics for the various MAV systems. The adaptation of integrated electronics can also reduce the power consumption of the MAV motor and other systems.

The other area, which is maybe the most critical, is the microwave conversion efficiency. That is, how much microwave power is converted to dc power. A number of factors affect the conversion efficiency. Starting at the front end of the system, the

antenna must be effectively designed to exhibit as high gain as possible at the frequency of operation, and at the same time should be compact to allow space minimization. These attributes can only be met in microstrip patch antennas and therefore, the design should not deviate from this practice. Moreover, microstrip patches are appropriate when dual polarization rectennas are required. In any case emphasis should be given to the impedance matching between the components of the rectenna. Since the reflected power is the primary factor that reduces the conversion efficiency, the design must be focused in minimizing the reflections.

The Schottky barrier diode plays a vital role in the system efficiency. An ideal diode should be one where minimum resistive losses are exhibited during the rectification process, and the impedance characteristics are predictable at the frequency of operation. Also the power handling capability of the diode should be as high as possible. This allows the number of diodes to be reduced leading to a more light and simple rectenna. Galium arsenide (GaAs) diodes can handle relatively more power than silicon (Si) diodes and potentially can be replace Si diodes in the future rectenna designs.

The selection of the microwave substrate together with the type of filters must be done in such a way that the power losses are minimized. Usually very thin substrates exhibit more losses than thicker ones when the dielectric constant remains the same. However, the thickness of the substrate seriously affects the weight of the rectenna, and therefore the weight of the MAV itself. Thus, the substrate thickness selection should be a compromise between weight and induced losses.

THIS PAGE INTENTIONALLY LEFT BLANK

LIST OF REFERENCES

1. Sang H. Choi, Sang-Hyon Chu, Kyo D. Song and Glen C. King, "Microwave-Driven Multifunctional Capability of Membrane Structures," NASA Langley Research Center, Hampton Virginia, 23681-2199, Norfolk State University, Norfolk, Virginia.

2. W. C. Brown, "The History of Power Transmission by Radio Waves," *IEEE Trans. Microwave Theory and Techniques*, Vol. MTT-32, No. 9, pp. 1320-1242, September 1984.

3. W. C. Brown, "Thermionic Diode Rectifier," *Okress, Microwave Power Engineering,* Vol. I, Academic Press 1968, pp. 195-198.

4. W. C. Brown, "Microwave Powered Aerospace Vehicles," *Okress, Microwave Power Engineering,* Vol. II, Academic Press 1968, pp. 268-285.

5. W. C. Brown, "Experimental Airborne Microwave Supported Platform,*"* Rome Air Development Center, Griffis Air Force Base, New York, Tech Rep. RADC-TR-65-188, December 1965.

6. J. J. Nahas, "Modeling and Computer Simulation of a Microwave-to-dc Energy Conversion Element," *IEEE Transactions on Microwave Theory Technique*, Vol. MTT-23, No. 12, pp. 1030-1035, December 1975.

7. R. J. Gudmann and J. M. Borrego, "Solar Power Satellite Rectenna Study: Directional Receiving Elements and Parallel-Series Combining Analysis," Rensselaer Polytechnic Institute, Troy, NY, NASA Contract No. NAS. 9-15453, NASA-CR-151866, December 1978.

8. J. O. McSpadden, "Theoretical and Experimental Study of 2.45 GHz Rectifying Antennas," Master's Thesis, Texas A&M University, December 1993.

9. R. M. Dickinson, "Performance of a High-Power 2.388 GHz Receiving Array in Wireless Power Transmission Over 1.54 km," *IEEE MTT-S International Microwave Symposium*, 1976, pp. 139-141.

10. W. C. Brown and J. F. Triner, "Experimental Thin-Film, Etched-Circuit Rectenna," *IEEE MTT-S International Microwave Symposium Digest*, 1982, pp. 185-187.

11. W. C. Brown "Experimental Low Power Density Rectenna," *IEEE MTT-S International Microwave Symposium Digest*, 1991, pp. 197-200.

12. J. J. Schlesak, A. Alden and T. Ohno, "A Microwave Powered High Altitude Platform," *IEEE MTT-S International Microwave Symposium*, 1988, pp. 283-286.

13. James O. McSpadden, Taewhan Yoo and Kai Chang, "Theoretical and Experimental Investigation of a Rectenna Element for Microwave Power Transmission," *IEEE Transactions on Microwave Theory and Techniques*, Vol. 40, No. 12, pp. 2359-2366, December 1993.

14. T. Yoo, James O. McSpadden and Kai Chang, "35 GHz Rectenna Implemented with a Patch and a Microstrip Dipole Antenna," *IEEE MTT-S International Microwave Symposium Digest,* 1992, pp. 345-348.

15. Tae-Whan Yoo and Kai Chang, "Theoretical and Experimental Development of 10 and 35 GHz Rectennas," *IEEE Transactions on Microwave Theory and Techniques,* Vol. 40, No. 6, pp. 1259-1266, June 1992.

16. A. Alden and T. Ohno, "Single Foreplane High Power Rectenna," *Electronics Letters,* Vol. 28, No. 11, pp. 1072-1073, 21 May 1992.

17. James O. McSpadden and Kai Chang, "A Dual Polarized Circular Patch Rectifying Antenna at 2.45 GHz for Microwave Power Conversion and Detection," *IEEE MTT-S International Microwave Symposium Digest,* 1994, pp. 1749-1752.

18. Larry W. Epp and Abdur R. Khan, "Microstrip Patch Antenna with High Output Voltage," JPL New Technology Report, California, Contract No. NAS 7-918, NPO-20641, NASA Tech Brief Vol. 24, No. 8, August 2000.

19. Y. Fujino, N. Kaya, and T. Saka, "Development of a C-Band Rectenna for Microwave Power Transmission toward a Space Robot," *Acta Astronautica,* Vol. 50, No. 5, pp. 295-300, 2002.

20. Y. Fujino, T. Ito, M. Fujita, N. Kaya, H. Matsumoto, K. Kawabata, H. Sawada and T. Odonera, "A Driving Test of a Small dc Motor with a Rectenna Array," *IEICE Transactions on Communications,* Vol. E77-B, No. 4, pp. 526-528, April 1994.

21. W. C. Brown, "Design Definition of a Microwave Power Reception and Conversion System for Use on High Altitude Powered Platform," Wallops Flight Facility, VA, NASA Report No. CR-156866, NASA Contract No. NAS 6-300, July 1980.

22. W. C. Brown, "A Microwave Powered, Long Duration, High Altitude Platform," *IEEE MTT-S Digest*, 1986.

23. W. C. Brown, "Beamed Microwave Power Transmission and its Application to Space," *IEEE Transactions on Microwave Theory and Techniques*, Vol. 40, No. 6, June 1992.

24. James M. McMichael and Colonel Michael S. Francis (Ret.), *"Micro Air Vehicles. Toward a New Dimension in Flight,"* 7 August 1997, Available from [http://www.darpa.mil/tto/MAV/mav_auvsi.html], Accessed January 2003.

25. Arthur F. Huber, II, Lt Col, USAF, "Death by Thousand Cuts: Micro Air Vehicles (MAV) in the Service of Air Force Missions" Air War College, Air University, Maxwell Air Force Base, Alabama, April 2001.

26. Page, Douglas, "Micro Air Vehicles: Learning from the Birds and the Bees," *High Technology Careers Magazine*, 1998, Available from [http://www.hightechcareers.com/doc198e/mav198e.html], Accessed January 2003.

27. G. Tsolis, "Experimental Study of the Unsteady Aerodynamics Phenomena of a NACA 0012 Airfoil Oscillating in Pitch Axis," Bachelor's Thesis, Hellenic Air Force Academy, Athens, Greece, March 1990.

28. Stephen J. Morris, "Design and Flight Tests Results for Micro-Sized Fixed-Wing and VTOL Aircraft," Palo Alto, California.

29. B. Vitale, J., "Design and Prototype Development of a Wireless Power Transmission System, for a Micro Air Vehicle (MAV)," Master's Thesis, Naval Postgraduate School, Monterey, California, June 1999.

30. G. P. Boyakchyan, V. A. Vanke and S. K. Lesota, "Problems in Optimization of Parameters of a Schottky-Barrier Diode in a Rectenna Element," "Radio Engineering and Electronic Physics (English Translation of *Radiotekhnika i Electronika*), Vol. 29, No. 2, pp. 131-135, February 1984.

31. Adel S. Sedra and Kenneth C. Smith, *"Microelectronic Circuits,"* Oxford University Press, New York, 1998.

32. David M. Pozar, *Microwave Engineering*, John Wiley & Sons, Inc., New York, 1998.

33. Rolando R. Buted, "Zero Bias Detector Diodes for the RF/ID Market," *Hewlett-Packard Journal,* December 1995.

34. Hewlett-Packard Application Note 988, "*All Schottky Diodes are Zero Bias Detectors."*

35. Hewlett-Packard Application Note 969*, "The Zero Bias Schottky Detector Diode."*

36. Agilent Technologies "Surface Mount Microwave Schottky Mixer Diodes," *Technical Data for HSMS Schottky Barrier Diode.*

37. Hewlett-Packard Application Note 1088, "*Designing the Virtual Battery.*"

38. Robert G. Harrison, Xavier de Prolozec, "Nonsquarelaw Behavior of Diode Detectors Analyzed by the Ritz-Galerkin Method," *IEEE Transactions on Microwave Theory and Techniques,* Vol. 42, No. 5, May 1994.

38. W .J. Wagtendock, *Principles of Helicopter Flight*, Aviation Supplies and Academics, Inc., Newcastle, Washington, 1996.

39. W. Z. Stepniewski, C. N. Keys, *Rotary-Wing Aerodynamics*, Dover Publications, Inc., New York.

40. SRI International, "Flapping-Wing Propulsion Using Electroactive Polymer Artificial Muscle Actuators, Phase 2: Radio Controlled Flapping Wing Testbed," SRI Project 3470, DARPA Order Number DABT63-98-C-0024, ITAD-3440-FR-03-009," Final Report Covering the Period 1 March 1998 through December 2002.

41. Personal Communication with Dr. Kevin Jones, Naval Postgraduate School, Monterey, California.

42. Thomas J. Mueller, *Fixed and Flapping Wing Aerodynamics for Micro Air Vehicle Applications,* American Institute in Astronautics and Aeronautics, Volume 195, 1998.

43. Warren L. Stutzman and Gary A. Thiele, *Antenna Theory and Design*, 2nd Edition, Wiley, 1998.

44. Balanis, Constantine A., *Antenna Theory: Analysis and Design*, Wiley, New York, 1997.

45. Robert A. Sainati "*CAD of Microstrip Antennas for Wireless Applications*," Artech House Inc., Boston, 1996.

46. W. C. Brown, "A Survey of the Elements of Power Transmission by Microwave Beam" *IRE Transactions on Antennas and Propagation*, Vol. AP-9, pp 248-256, May 1961.

47. R. J. Gudmann and J. M. Borrego, "Power Combining in an Array of Microwave Power Rectifiers", *IEEE Transactions of Microwave Theory and Techniques*, Vol. MTT-27, No. 12, December 1979.

48. Takeo Ito, Yoshiyuki Fujino and Masaharu Fujita, "Fundamental Experiment of a Rectenna Array for Microwave Power Reception," *IEEE Transactions on Communications*, Vol. ET-6B, No. 12, pp. 1508-1513, December 1993.

INITIAL DISTRIBUTION LIST

1. Defense Technical Information Center
   Ft. Belvoir, Virginia

2. Dudley Knox Library
   Naval Postgraduate School
   Monterey, California

3. Chairman
   Information Sciences Department
   Naval Postgraduate School
   Monterey, California

4. Professor David C. Jenn, Code EC/Jn
   Department of Electrical and Computer Engineering
   Naval Postgraduate School
   Monterey, California

5. Professor Jeffrey B. Knorr, Code EC/Ko
   Department of Electrical and Computer Engineering
   Naval Postgraduate School
   Monterey, California

6. Professor Kevin Jones
   Department of Mechanical Engineering
   Naval Postgraduate School
   Monterey, California

7. Major George Tsolis
   Greece

View publication stats